Agile Multi-PHY Wireless Networking

Mina Rady

Thesis

of the

École Doctorale Informatique, Télécommunications
et Électronique (Paris)

Agile Multi-PHY Wireless Networking

presented by

Mina Rady Abdelshahid Mouawad

A dissertation submitted in partial satisfaction of the
requirements for the degree of

Doctor of Philosophy

in

Computer Science

at

Sorbonne Université

Presented on 9 December 2021.

Jury:

Xavier Vilajosana	Universitat Oberta de Catalunya, Barcelona, Spain	Reviewer
Bernard Tourancheau	Université Grenoble Alpes, Grenoble, France	Reviewer
Nathalie Mitton	Inria, Lille , France	Examiner
Fabrice Theoleyre	CNRS, Strasbourg, France	Examiner
Oana Iova	INSA, Lyon, France	Examiner
Georgios Papadopoulos	IMT Atlantique, Rennes, France	Examiner
Paul Muhlethaler	Inria, Paris, France	PhD Adviser
Thomas Watteyne	Inria, Paris, France	PhD co-Adviser
Dominique Barthel	Orange Labs, Meylan, France	Industrial Advisor
Quentin Lampin	Orange Labs, Meylan, France	Industrial Advisor

Résumé

Cette thèse contribue au domaine émergent des réseaux sans-fil agiles utilisant plusieurs couches physiques. Traditionnellement, les réseaux sans-fil industriels n'emploient qu'une seule interface radio, à l'instar des implémentations de la pile protocolaire réseau IETF 6TiSCH qui s'appuient sur la radio IEEE 802.15.4 O-QPSK opérant dans la bande de fréquence à 2,4 GHz. Des progrès dans l'intégration de plusieurs schémas de modulation/codage au sein d'un même circuit radio et capable d'opérer dans différentes bandes de fréquence permettent aujourd'hui l'exploitation au sein d'un même réseau d'une diversité de configurations radios. Nous utilisons le terme "PHY" pour désigner toute combinaison de : modulation, bande de fréquence et schéma de codage. Dans cette recherche, nous soutenons que la combinaison de PHY longue portée et courte portée peut offrir des performances de bout en bout de réseau équilibrées qu'aucun PHY unique n'atteint. Nous démontrons comment un ensemble de PHY courte et longue portée peut être intégré sous une architecture 6TiSCH généralisée ("g6TiSCH") et nous évaluons expérimentalement ses performances dans un banc d'essai de 36 nœuds à Inria-Paris. De plus, nous montrons, expérimentalement, comment un slotframe TSCH peut adapter la durée du slot, slot par slot, en fonction du débit du PHY utilisé ("6DYN"). Enfin, nous concevons et évaluons, par simulation, une fonction d'objectif pour RPL qui optimise la durée de vie du réseau ("Life-OF"). Nous démontrons comment Life-OF combine divers PHYs pour augmenter la durée de vie du réseau de jusqu'à 470% par rapport à la fonction d'objectif MRHOF du staandard IETF actuel.

Summary

This thesis contributes to the emerging field of agile multi-PHY wireless networking. Industrial wireless networks have relied on a single physical layer for their operation. One example is the standardized IETF 6TiSCH protocol stack for industrial wireless networking, which uses IEEE 802.15.4 O-QPSK radio in the 2.4 GHz band as its physical layer. Advances in radio chip manufacturing have resulted in chips that support a diverse set of long range and short range PHYs. We use the term "PHY" to refer to any combination of: modulation, frequency band, and coding scheme. In this research, we argue that combining long-range and short-range PHYs can offer balanced network end-to-end performance that no single PHY achieves. We demonstrate how a set of short-range and long-range PHYs can be integrated under one generalized 6TiSCH ("g6TiSCH") architecture and we evaluate its performance experimentally in a testbed of 36 motes at Inria-Paris. We further demonstrate, experimentally, how a TSCH slotframe can adapt the slot duration on a slot-by-slot basis, as a function of the bitrate of the used PHY ("6DYN"). Finally, we design and evaluate, through simulation, an objective function for RPL that optimizes for network lifetime ("Life-OF"). We demonstrate how Life-OF combines diverse PHYs to boost network lifetime to be up to 470% compared to the IETF standard MRHOF.

Acronyms

6LoWPAN	IPv6 over Low-Power Wireless Personal Area Networks
6P	6top Protocol
6top	6TiSCH Operation Sublayer
6TiSCH	IPv6 over TSCH
ASN	Absolute Slot Number
DIO	Destination Information Object
DMC	DAG Metric Container
DODAG	Destination-Oriented Directed Acyclic Graph
ETSI	European Telecommunications Standards Institute
FSK	Frequency Shift-Keying
GFSK	Gaussian Frequency Shift-Keying
GW	Gateway
HART	Highway Addressable Remote Transducer
IEEE	Institute of Electrical and Electronics Engineers
IETF	Internet Engineering Task Force
IIoT	Industrial Internet of Things
IoT	Internet of Things
IPv6	Internet Protocol version 6
JSON	JavaScript Object Notation
KPI	Key Performance Indicators
LLN	Low-power and Lossy Network

MAC	Medium Access Control
MCS	Modulation and Coding Scheme
MQTT	Message Queuing Telemetry Transport
O-QPSK	Offset quadrature phase-shift keying
OF	Objective Function
OFDM	Orthogonal frequency division multiplexing
PDR	Packet Delivery Ratio
PHY	Physical layer
PLC	Power Line Communications
QoS	Quality of Service
RFC	Request For Comments
RPL	Routing Protocol for Low-Power and Lossy Networks
RSSI	Received Signal Strength Indicator
SPI	Serial Peripheral Interface
TSCH	Time Slotted Channel Hopping
UDP	User Datagram Protocol

To the man who taught me how to walk.
Until we meet again.

"the thought that makes me smile now,
even as the tears fall down
is that the only scars in heaven
are on the hands that hold you now"

In memory of my father Rady Abdelshahid
9 November 1953 - 22 December 2020.

Acknowledgements

I have been blessed with a wonderful family: no words or actions of gratitude can outweigh how each and every one of you supported and guided me during tough and dry seasons: My Mom and my sisters Mariana and Merna, Nahamia Nathan and Lydia Hanna, Pierre-Alain and Viviane Brunel, Jean-Luc and Jeannie Tabailloux, Blaine and Olivia Vorster, Roy and Jennifer Nagelkirk, Jean-Pierre and Ruth Hoonakker, Fadia and Fawwaz Dalloul, Kathryn and Kamal Loudiyi. I am grateful from all my heart. This work would not have been even nearly possible without your wholehearted presence in my life.

If I ever happen to seem tall, it is only because I stood on the shoulders of giants. Dominique Barthel, Quentin Lampin and Thomas Watteyne are true giants that held me up during incredibly turbulent times and who did not cease to give me their absolute best, in time, effort, and sincere unfiltered advice. I could not wish for stronger or more supportive supervisors. Thank you for everything and for bearing every time I, unintentionally, tested your patience. A good sailor is known in the storm and you are the best sailors I know. No words can suffice to serve you due honor.

I would not have been here without my role model: Professor Nazli Choucri, MIT Faculty of Political Science, who was the first to teach me how to think like researcher and how to remain human during a work that can get cold and tough. I could not be more grateful to everything you taught me. To this day, I still have no clue why you picked me to work with you.

If I know anything today about networks, it is thanks to Professor Francis Lepage and Professor Jean-Philippe Georges in Université de Lorraine in Nancy and to the whole Erasmus Mundus PERCCOM Program. They had me as their student when I had not touched a network in my life and when I was still googling: "what is a protocol stack". Again, to this day, I still have no clue why you picked me to work with you.

I would like to thank my undergraduate supervisors when I was at the American University in Cairo: Professor Awad Khalil and Professor Ahmed Rafea as you made computer science seem so easy.

Thank you all for being the role models you are.

I would like to express my special gratitude for my team in Orange and in Inria for this wonderful time. I specially thank my boss Nadège Favre: thank you for all your hard efforts to help me have my life as smooth as possible. I feel incredibly fortunate (and a bit spoiled) to have you as my boss!

I thank my comrades in the Inria AIO team who helped me patiently and unswervingly as I was figuring out my way around this work. Tengfei Chang: thank you for your incredible effort and patience in walking me around OpenWSN and 6TiSCH. Jonathan Muñoz: you know this work is only possible thanks to the fruit of your hard work in your PhD titled "km-scale industrial networking". I am truly grateful for your support and your friendship.

I specially thank my Comité de Suivi: Marcelo Amorim and Samia Bouzefrane for their precious advice at both meetings. It was an eye opening advice that made a real difference to my thesis and to my thinking as a researcher.

Chapter 1

Introduction

This thesis contributes to the growing research topic of low-power wireless networking and IoT. Specifically, it focuses on exploring the potential for multi-PHY wireless networking for increasing the agility of network architectures. This chapter is organized as follows. Section 1.1 introduces a historical perspective on the concept of "agility" in computer systems. Section 1.2 provides an introduction on the IoT use cases and main technologies using both short-range and long-range PHYs. Section 1.3 presents why multi-hopping is still needed even with use of long-range PHYs. Section 1.4 introduces the vision of this thesis for an agile IoT networking. Finally, Section 1.5, introduces the outline of the thesis manuscript.

1.1 Agility: A Story

Agility can be defined by its french root *agilité* as "the ability to move and adapt lightly, fast, and smoothly". It has historically marked the technical epochs in software engineering and systems development.

In 1880, the United States experienced a large wave of immigration. The U.S. Census Bureau had a challenge to process the paper records of all U.S. residents. It took employees of the bureau full eight years of work to complete the census processing. Herman Hollerith, an engineer of mines and a clerk at the bureau, proposed a solution to accelerate the census processing. He proposed to store the records in the form of punched cards and he proposed an electro-mechanical machine that can translate the locations of holes on the cards to mechanical rotations of counting gears. In 1890 the U.S. Census Bureau adopted those machines which led to reducing census processing time down to two years only instead of eight. The first card format had 22 columns, specifically designed for the census application.

Later, Hollerith generalized the solution under his new company: *International Business Machines* (IBM). It was used in banking, commercial, and even police record keeping and processing. As the use cases became more diverse, different punched cards were needed with more columns and different hole shape. In 1928, IBM adopted a new 80-column punched card that was designed to allow as versatile applications as possible.

However, as the use cases increased in diversity, it became clear that the punched cards were not able to keep up with the diverse requirements. IBM researched several options to the best design of its punched cards. A grand challenge was ahead: adopting new/larger cards meant to customize the mechanical design of the equipment for each potential card (let alone backward-compatibility).

In 1952, instead of attempting to find "the best" configuration of a punched card, IBM introduced the magnetic tape storage with IBM 701 computer. This storage system was large, fast, and cost-effective enough that it was able to be generalized to diverse use cases via the IBM 701, the IBM's first released scientific computer. Magnetic tape storage paved the road later for the magnetic disk storage (i.e. hard disk storage).

One can observe a factor behind the evolution of modern storage systems: there was no single design of punched cards that was best fit for all use cases.

Later technological developments followed suite with a similar pattern. Networks were developed with different MAC protocols and physical mediums that varied between focus on reliability, delay, and simplicity. Examples of these networks were ARCNET, Ethernet, and Token Ring. Each network was advanced in the market by industrial players behind them. The networking market did not converge on one solution that seemed "the best". Instead, the Internet Protocol was introduced to allow harnessing the advantages of diverse networks by integrating them into one larger network: the Internet. This way, a network solution can be adapted to diverse use cases by integrating the different networks under one larger logical network.

Therefore, a key factor behind the evolution of both modern storage systems as well as the Internet Protocol is this: *how to adapt as quickly as possible to changing and diverse requirements when no single solution seems to be always the best?*

1.2 The Internet of Things

In the recent two decades, the world witnessed a renaissance in industrial wireless networking with the advent of the IoT. This was motivated by industrial interest in remote monitoring of huge and complex machinery in industrial plants (i.e. the fourth industrial revolution). Wireless is preferred in such a case since it can be easily deployed and maintained without invasion to the plant infrastructure [1]. It was also motivated by a need to automate monitoring for utility metering in remote or dense areas.

In 2003, the IEEE standardized a physical layer for IoT applications in the IEEE802.15.4 standard. It is the O-QPSK modulation at 2.4 GHz with 250 kbps raw bitrate. There has been one major limitation of this configuration: its usual physical range is considerably small. It may not exceed a dozen meters in a typical office building. To overcome this limitation, IoT networks using this physical layer rely on multi-hopping within the network: a node uses its neighbors to route its traffic to the gateway. It has been adopted at the base of several commercial solutions such as Zigbee [2] and SmartMeshIP [3].

Therefore, a typical "short range" IoT network using the O-QPSK 2.4 GHz PHY is depicted in Fig. 1.1. It consists of a number of embedded nodes where each node

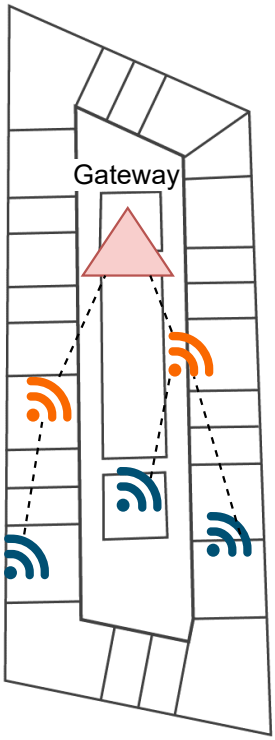

Figure 1.1: A short-range multi-hop network can be sufficient for a local deployment in a building floor. Some end devices may rely on routers for coverage extension (marked in orange).

contains a low-power micro-controller, attached sensors to monitor physical phenomena (e.g. temperature, gas concentration, vibration intensity), and a radio chip that is used to transmit the sensor readings using a communication protocol. Nodes can send their readings periodically or based on alarm event triggers.

Applications of IoT began spanning a growing number of use cases. These use cases covered areas such as environmental monitoring [4], smart building [5], [6], precision agriculture [7], automated meter reading [8], indoor localization [9], micro-robot connectivity [10], smart grid management [11] and predictive maintenance [1]. Each application poses its own requirements for the QoS expected from the network. The average current draw is often a key performance factor as devices are typically battery-powered and deployed in hard-to-reach areas. For some applications, the ability to communicate over a long distance is important as the network is deployed over a large area, or an area with poor propagation conditions. Other important network performance metrics include end-to-end reliability and latency.

A short-range radio such as O-QPSK 2.4 GHz can be sufficient in meeting the requirements for some applications where energy saving has higher priority than latency and reliability. But since it relies on routers for multi-hopping, this made it less suitable for wide area coverage (such as a $2 \times 2\ km^2$ industrial plant). In this case, more routers are needed to bridge the link between the nodes and the gateway, which means more maintenance overhead and therefore less financial and practical feasibility.

In response to these limitations, a new family of long-range PHYs have been introduced to serve the IoT market. They rely on use of a combination of slower bit-rates, sub-GHz frequencies, and narrow-band PHYs to improve their link budget (i.e. their potential range). Their range typically spans between a few hundred meters to a dozen kilometers, depending on the environment (indoor, outdoor, dense urban, etc). This way, nodes can communicate directly to the root without need for intermediate routers and therefore with minimal maintenance overhead. These networks are typically deployed in star or connected-star topologies as shown in Fig. 1.2. This, however, comes at the expense of battery lifetime (or low application datarates) as the energy consumption of the node is increased significantly to achieve this long-range connectivity. Such networks have been identified as Low Power Wide Area Networks (LPWANs). Several commercial LPWAN technologies have been available in the market such as LoRaWAN [12], SigFox [13], and Narrow Band IoT (NB-IoT) [14].

LoRaWAN uses the LoRa PHY layer which is based on Chirp Spread Spectrum modulation [12], [15]. LoRa relies on a combination of low data rate and sub-GHz frequencies to achieve an improved link budget and, subsequently, long range connectivity. The network architecture is based on connected-star topology. It relies on a central network server that determines how each end device connects to the nework. A typical LoRaWAN network operates on 125 kHz channel bandwidth in a sub-GHz (license-free) frequency band (e.g. 868 MHz in Europe), with raw bitrate varying from 293 bps up to 5.4 kbps. It offers a maximum payload of 243 bytes.

SigFox relies on a proprietary ultra narrow band (UNB) Binary Phase Shift Keying modulation for its PHY layer [15]. It relies on a combination of low fixed bitrate of

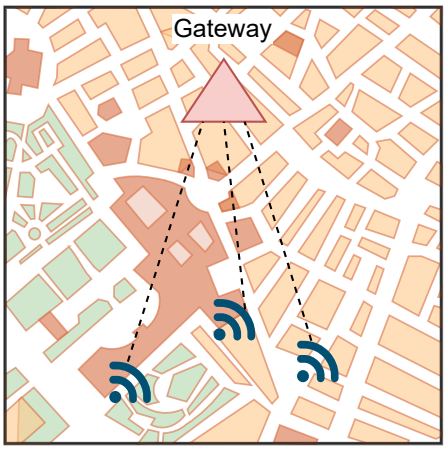

Figure 1.2: A long-range star network can serve metropolitan area deployments. End devices rely on the robust modulations to communicate directly with the gateway.

100 bps, UNB channel width of 100 Hz, and use of sub-GHz (license-free) frequencies. Its architecture is also based on multiple-antenna sites and a cloud-based network server [13]. It limits the available data payload to 12 bytes with an allowance of 140 up-link messages per device per day [15].

NB-IoT uses narrow-band Quadrature Phase Shift Keying and Frequency Division Multiple Access as uplink PHY layer. It further uses Orthogonal Frequency Division Multiple Access at its downlink PHY layer [14], [15]. It relies on a combination of narrow-band channel width of 200 kHz and use of licensed sub-GHz frequency. It offers a maximum throughput of 20 kbps and 200 kbps for uplink and downlink, respectively, with a maximum allowed payload of 1600 bytes [15]. Its architecture is also based on cellular topology with cellular coverage.

There are three common factors among the three technologies. First, each technology is developed as a full protocol stack backed by an industrial body or alliance (e.g. LoRaWAN Alliance and 3^{rd} Generation Partnership Project – 3GPP). Second, these technologies rely on base stations for cellular coverage which can cost anywhere between 1 k and up to 15 k euros in capital expenditure (excluding operational expenditure) [15]. Third, the protocol stack of each technology is packaged with pre-specified PHY layer that is often proprietary.

In 2012, the IEEE introduced the 802.15.4g amendment to include a family of 31 modulations in the sub-GHz band as well as 2.4 GHz band [5], [16]. They vary in performance, from long range to high bit-rate, to serve the requirements for diverse use cases. The advent of these standardized PHYs paves the way for more open network architectures as it allows the network solution architect more diverse set of standard PHYs that can be supplied from multiple vendors.

The diversity in use case requirements opens pathways where either short- or long-range approaches are beneficial. Short-range radios generally run at faster datarates leading to shorter air time. This leads to an improved battery lifetime and can offer

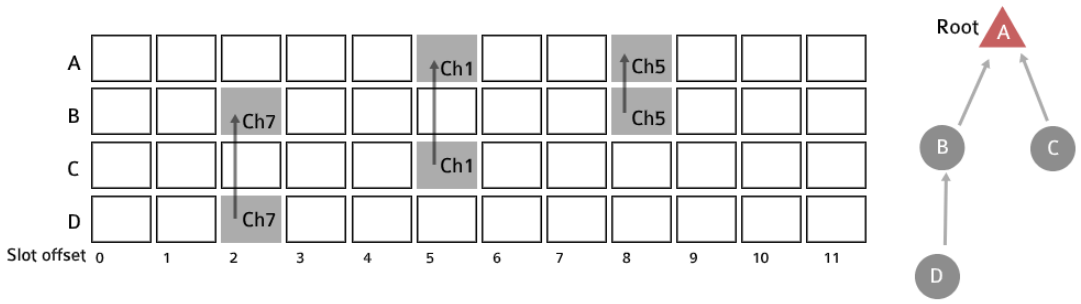

Figure 1.3: A typical TSCH slotframe for Motes A–D, using a uniform slot duration and single PHY at a fixed bitrate. Each node allocates a specific slot offset and channel offset for transmissions to its parent.

satisfying coverage for some applications involving few nodes within a building-floor [5], [6], a peach orchard [7], [9], or a few single-chip micro-motes [10]. Conversely, long-range radios can offer the necessary coverage for deployments spanning multiple km^2 such as a large factory [1] or a power grid [11], at an acceptable compromise in battery lifetime [16].

Battery lifetime has been a key performance indicator in IoT networks. In many use cases, an area is covered with a wireless network of battery-powered devices where mains power is not available. Even when mains power is available, a none-invasive deployment is often inevitable in sensitive infrastructures (e.g. hospitals [9], complex industrial plants [1]). This creates a need to manage the network protocol in such as way as to result in the longest battery lifetime possible. IoT network protocols have been introduced to save the average battery lifetime by using MAC techniques that allow the radios to go into sleep mode when they are not needed.

One of these MAC techniques is the class of protocols under the TSCH paradigm [17], [18]. While early low-power wireless networks used contention-based MAC approach, TSCH, initially developed for industrial applications, is now supported by many commercial products and open-source implementations [19]. In a TSCH network, time is cut into timeslots and a schedule orchestrates all communication; it indicates to every node what to do in each timeslot: transmit, listen or sleep. An example of a TSCH slot-frame is presented in Fig. 1.3. TSCH is the key principle of the IEEE802.15.4e standard which is the standard MAC layer for several industrial protocol stacks such as WirelessHART, ISA100.11a, and more recently, 6TiSCH. In today's TSCH networks, for each cell, the schedule indicates the frequency to communicate on, resulting in "channel hopping", a technique known to efficiently combat external narrowband interference and multi-path fading.

Within this context, the IETF standardized the 6TiSCH protocol stack, which combines the high reliability of TSCH and the low power operation of the IEEE 802.15.4 PHY [20] (e.g. 24 mA current draw for transmission [21]). It is a fully distributed protocol stack for mesh networking (i.e. no central controller). Specifically, 6TiSCH combines IPv6 with the TSCH mode of IEEE802.15.4e standard.

1.3 Why Multi-hopping Still Makes Sense for Long-Range PHYs?

A common question is raised when discussing specifically the use of long-range PHYs in a multi-hop network: multi-hopping was useful with short-range PHYs, but now if all nodes are equipped with long-range PHYs such as LoRa, *do we still need multi-hopping?* There is at least two reasons why multi-hopping makes sense even with long-range PHYs: extreme connectivity barriers and budget barriers.

Even with long-rang PHYs, connectivity barriers are still unavoidable. Orange provides extensive LoRaWAN coverage of France, as illustrated in Fig. 1.4a. Blind spots are unavoidable in deep indoor locations where utility meters or parking sensors are deployed, as shown in Fig. 1.4b. From the point of view of a network operator such as Orange, the LoRaWAN network is deployed in a way similar to a cellular network. Users cannot add gateways on their own to improve the coverage in areas where the connectivity is not sufficient. An example of this scenario can be seen at Orange Labs site in Meylan, France in Fig. 1.5. The gateway is placed right on top of the garage building, yet the LoRaWAN network is inaccessible in this garage because of the layers of concrete walls and ceilings. Consumer interest or regulatory requirements normally necessitate pervasive coverage of end devices in different contexts. For instance, the European Commission (EC) mandate M/441 draws the regulatory requirements for open bidirectional communications interfacing of metering instruments [22]. This is in order to comply with utility monitoring standards outlined in several EC directives such as directive 2006/32/EC (Article 13) [23]. Also, an owner of an underground deployment of sensors (e.g. parking sensors) requires all sensors to be covered.

In a long-range star topology (Fig. 1.2), this connectivity gap is addressed today by adding more GWs, thereby creating more stars. However, this is challenged by a budget barrier. GWs provide hot spots for end devices and then forward the traffic via a high-throughput link such as Ethernet or cellular network. However, GWs come with significant financial costs for their installation. Mainly, the main cost element is that operator has to dispatch employees to access mobile towers to install these GWs (often in remote areas). In addition, the cost of a GW ranges between a few hundred euros to a few thousand euros depending on its capacity, antenna, and network interfaces. Furthermore, GWs need to be constantly powered, and mounted to an infrastructure with a grid power and a high throughput connection. This is the normal setting of a cellular tower, and it is where a network operator would usually mount their LPWAN GWs.

Network operators want to provide an affordable subscription cost to their users, typically in the order of one euro per end-device per month. Therefore, efficient capacity utilization of the network, to enable reasonable subscription costs, is a common interest. Maybe in some situations, the number of poorly covered devices are numerous enough to justify the cost of adding a GW. *But what if this is not the case?* For instance, the area of the indoor blind-spots observed in Fig. 1.4b is likely to contain too few devices/subscriptions to offset the cost of adding another GW. This invites efforts to

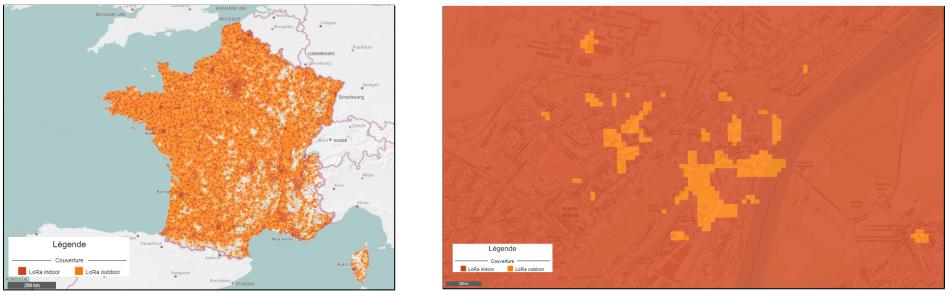

(a) Orange LoRaWAN extensive coverage in France

(b) Isolated blind spots in indoor coverage in complex urban areas with good coverage

Figure 1.4: LoRaWAN coverage by Orange in France in August 2021 [24]. Despite pervasive national coverage (*left*), blind spots are unavoidable, especially indoor (*right*), let alone deep indoors. Therefore, some end devices can potentially be unreachable.

Figure 1.5: Example of concrete structure environments of underground parking sensors parking in Orange Labs Meylan

find cheaper and more flexible coverage extension alternatives. Cheap low capacity multi-hop routers, in this sense, can be a promising approach to improve coverage at a cost proportional to ROI from the few affected end devices.

1.4 The Vision: Agile IoT Networking

Advances have been accomplished in the manufacturing of radio chips and Systems-on-Chip (SoCs), leading to lower costs with more features and more advanced PHY capabilities. For example, the CC2538 SoC by Texas Instruments implements the IEEE802.15.4 PHY in the 2.4 GHz band which serves a sector of the short-range PHY market [21]. The Nordic Semiconductor nRF52840 SoC offers support of multiple protocol stacks for short-range PHYs such as IEEE802.15.4 and Bluetooth Low Energy

(BLE) [25], both at 2.4 GHz. The AT86RF215 by Atmel implements the full range of modulations under the IEEE802.15.4g amendment [26] in both the 2.4 GHz and sub-GHz bands. Its design allows switching between modulations on a frame-by-frame basis, which enables it to serve both long-range and short-range applications [27].

The approach traditionally followed by network architects is to compare different PHYs and choose the one most suitable for a given application. However, this approach leads to further constraints: if one PHY is used, the benefits of other PHYs are forfeited. If the application demands a change or a tuning (for example, a subset of nodes requires longer-range PHY), the entire network must be re-engineered to integrate a separate network using the new PHY running side-by-side (as discussed in Section 2.6). This leads to an agility challenge as the network is becoming more complex to maintain and to improve.

This leads to the question: *Since both short-range and long-range approaches can be useful in different ways, is it possible to have an* ***agile*** *approach where a network can adapt to different requirements my using any mix of PHYs as needed by the uses case?*

The vision of this thesis is to have an agile wireless network where different PHYs can co-exist in the same network. This allows nodes to choose the most appropriate PHY on a frame-by-frame basis. A node dynamically switches between PHYs: a short-range PHY when the next hop is close by, a long-range PHY when the next hop is far away. On top of saving energy, this approach allows increasing robustness as some long-range PHYs are more robust against path-loss (e.g., FSK 868 MHz [5]) while others are more robust against multi-path fading and channel selective interference (e.g. OFDM 868 MHz [4], [5], [28]). All motes are still part of the same network in spite of their diverse PHYs.

This leaves us with three questions: *Does this vision make sense? How to realize this vision with a full protocol stack in a real network on a testbed setup?* and *Does this vision still make sense for improving network lifetime, in large scale simulations, apart from the variable specifics of the implementation details?*

This vision translates into the following scientific objectives:

- Study the "no free lunch" principle, where the intuition is that no single PHY offers best performance across all end-to-end network KPIs.
- Generalize the 6TiSCH protocol stack, by integrating a combination of short- and long-range radios into one network architecture.
- Introduce a new Objective Function (OF) for the RPL routing protocol, that combines diverse PHYs to boost network lifetime using multi-PHY networking.

1.5 Organization of the Thesis

Chapter 2 introduces the state of the art related to the subject of the thesis and we state our contributions. It is divided into six sub-areas on both research and standardization fronts. Section 2.1 concludes with the interest in multi-PHY integration. Section 2.2 highlights the reliability of the 6TiSCH protocol stack using the canonical

O-QPSK 2.4 GHz PHY. Section 2.3 highlights the regulation constraints to medium access in the ISM band. Section 2.4 highlights related work that improves TSCH schedule compactness using a centralized controller in a single-PHY network. Section 2.5 highlights related work on improving RPL performance either by improving network lifetime or by improving network stability in hybrid RF-PLC networks. Section 2.6 highlights the state of the art in multi-PHY industrial networks which confirms the intuition of the potential benefits of multi-PHY integration. Chapter 2 concludes with the key contributions of this thesis.

Chapter 3 describes the experimental and evaluation methodologies used throughout the thesis. We deploy three different setups to investigate the different research questions addressed. First, we describe a floor-scale testbed for network-wide evaluation protocol stack performance evaluation, used in Chapter 4 and Chapter 5. Second, we describe a local experimental setup for real-time performance demonstration using hardware probes, used in Chapter 6. Third, we describe the RPL simulator for high-level performance evaluation of RPL OFs, used in Chapter 7.

Chapter 4 addresses the question of why multi-PHY integration makes sense. Low-power wireless applications require different trade-off points between latency, reliability, data rate and power consumption. Given such a set of constraints, which PHY should I be using? We study this question in the context of 6TiSCH, a state-of-the-art recently standardized protocol stack developed for harsh industrial applications. Specifically, we augment OpenWSN, the reference 6TiSCH open-source implementation of our choice, to support one of three PHYs from the IEEE802.15.4g standard: FSK 868 MHz which offers long range, OFDM 868 MHz which offers high data rate, and O-QPSK 2.4 GHz which offers more balanced performance. We run the resulting firmware on the 42-mote OpenTestbed deployed in an office environment, once for each PHY. Performance results show that, indeed, no PHY outperforms the other for all metrics. The long range FSK 868 MHz radio leads to fastest network formation and lowest latency at the expense of battery lifetime. The short range O-QPSK 2.4 GHz radio leads to best network lifetime at the expense of latency and reliability, and network formation time. Chapter 4 proposes a principle of "no free lunch": advantages gained from one PHY will lead to forfeiting advantages of another PHY in terms of industrial KPIs. Subsequently, it argues for combining the PHYs, rather than choosing one, in a generalized 6TiSCH architecture. This is possible with technology-agile radio chips (of which there are now many), driven by a protocol stack which chooses the most appropriate PHY on a link-by-link basis.

Chapter 5 generalizes the 6TiSCH protocol stack with multi-PHY integration. We call the resulting protocol "g6TiSCH", which we evaluate on a real testbed setup. Wireless networks traditionally use a single PHY for communication: some use high bit-rate short-range radios, others low bit-rate long-range radios. g6TiSCH allows nodes equipped with multiple radios to dynamically switch between them on a link-by-link basis, as a function of link-quality. This approach results in a dynamic trade-off between latency and power consumption. We evaluate the performance of the approach experimentally on an indoor office testbed of 36 OpenMote B boards. Each OpenMote B can communicate

using FSK 868 MHz, O-QPSK 2.4 GHz or OFDM 868 MHz, a combination of long-range and short-range PHYs. We measure network formation time, end-to-end reliability, end-to-end latency, and battery lifetime. We compare the performance of g6TiSCH against that of a traditional 6TiSCH stack running on each of the three PHYs. Results show that g6TiSCH yields lower latency and network formation time than any of the individual PHYs, while maintaining a similar battery lifetime.

Ch. 6 goes a step further by showing how a multi-PHY TSCH slot frame can have heterogeneous slot-durations that vary by the bit rate of the each PHY. This chapter introduces 6DYN, an extension to the g6TiSCH multi-PHY protocol stack. In a 6DYN network, nodes switch PHYs dynamically on a link-by-link basis, in order to exploit the diversity offered by this new technology agility. To offer low latency and high network capacity, 6DYN uses heterogeneous slot durations: the length of a slot in the 6TiSCH schedule depends on the PHY used. This chapter shows how reserved bits in 6TiSCH headers can be used to standardize 6DYN and details its implementation in OpenWSN, a reference implementation of 6TiSCH.

Chapter 7 addresses the question of whether multi-PHY integration makes sense for improving network lifetime within high-level simulation setup. We propose a routing mechanism based on the RPL protocol in a wireless network that is equipped with a mix of short-range and long-range radios. We introduce Life-OF, an objective function for RPL which uses a combination of metrics and the diverse PHYs to boost the network's lifetime. We evaluate the performance of Life-OF compared to the standardized MRHOF objective function in simulations. Two KPIs are reported: network lifetime and network latency. Results demonstrate that MRHOF tends to converge to a pure long-range network, leading to short network lifetime. However, Life-OF improves network lifetime by continuously adapting the routing topology to favor routing over nodes with longest remaining lifetime. Life-OF combines diverse radios and balances power consumption in the network. This way, nodes switch between using their short-range radio to improve their own battery lifetime and using their long-range radio to avoid routers that are close to depletion. Results show that using Life-OF improves the lifetime of the network by up to 470% compared to MRHOF, while maintaining similar latency.

Chapter 8 concludes this manuscript and discusses the avenues for future work it opens. The list of publications and software contributions made as part of this work are listed in Chapter 9.

Chapter 2

State of the Art

Key Takeaways: This chapter surveys the research and standards related to this thesis. We introduce in Section 2.1 related work on performance evaluation of IEEE802.15.4g PHYs and we present why multi-PHY integration can be of interest. We then introduce in Section 2.2 an overview of the IETF 6TiSCH protocol stack for a reader without former knowledge on 6TiSCH and we present how it achieves high reliability. We introduce in Section 2.3 the regulation constraints to medium access in the unlicensed band and we present why multi-PHY integration can help relax these constraints. Furthermore, in Section 2.4, we present related work on schedule compactness in TSCH networks and we highlight that it only exists in centralized networks. We then provide an overview on RPL in Section 2.5 and we introduce related work on improving network lifetime in RPL or use of hybrid interface networks. Section 2.6 presents related work on state of the art in multi-PHY industrial networks. Finally, Section 2.7 summarizes the related work, and lists the key contributions of this thesis.

2.1 Evaluation of IEEE802.15.4g PHYs

As previously discussed in the introduction, the IEEE adopted a standard and diverse set of 31 PHYs in the IEEEE802.15.4g amendment [26]. The set consists of 31 PHYs for SUNs and their advantages vary to serve a wide array of use cases. Some PHYs are more suitable for long-range applications such as the family of FSK PHYs. The OFDM family of PHYs are more robust against multi-path fading in urban or indoor environments while offering high bitrates up to 800 kbps. Therefore, we consider this standard as a reference for our PHY selection because of its wide diversity.

This section introduces the related work on the performance evaluation of the IEEE802.15.4g PHYs (without the 6TiSCH stack).

Kojima et al.[28] examine the impact of interference between multi regional

FSK mode 2 and multi regional OFDM option 4 MCS 3. FSK mode 2 offers 100 kbps raw datarate at 400 kHz channel spacing whereas OFDM option 4 MCS 3 offers the same datrate but at only 200 kHz channel spacing. Generally, FSK requires less circuitry than OFDM and it is less immune against multi-path fading. Conversely, OFDM is capable of withstanding multi-path fading in complex environments at higher bit-rate than FSK at the expense of complex circuitry. The authors deploy IEEE802.15.4e MAC with multi-hop capability on top of each PHY layer and measure the impact of the interference between two networks, each running one PHY. Results are reported in terms of the degradation of throughput of each network in the presence of the other interfering network. Kojima et al.demonstrates that, since the OFDM modulation scheme uses multiple sub-carriers, it performs better than FSK in the presence of frequency selective interference.

Muñoz et al. [5] run an experimental campaign to compare the performance of IEEE802.15.4 O-QPSK 2.4 GHz at 250 kbps, and IEEE802.15.4g OFDM. They show a higher robustness of OFDM, even though it operates at a higher bit rate (800 kbps). They show that, although a radio draws less current when running O-QPSK 2.4 GHz, using OFDM 868 MHz leads to an overall lower power budget as transmission happens much faster.

The same authors also evaluate the performance of all IEEE802.15.4g PHYs [4]. They conduct a complete range-testing campaign for the 31 PHYs on the four scenarios they consider the most prevalent in outdoor applications: line of sight, smart agriculture, urban canyon, smart metering. Their results of the range-tests are reported in terms of PDR measurements, throughput, and electric charge consumption. They demonstrate the longer range of FSK and O-QPSK in the sub-GHz band compared to OFDM options due to their higher receiver sensitivity. Muñoz et al.provide interesting results as to which radio could be better in certain scenarios.

My thesis goes one step further to address the end-to-end performance of a full 6TiSCH stack using these PHY layers. We show in Chapter 4 the performance of 6TiSCH stack using each PHY. We demonstrate that there is not a single PHY that offers the best performance across all relevant network KPIs. This is the key motivation for generalizing the 6TiSCH architecture so it offers a balanced performance by integrating diverse PHYs.

2.2 IETF 6TiSCH Protocol Stack

This section provides an overview of standards and research related to the 6TiSCH protocol stack. It presents an overview of the standards of the protocol stack (Section 2.2.1), related work on the schedule management in 6TiSCH (Section 2.2.2), and related work on performance evaluation of 6TiSCH (Section 2.2.3).

2.2.1 6TiSCH Overview

The IETF is organized in Working Groups, some of which standardize IoT protocols. One of these Working Groups formalized a set of standards for Industrial IoT applications,

which require high reliability: the IPv6 over the Time Slotted Channel Hopping mode of IEEE802.15.4e (6TiSCH) Working Group. At the MAC layer, 6TiSCH uses the IEEE802.15.4e TSCH mode, which is also at the root of industrial wireless protocols such as WirelessHART and ISA100.11a. In TSCH, a node cuts time into slots. A communication schedule orchestrates all communication, indicating to each node what to do in each slot: transmit, receive or sleep. Combined with channel hopping, this leads to high end-to-end reliability, and can be used in networks with a high traffic rate. At the PHY layer, 6TiSCH only supports a single PHY for the entire network. Currently, the chosen PHY for the standard stack is IEEE802.15.4 O-QPSK at 2.4 GHz [29].

Several articles shed light on 6TiSCH evolution and state of the art. Vilajosana et al. [30] provide a detailed tutorial on the stack of protocols adopted by the IETF 6TiSCH working group. For the purpose of this thesis, we focus on the basic overview of the protocol stack for a reader without previous knowledge of 6TiSCH. An outline of the relevant 6TiSCH standards is presented in Table 2.1.

The main vision of 6TiSCH is to benefit from the industrial reliability of IEEE802.15.4e TSCH under a generic IP routing layer [31]. To achieve such integration, an adaptation layer called 6LoWPAN has been introduced to enable IP operation on over IEEE 802.15.4 PHY. Furthermore, the Minimal 6TiSCH standard RFC8180 [29] describes how neighbor advertisement and discovery should take place using the "minimal" shared cells. These advertisements are carried in 802.15.4 TSCH Enhanced Beacons (EBs) [18]. As neighbors are being discovered, the RPL routing algorithm chooses one or more neighbors to be routing parents, according to an objective function [32]–[34]. The objective function can consider one or more parameters for link cost estimations [34]. When a parent is selected, a node negotiates with its parent to add dedicated cells for uplink traffic using the 6TiSCH Operation Sublayer Protocol (6top) [35]. 6top negotiations occur via autonomous cells: each node allocates a default cell to receive negotiation requests, the index of this cell is calculated by a hashing function based on the slotframe length and the mote's MAC address [36]. After cells are allocated, the node broadcasts its routing information and the cost of the path between the node and the root (i.e. rank). These RPL broadcasts are called Destination-oriented directed acyclic graph Information Objects (DIOs). This information allows neighboring nodes to calculate the best route (according to some objective) to use for their traffic.

2.2.2 Scheduling in 6TiSCH

This section takes a closer look into the scheduling mechanisms in 6TiSCH. The 6TiSCH protocol stack [19], [31] combines the ease of use of IPv6 with the industrial performance of TSCH. A 6TiSCH schedule is a matrix of cells, each identified by its slot offset and channel offset(a cell is the combination of a location of a time-slot in the schedule and a frequency setting). There are three types of cells:

- A *dedicated* cell is negotiated between neighbor nodes. A TX cell is allocated at the source mote and an RX cell is allocated at the destination motes.

Table 2.1: An outline of the relevant standards of the 6TiSCH protocol stack.

Routing Layer (RPL)	RFC6550	2012	Main RPL Specification
	RFC6551	2012	Definitions for RPL Metrics
	RFC6552	2012	RPL default Objective Function Definition
6LoWPAN Adaptation Layer	RFC8505	2018	Describes neighbor discovery, registration, and managment policies
6TiSCH MAC Scheduling Layer	Minimal Scheduling Function draft	WIP	Describes the distributed schedule allocation
	Minimal security draft	WIP	6TiSCH Security and Constrained Join Protocol
	RFC8480	2018	6TiSCH Operation Sublayer Protocol (6top) describing how neighbors negotiate their links
	RFC8180	2017	Minimal 6TiSCH standard: detailing neighbor advertisement and discovery
	IEEE802.15.4e	2012	Standardized time-slotted channel hopping for medium access for deterministic IoT networks used in industrial applications
Physical Layer	IEEE802.15.4g	2015	An amendment to the IEEE802.15.4 standard, which introduces 31 PHYs for IoT networks in the 2.4 GHz band and the sub-GHz band
	IEEE802.15.4	2001	Standardized O-QPSK radio for IoT networks in the 2.4 GHz band

- A *broadcast* cell (also called "Minimal cell") is used for network-wide broadcast messages and network routing information. This allows a mote to synchronize to the network, discover its neighbors and the network routing details.
- Each node allocates an *autonomous* cell in its schedule where it can receive negotiation requests for cell allocations from its neighbors.

6top coordinates a mote's negotiations with its neighbors to allocate cells [35]. It further defines a default scheduling algorithm, called Minimal Scheduling Function (MSF) [36], which defines how cells are allocated for unicast or broadcast activities. 6TiSCH uses the 6LoWPAN adaptation layer [37] to transport IPv6 packets over IEEE 802.15.4e MAC layer, and the IPv6 Routing Protocol for Low-Power and Lossy Networks (RPL) [32] routing protocol. Chang et al.provided a comprehensive overview of the 6TiSCH protocol stack [10].

Schedule management can be done in a centralized or distributed manner. In a centralized approach [3], [9], a central entity manages the schedule based on a complete view of the network. In a distributed approach, nodes manage their resources locally. 6TiSCH uses the latter.

2.2.3 6TiSCH Performance Evaluation

Related research provides performance evaluation of 6TiSCH in different situations.

Yang et al. [38] evaluate the performance of the full 6TiSCH stack on the OpenWSN reference architecture in terms of responsiveness to time critical event triggers. They vary the number of active slots in a frame of length 11 slots and measure how packet end-to-end latency is affected.

Theoleyre et al. [39] evaluate the performance of the 6TiSCH stack with the deployment of traffic isolation mechanisms that allow reservation of dedicated slots for certain applications and reservation of shared slots for alarm events. They report end-to-end latency and PDR under various schedule management strategies, including using uniformly distributed shared cells instead of contiguous (adjacent) shared cells in the slot-frame.

Teles Hermeto et al. [40] execute a performance evaluation of the 6TiSCH protocol stack in an indoor environment with a focus on the stability of the stack performance. They report the end-to-end reliability and the number of parent changes as the network is converging. They also propose a stable link quality metric and a simplified method for schedule inconsistency management.

Ben Yaala et al.[41] evaluate the performance of the 6TiSCH stack in co-located networks. They consider both cases where the coexisting 6TiSCH networks are either synchronized or un-synchronized.

In all of related works listed above, the PHY used is IEEE802.15.4 O-QPSK 2.4 GHz. Sum et al. [8] use different approach: they provide an experimental evaluation of IEEE802.15.4e TSCH MAC based on IEEE802.15.4g FSK 868 MHz radio. The experiments report range and performance testing results in terms of PDR and Packet

Error Rate in four situations: Line-of-Sight conditions, Non-line-of-sight conditions, tree topology in corridor setting and line topology across buildings.

This thesis goes a step further by conducting performance evaluation of 6TiSCH on top of three different PHYs (Chapter 4). We report the end-to-end performance based on industrial KPIs [42]: network formation time, end-to-end reliability, end-to-end latency, and battery lifetime. We further propose a generalized 6TiSCH architecture (Chapter 5) where a node can use a short-range PHY to communicate with nearby neighbors and long-range PHY to communicate with neighbors further away. g6TiSCH is configured to include the following PHYs: FSK 868 MHz as low bitrate PHY, OFDM 868 MHz as high bitrate PHY, and O-QPSK 2.4 GHz as an in-between option. We compare the performance of g6TiSCH against that of a traditional 6TiSCH stack running on each of the three physical layers.

2.3 Unlicensed Band Considerations

This section details practical limitations on network performance when operating in publicly shared spectrum. When the wireless network is operating in an unlicensed band, it faces constraints by regulations or by medium scarcity. There are two main considerations to take into account related to the frequency band used: co-existence with other technologies in unlicensed band, and duty cycle limits on sub-GHz unlicensed bands.

Hermeto et al.indicated that the articles they surveyed [43]–[46] do not consider packet loss due to interference from IEEE802.11 WiFi networks [47]. Since the IEEE802.15.4 PHY operates using O-QPSK 2.4 GHz, it has classically suffered interference from co-existing Wi-Fi networks. Musaloiu et al.showed how IEEE802.15.4 networks exhibit packet losses ranging 22–58% when WiFi networks are operating in the same area [48]. Gonga et al.showed that up to 95% of the links in a IEEE802.15.4 channel hopping network can suffer independent packet losses due to WiFi interference [49].

Furthermore, Liu et al. [50] proposed an IIoT architecture that integrates satellite IIoT with ground cellular IIoT to extend coverage in satellite-blocked areas. This integration leads to co-channel interference from both networks operating on the same frequencies. The authors therefore propose a mechanism to optimize the satellite power resource allocation to mitigate the interference and guarantee a QoS level.

In Europe, ETSI is the regulatory body which governs frequency bands. Section 7.2.3 of ETSI 300-220 [51] limits the transmit duty cycle (the portion of the time a radio is actively transmitting) in the 868 MHz band between 0.1% and 1% depending on the sub-band. Similar regulation is in place in the U.S. (under the guidance of the FCC) and other parts of the world. Such regulations must be taken into account by scheduling policy using these frequencies.

g6TiSCH proposed in Chapter 5 uses both the 2.4 GHz and sub-GHz bands. By increasing the available frequency resources, it reduces the probability of interference from co-existing networks. Furthermore, it reduces the impact of the duty-cycle regulation by splitting the amount of traffic between the two bands.

2.4 TSCH Schedule Compactness

This section presents articles that focused on improving TSCH schedule compactness. Schedule compactness can be defined as "[the maximization of] the number of channel offsets and timeslots not used by any transmitter" [47]. A schedule that is compact allows to accept new flows as there is enough space available to allocate more bandwidth. This permits the improvement of end-to-end throughput by allocating more slots and by increasing the number of available channels for hopping, which increases link robustness [52], [53].

Hermeto et al.focus on scheduling in IEEE802.15.4-TSCH industrial networks, surveying both centralized and distributed approaches [47]. They indicate that research on improving schedule compactness has been done exclusively for centralized networks.

Palattella et al.propose the Traffic Aware Scheduling Algorithm (TASA) for schedule optimization [43]. TASA relies on a central manager to reserve slots as early as possible in the schedule. It relies on minimizing the maximum offset of used slots in the schedule. The authors port TASA to the 6TiSCH architecture in combination with the IEEE802.15.4e MAC, and provide a simulation of its performance [44]. They show that TASA-based IEEE802.15.4e MAC shows 80% improvement in the power efficiency compared to the legacy IEEE802.15.4 MAC.

Soua et al.propose MODESA, a centralized slot allocation algorithm which relies on a root node having multiple radio interfaces [45]. MODESA reduces the slotframe length by optimizing slot and channel allocation across a tree-topology network. The authors provide a linear programming model that runs on the central controller and optimizes slot and channel assignment. They show how this approach reduces slotframe length by 13% in a 100-node network.

The related work surveyed in this section is based on a centralized controller, and it all assumes the same PHY is used across the network (hence, a uniform slot duration). This thesis proposes 6DYN (Chapter 6), a distributed mechanism for increasing schedule compactness, combined with a multi-PHY approach and heterogeneous slot durations. 6DYN allows nodes to allocate shorter slots for faster transmissions and longer slots when necessary for slower transmissions. This allows for better packing of the schedule, which reduces latency and increases network capacity.

2.5 IETF RPL Protocol

Another IETF working group is the Routing Over Low power and Lossy networks (ROLL) group focused on the routing layer in IoT applications. The group standardized RPL, the IPv6 Routing Protocol for LLNs [32]. An LLN can be defined as different name for IoT low-power wireless mesh networks. This section presents previous work related to routing with RPL. We present the work in two sections. Section 2.5.1 gives the a background on the RPL standard and related RFCs. Section 2.5.2 introduces related work on RPL Objective Functions (OFs) that intersect with this work.

2.5.1 RPL Standardization

RPL was first standardized in 2012 as a proactive, distance-vector, distributed algorithm, aligned on Destination Oriented DAGs rooted at the internet border routers [32]. It was extended later with options to do point-to-point proactive routing, and to do reactive routing. It is currently being extended to enable centralized routing.

RPL provides an elaborate framework with a wide range of features that allow it to address simple as well as complex use cases. A key advantage of RPL is that it is a distributed protocol: decisions are taken independently by each node. This way, it minimizes the risk of having a single point of failure, which occurs when the network is using a centralized controller (i.e. Path Computation Element). It also reduces the network control overhead as nodes do not send all their state information to the controller. The core routing decision in RPL is taken by the OF which evaluates each available path according to "an objective", and decides which path best meets that objective. There are currently two IETF-adopted OFs that aim to improve latency and energy by choosing paths with the least possible number of hops or transmissions.

The Root advertises metrics [33] that are used by intermediate nodes to select routes according to the OF. Standardized OFs include route selection by hop-count (called OF0 [34]) or by minimum end-to-end ETX with hysteresis (called MRHOF [54]). The network DODAG is guaranteed to be acyclic (in steady state) by having each node assign itself and advertise a rank that is strictly monotonic along any path to the Root. In addition to defining how routes are selected, the OF also specifies how the rank is calculated. The RPL protocol is extensible with other objective functions, yet to be defined. The currently defined metrics include node metrics such as: node remaining energy, node workload, or hop-count. Link metrics are also defined such as: link throughput, latency, reliability, or link color.

Metrics are shared in the network via Destination Information Object (DIO) multicasts among router nodes. DIOs contain DAG Metric Containers (DMCs) which describe the utilized metrics and how they are shared in the network. We note two particular control points in the routing metric flag field that define how metrics are shared (which will be referred to later in the Chapter 7).

- "`R-Flag`": if set, the metric is recorded by separate entry for each node along the path. Otherwise, the metric is aggregated along the path in one entry.
- "`A-Field`": in case an aggregate metric is defined (i.e. `R-Flag` set to 0). It allows choosing the mode of aggregation: additive, minimum, maximum, or multiplicative.

This way, metrics can be combined in different ways to optimize the routing topology for different use cases.

2.5.2 OFs for a Hybrid RPL Topology

The main RPL standard RFC6550 [32] does not specify an OF for a RPL implementation. Specification of the OF is left to the architects of each network since the criteria of

optimization can vary by use case. Some applications using alarms may prioritize delay over energy savings. Other applications for utility metering in remote areas may prioritize energy saving over delay.

Extensions to the standard have proposed OFs that can serve as reference points for RPL implementations. RFC6552 [34] introduces OF0 which serves as a minimal OF that can allow basic interoperation of RPL implementations in simple use cases. It uses the hop-count as an additive aggregate metric along the path. This way, nodes closer to the root in the routing tree will be favored, irrespective of the link quality.

RFC6719 [54] introduces the Minimum Rank with Hysteresis Objective Function (MRHOF). It goes one step further than OF0 by expressing the link quality across the path using Expected Transmission Count (ETX) as a path metric. This way, it can be sensitive to temporary fluctuations in link quality across the path due to interference or multi-path fading. For instance, a link between a node and the root can suffer temporary interference that leads to degrading the link quality from 99% down to 75% PDR. The node may choose an alternative route through a neighbor where each hop has 95% PDR. In this case, 2-hop route has a higher PDR (90%) than the one hop route. When the interference ends, the node can return to the one-hop route of 99% PDR.

Ben Saad et al. [55] propose a heterogeneous infrastructure for IPv6 using a combination of diverse PHYs: PLC interface, Sub-GHz radio at 250 kbps, and 2.4 GHz radio at 250 kbps. The authors propose an infrastructure where PLC-RF routers are introduced to improve lifetime of an RF network. They emulate a testbed of 25 motes in a 50×50 m^2 area, with a fixed RF range of 10 m and placed in a grid topology. They place mains-powered RF-PLC routers in optimal points and show how it leads to improvement of network lifetime.

Lemercier et al. [56], [57] address the challenge of routing when each node is equipped with heterogeneous interfaces, namely IEEE 802.15.4g RF and PLC. The authors compare three approaches for multi-PHY routing in RPL: *(1)* a multi-instance RPL where RPL maintains a separate DODAG per each PHY, *(2)* a parent-oriented design where switching between PHYs is more favorable for interfaces of the same neighbor node, and *(3)* an interface-oriented design where each combination of node/interface is considered as an independent neighbor. The objective of the study is to arrive at a solution that yields the best network reliability in case of interface failure. This is expressed as the number of parent changes and degree of connectivity of the resulting topologies. The authors propose an OF that aims at optimizing the link quality and expected transmission time. They show that the parent-oriented design yields network with the best reliability performance in terms of number of parent-changes and link quality in the DODAG.

Iova et al. [58] propose an OF for RPL that optimizes for network lifetime (i.e. the time until the first battery depletion of a node in the network). They propose that the routing algorithm avoids nodes that appear as energy bottlenecks. They also propose to use multi-parent routing to balance the load across the network. Their OF defines expected lifetime node metric that is based on: node energy consumption, remaining battery energy, ETX, and estimated node traffic rate. They simulate the performance

of the proposed multi-path routing technique in a single-PHY topologies of 30–90 nodes in a 300×300 m^2. They show that the hybrid OF with probabilistic multi-path routing is able to improve network lifetime by several orders of magnitude (depending on the network's density) compared to MRHOF.

The related work presented in this section demonstrates significant advances in adapting RPL for multi-PHY integration or network lifetime. Both OF0 and MRHOF offer a basic PHY-agnostic routing approach that leaves room for improvement in the case of multi-PHY networks or specialized use cases. Ben Saad et al. [55] demonstrate how introducing heterogeneous mains-powered routers can improve network lifetime. This confirms out intuition about the benefit of having heterogeneous network for improving lifetime. Lemercier et al. [56], [57] demonstrate that having a heterogeneous network with mix of wired/wireless interfaces can improve network reliability and stability.

My work goes a step further by demonstrating in Chapter 7 how heterogeneous nodes that are fully wireless and fully battery-powered can improve network lifetime by integrating a mix of long-range and short-range PHYs. Iova et al. [58] demonstrate the benefit of optimizing for a node's estimated lifetime to yield an energy balanced network with improved lifetime. This confirms the intuition behind using combined metrics for network lifetime optimization and how that path diversity can allow improving the network lifetime. This thesis designs in Chapter 7 an OF that makes use of heterogeneous PHYs to improve the network lifetime and how the characteristics of each PHY can be taken into account by the routing layer. Finally, this work simulates the resulting networks in a setting of 100 nodes in 2×2 km^2. This is to demonstrate the potential impact of this function in wide area coverage.

2.6 Multi-PHY Integration

This section presents recent related work that uses hybrid PHYs in an integrated network.

The study by Brachmann et al. [59] demonstrates enabling multi-PHY capability in the 6TiSCH stack. The authors run link performance testing campaigns using multiple PHYs: 2-GFSK (at 1.2 kbps, 8 kbps, 50 kbps, 250 kbps), 4-GFSK (at 1000 kbps), O-QPSK 2.4 GHz (at 250 kbps). The authors choose two PHYs in the sub-GHz band for integration in the 6TiSCH MAC layer: 2-GFSK at 1.2 kbps for transmitting Enhanced Beacons (EB), 4-GFSK at 1000 kbps for data traffic. The slot templates for the PHY layers are defined in accordance with the IEEE802.15.4 standard, and used in Contiki-NG. They demonstrate that the faster bit-rate of 4-GFSK at 1000 kbps for data packets reduces the collision probability and leads to less than 0.1% channel utilization despite the higher re-transmission rate. Furthermore, the slower bit-rate of 2-GFSK at 1.2 kbps leads to higher channel occupancy, at 2% duty cycle.

The proposal by Van Leemput et al. [60] is the state-of-the-art in multi-PHY integration in TSCH networking. The authors propose using slower PHYs for unicast links in case the RSSI is persistently below a certain threshold. PHY switching occurs at the MAC layer by continuously assessing the link's RSSI, using an Exponentially Moving Average filter. The timeslot is long enough for a single packet when using a low bit-rate

radio, or multiple back-to-back packets when using a high bit-rate radio. The authors demonstrate that a link's throughput can be increased by 153 % with only 84 % power consumption. This is achieved by using single acknowledgment for multiple packets in the same slot.

Garrido-Hidalgo et al. [61] develop a body-area network (BAN) using BLE mesh in the 2.4 GHz band. The mesh connects BLE wrist-bands worn by factory workers along with BLE-based machine sensors. The devices capture data relevant for safety in a real industrial setting. Collected data is forwarded to a BLE gateway which has a LoRaWAN interface that relays the data over long-range PHY in the sub-GHz band to a LoRaWAN gateway connected to the cloud.

Al-Saadi et al. [62] propose a hybrid network architecture integrating Long Term Evolution (LTE) "eNodeB" base stations with a WiFi mesh based on an IEEE802.11 stack. The architecture enables relaying traffic among nodes with multiple interfaces: LTE, WiFi, and Ethernet. This enables the utilization of unlicensed band of WiFi to improve LTE coverage via WiFi mesh networks, without having to buy more of the licensed spectrum of LTE. The authors make use of the multi-rate feature of WiFi to combat interference and use a re-enforcement learning algorithm that determines for each node which technology to use for forwarding. They use simulations to demonstrate that the overall network throughput is increased.

These papers provide insightful performance evaluation of three kinds of multi-PHY networks.

First, Brachmann et al. [59] integrate two PHYs under one protocol stack; however, only one PHY is used as a default setting for data packets. Our proposed g6TiSCH architecture (Chapter 5) introduces a fully generalized stack where nodes can use hybrid PHYs for different neighbors for data transmission or reception and a node can switch its PHY dynamically depending on the neighbor.

Second, the architecture proposed by Van Leemput et al. [60] also integrates two sub-GHz PHYs under one protocol stack; however, the link switching mechanism occurs at the MAC layer. The authors show significant throughput improvement and energy savings using their multi-PHY architecture at the MAC layer. This confirms the intuition behind using multiple PHYs in the same TSCH-network. g6TiSCH goes a step further by allowing the integration of any number of (multi-band) PHYs. g6TiSCH also allows exposing the different costs associated with each PHY to the routing layer. The latter becomes aware of such costs and can improve the network energy footprint by selecting less costly PHYs when possible. This way, the routing layer cooperates with the lower layers. Furthermore, they demonstrate how the PHY-switching mechanism adapts the used PHY in case of switching to another PHY *of the same parent node.* g6TiSCH goes a step further by proposing a PHY-switching mechanism that is demonstrated in case of switching to a PHY of the same parent node or of a different parent node, since both cases are treated the same way. We further demonstrate the end-to-end performance of the resulting architecture for a holistic performance evaluation and we compare it to single-PHY architectures.

Third, Garrido-Hidalgo et al. [61] integrate two full stack networks side-by-side:

LoRaWAN and BLE mesh to benefit from long-range and short-range PHYs. Since the g6TiSCH architecture proposed in this paper allows for the co-existence of multiple PHYs under one protocol stack, it allows less network management overhead and easier integration than multiple independent full-stacks.

Finally, Al-Saadi et al.propose running WiFi and LTE side-by-side on relay nodes. My thesis goes a step further by introducing a unified multi-PHY protocol stack and providing experimental evaluation of its performance.

2.7 Summary and Contributions

This section describes related work on both research and standardization fronts. We demonstrate the potential of multi-PHY integration and we provide an overview of the 6TiSCH protocol stack and its related work that we later extend with multi-PHY capabilities. We further present how multi-PHY integration can help in relaxing MAC constraints in the unlicensed band. We then show that TSCH schedule compactness is currently addressed only in the context of centralized single-PHY network, which leaves room for contribution in the context of a distributed multi-PHY network. We give an overview of RPL and related RPL OFs that address either improving network lifetime or improving network stability in hybrid RF-PLC networks. This leaves room for contribution with an OF that improves network lifetime by use of multi-PHY network. Finally, we highlight the state of the art in multi-PHY industrial networks which shows the growing intuition in the research community for the potential benefits of multi-PHY integration.

My works builds upon this related work, and bring the following key contributions:

1. Instead of trying to find the best PHY from those surveyed in Section 2.1, we argue for a "no free lunch" principle: that no single PHY can offer best performance across all end-to-end network KPIs. This is developed in Chapter 4.

2. We generalize the 6TiSCH architecture (surveyed in Section 2.2): we demonstrate how a set of short-range and long-range radios can be integrated under one generalized 6TiSCH architecture and we evaluate its performance experimentally in a testbed of 36 motes at Inria-Paris. This is developed in Chapter 5.

3. While related work in Section 2.4 improves schedule compactness in centralized single-PHY networks, we demonstrate in Chapter 6 how to enable compact scheduling in a TSCH slot-frame in a decentralized multi-PHY network. The schedule can adapt slot-duration on a slot-by-slot basis depending on the bit-rate of the used PHY ("6DYN") and we show how this can help mitigate the unlicensed band limitations surveyed in Section 2.3.

4. We extend RPL based on the work in Section 2.5 and we demonstrate, using simulation, a RPL OF that optimizes for network lifetime ("Life-OF"). We show how it combines diverse PHYs to boost network lifetime using multi-PHY networking.

Chapter 3

Methodology

Key Takeaways: This chapter surveys the methodology followed for conducting the experiments in this thesis. We employ three different setups to investigate the different research questions addressed.

- Section 3.1 details the OpenTestbed [63], a set of nodes deployed across an office building. We use the OpenTestbed to test end-to-end network performance. The OpenTestbed is used in Chapters 4 and 5.
- Section 3.2 describes a lab-bench setup of 4 motes connected to lab equipment. This allows us to get an in-depth look into the real-time performance of the protocol stack using hardware probes. This setup is used in Chapter 6.
- Section 3.3 presents RPLSim, a RPL simulator that we built to examine the performance of the proposed OF for multi-PHY routing. The RPLSim is used in Chapter 7.

3.1 OpenTestbed

We are interested in the end-to-end performance of the 6TiSCH protocol stack (Chapter 4) as well as the g6TiSCH stack (Chapter 5) at in a realistic setting. For this reason, we use the OpenTestbed which is a real deployment in Inria Paris, which is a typical indoor office building setting. We outline the physical setup of the OpenTestbed in Section 3.1.1. We describe the methodology for experiment and measurement collection in Section 3.1.2.

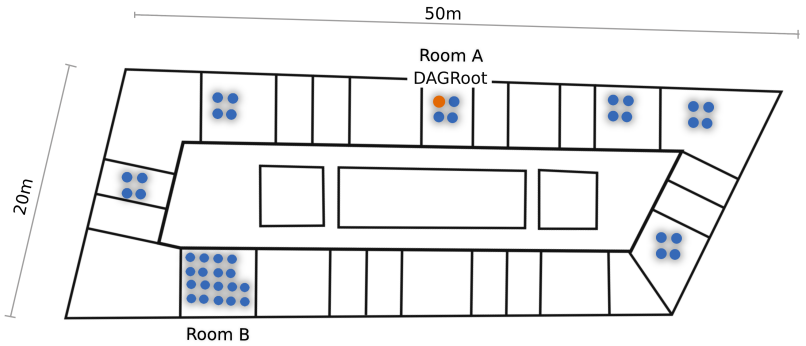

Figure 3.1: Locations of the 42 motes of the OpenTestbed across an office floor at Inria-Paris.

Table 3.1: Characteristics of the selected PHYs.

	FSK 868 MHz	**OFDM 868 MHz**	**O-QPSK 2.4 GHz**
Radio chip	AT86RF215	AT86RF215	CC2538
Data rate	50 kbps	800 kbps	250 kbps
Output power	+14.5 dBm	+10.0 dBm	+7.0 dBm
Sensitivity	-114 dBm	-104 dBm	-97 dBm
Link budget	128.5 dB	114.0 dB	104.0 dB
Channel Spacing*	0.2 MHz	1.2 MHz	2 MHz

(*) The number of channels varies by regional regulations of each band. We consider the European 863-870 MHz band. A full list of available license-free bands is provided in the IEEE 802.15.4g amendment [26].

3.1.1 Setup

The OpenTestbed is composed of 42 OpenMote B boards deployed across an office floor at the Inria research center in Paris in groups of 4 (see floorplan on Fig. 3.1). The distribution of the motes happens in clusters of 4–18 motes, mimicking nodes clustered around machines in an industrial setting [1]. The OpenTestbed is built from off-the-shelf components, networked together using the building's 5 GHz Wi-Fi network (i.e. no dedicated Ethernet network), without requiring back-end servers, and with an open access interface. Interaction with the OpenTestbed is done entirely over the MQTT protocol. The Raspberry Pi single-board computers to which the OpenMote B boards are attached implement a number of commands to reprogram and reset the boards. During an experiment, one can interact (read/write) with the serial port of each OpenMote B board, in real-time, using MQTT messages.

As shown in Fig. 3.2, the OpenMote B is an IoT platform which features both a CC2538 (a micro-controller and O-QPSK 2.4 GHz radio) and an AT86RF215 (an

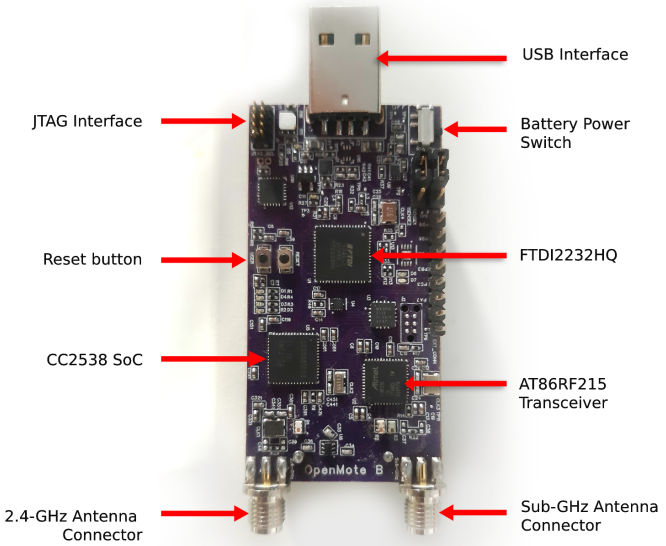

(a) The OpenMote B

(b) the OpenTestbox, part of the OpenTestbed

Figure 3.2: Components of the OpenTestbed.

FSK 868 MHz and OFDM 868 MHz radio) [64]. There are two antennas: a 2.4 GHz antenna connected to the CC2538, a sub-GHz antenna connected to the AT86RF215. Table 3.1 lists the main characteristics of the PHY layers tested; TX power and sensitivity number are taken for the chip used. The ARM Cortex-M3 on the CC2538 features 32 kB of RAM and 512 kB of flash. The OpenWSN firmware is loaded onto that micro-controller; that firmware then interacts with the CC2538's radio directly using the registers, and with the AT86RF215 over SPI. We use a combination of JTAG in-circuit debugging and a logic analyzer to verify the code.

3.1.2 Methodology

We run the OpenWSN network once with 6TiSCH for each of the three PHYs (Chapter 4) and for the g6TiSCH architectures (Chapter 5). During the experiments, the floor is mostly unoccupied, so we do not expect WiFi interference beyond the regular 100 ms beaconing interval of the 8 WiFi access points on that floor [5]. Each time, we load the firmware onto the testbed, then switch on the OpenVisualizer software, which connects to all motes over their serial port (over MQTT). In the OpenVisualizer, we then select the mote that we want to play the role of DAG root. We always select the same mote, shown in Fig. 3.1, which is positioned at the center of the floor in room A. We then let the network run for 90 min, recording all the data generated by the motes. The OpenVisualizer shows a live view of the routing topology in the network. We adapted

this live view to show the multi-PHY routing topology as shown in Fig. 3.3 (further details in Chapter 5).

We developed a custom application which runs at the application layer of each mote. That application sends a data packet every minute containing the following fields:

- a counter, which we use to detect lost data packets,
- the time at which the data packet is generated (ASN),
- the DAG rank of the sender,
- the size of the neighbor table of the sender,
- T_{on}, how long the sender's radio has been on since the previous data packet transmission,
- T_{TX}, how long the sender's radio has been on and transmitting since the previous data packet transmission,
- T_{total}, the amount of time since the previous data packet transmission,
- the maximum and minimum number of packets in the packet buffer since the previous packet.

After the experiment is done, we use that information to compute the following KPIs (recommended by Reference [42]):

- Network Formation Time: how much time elapses between the moment the root is selected and that root has received at least one packet from *each* mote.
- End-to-End Reliability: what portion of all packet generated in the network are received by the root.
- End-to-End latency: how much time elapses between the generation of the packet at the sender, and reception at the root.
- Radio duty cycle: what portion of the time a node's radio is on; a good indication for its power consumption.

We display the results in three forms:

- Time series. We show the mean and the inter-quartile range of the KPI, with a 3 min sliding window and a 1 s time resolution.
- Cumulative Distribution Function (CDF). We show the cumulative distribution of all data samples at steady state (starting 30 min into the experiment), using 100 bins. This allows for efficiently visualizing key performance indicators such as outages.

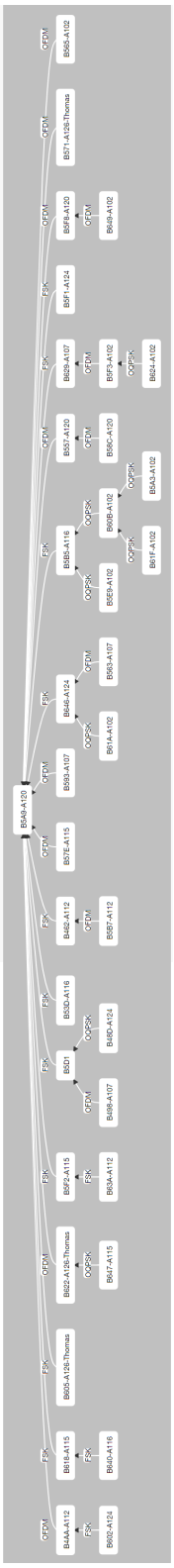

Figure 3.3: Live view from the OpenVisualizer is adapted to show the multi-PHY routing topology in the network.

- Probability Distribution Function (PDF). We show the probability distribution of all data samples at steady state using 100 bins. This allows for a more detailed assessment of the distribution of each data set.

We developed a data logging and processing tool for the OpenTestbed known as the KPI monitor (Chapter 9). The tool allows logging bulk measurements by experiment ID in distributed JSON files. This allows post-experiment analytics. Doing so allow you to extract new insights or KPIs without re-running experiments. For instance, plots can be reproduced by modifying the width or the time resolution of the sliding window. Similarly, CDFs and PDFs can be reproduced for the whole or a portion of the experiment dataset.

3.2 Local Experiment Setup

We are interested to show the real-time performance of 6DYN, 6TiSCH with heterogeneous slot-frames. For this purpose, we create a lab-bench experimental setup with 4 nodes connected to lab equipment, to inspect the real-time performance of the MAC layer. OpenMote B (Fig. 3.2a) is used as the development platform. A logic analyzer is used to capture the event-triggers from the different MAC layer components at real-time. We use a JTAG interface for in-circuit debugging and the IAR Embedded Workbench as the Integrated Development Environment.

The OpenMote B routes six general purpose input/output pins from the CC2538 to extension headers. We use those to follow the execution of the firmware using the logic analyzer. This setup is outlined in Fig. 3.4. We instrument the firmware to toggle the following pins:

- The `slot` pin is toggled at the start of each timeslot.
- The `radio` is set high when the radio is on, either in transmit or receive mode.
- The `fsm` pin toggles at each transition of the Finite State Machine of the implementation of the TSCH MAC layer. This pin allows us to identify transmit and receive slots and the timing inside the slot, defined in the timeslot template (see Section 4.3).

Fig. 3.5 shows the resulting real-time capture of MAC-layer events on both nodes during a ping session from the root to the node. This setup is expanded to four nodes as illustrated in Fig. 3.6 to enable capturing the real-time multi-hop/multi-PHY performance of 6DYN. The output of this setup is shown in Fig. 6.5 and the content details will be explained in Chapter 6.

3.3 RPLSim

We are interested in measuring the impact of the used RPL OF on network lifetime and latency. For this purpose, we have developed a high level RPL discrete-time simulator

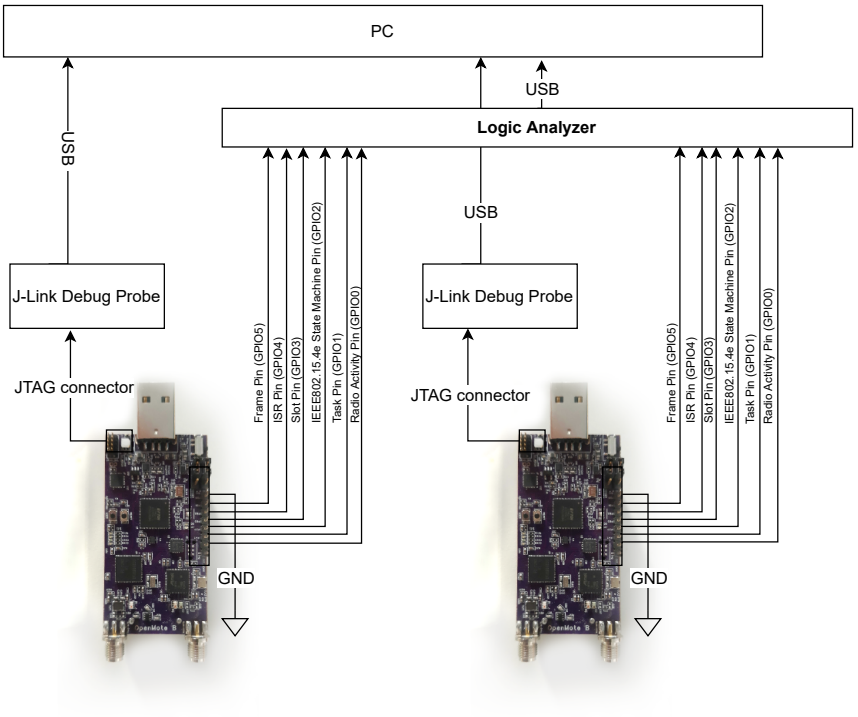

Figure 3.4: Full connection of two motes using logic analyzer and J-link debug probes.

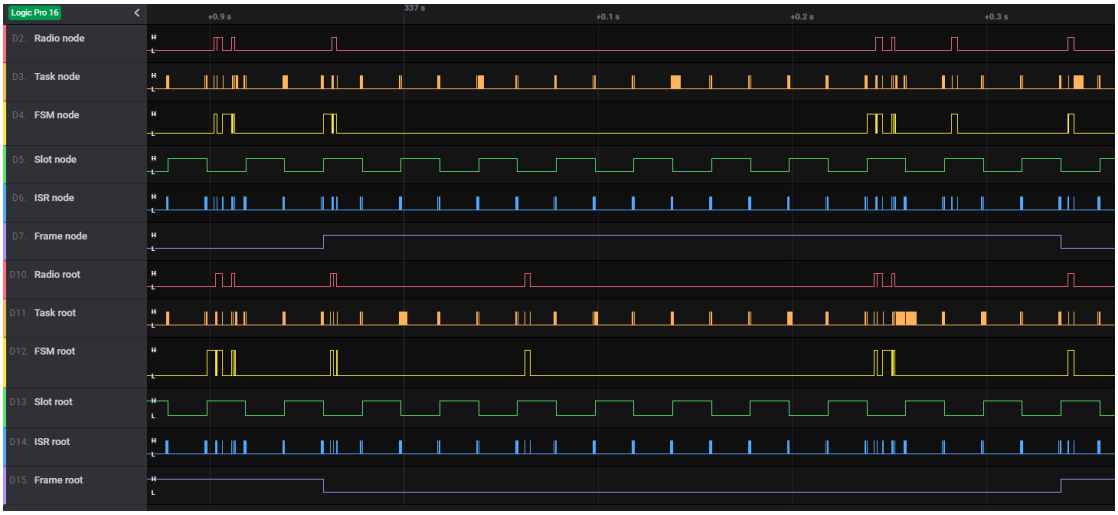

Figure 3.5: Resulting logic analyzer capture of firmware events on two nodes during a ping session from root to node using 6TiSCH.

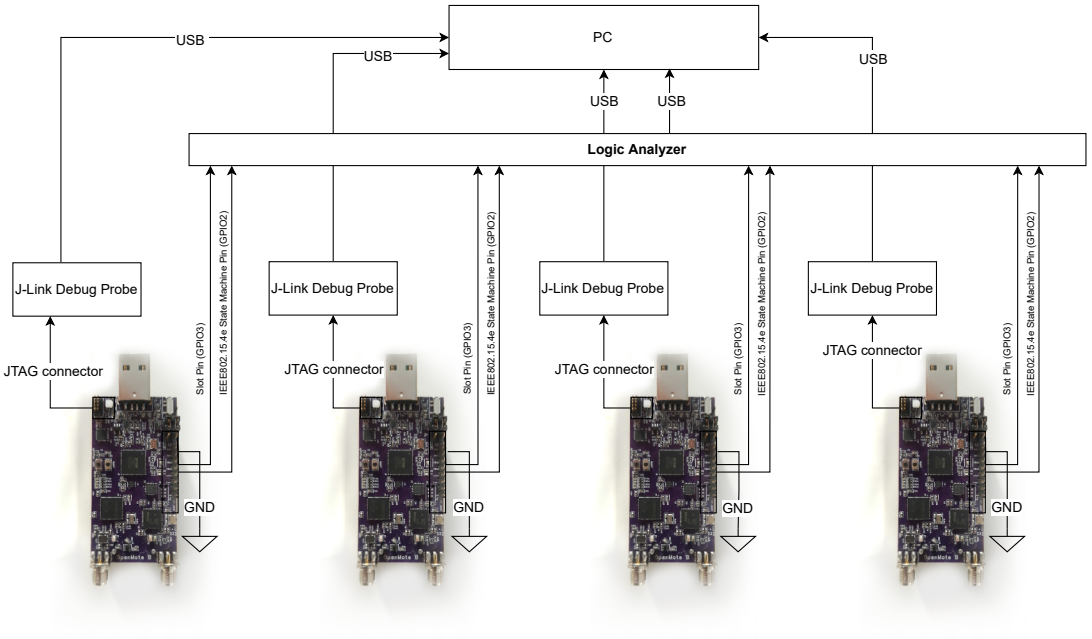

Figure 3.6: Connectivity of four motes to capture multi-hop performance of 6DYN.

Table 3.2: Power consumption of the simulated PHYs

	FSK 868 MHz	**OFDM 868 MHz**	**O-QPSK 2.4 GHz**
Radio chip	AT86RF215	AT86RF215	CC2538
Data rate	50 kbps	800 kbps	250 kbps
I_{TX}	62 mA	62 mA	24 mA
I_{RX}	28 mA	28 mA	20 mA
Supply voltage	2.5 V	2.5 V	3.0 V

with focus on the performance of the routing algorithm, irrespective of the dynamics of the used MAC layer. This section introduces the architecture of the RPL simulator ("RPLSim") in Section 3.3.1. We provide an overview of the simulation methodology in Section 3.3.2.

3.3.1 Architecture

RPLSim mimics the behavior of RPL in a multi-PHY setting. For the propagation loss model, we use the Pister-Hack trace-based propagation loss model recently utilized in other simulators [65]–[67]. The model is tuned for the sub-GHz PHYs to match the traces obtained from the range tests by Muñoz et al. [4]. Links are assumed to be asymmetrical as observed in [4], [59]. RPLSim allows simulating RPL topology convergence in a distributed network where nodes are equipped with multi-PHY interfaces with diverse

Table 3.3: RPL configuration used for MRHOF and Life-OF

	MRHOF	Life-OF
HYSTERISIS	512	0.01
DAGMAXRANKINCREASE	768	0.05
MINHOPRANKINCREASE	256	1
MAX_RANK	65535	-50

bit-rates, power-consumption, and link qualities. We refer to the power characteristics of the AT86RF215 radio chip by Atmel for the Sub-GHz PHYs and the CC2538 radio chip by Texas Instruments for the 2.4 GHz PHY (as used in previous research [68]–[70]). These characteristics are outlined in Table 3.2. Furthermore, RPLSim estimates the power consumption of each node depending on its load and the link quality with each neighbor. This follows the same process for duty cycle estimation as Iova et al. [58]. We extend it to use different power characteristics and bit-rate for each neighbor depending on the used PHY. This allows to mimic the battery discharge for each node at discrete-time epochs. This way, we are able to observe how Life-OF adapts the routing topology at each epoch to optimize for the network's lifetime.

Fig. 3.7 depicts a high level flowchart of RPLSim. At the beginning of a run, a random 2-dimensional topology is generated with specified number of nodes and area side length. After a topology is generated, the routing algorithm is run on nodes in the network in a random order until each node converges on a selected parent. Then the simulator estimates the up-link traffic of each mote based on how many nodes use it as a router (directly or indirectly), the bit-rate of the PHY of each neighbor, and ETX of each link. We assume a periodic traffic pattern where a node generates 4 frames per minute of 127 bytes each. Nodes are assumed to be equipped with 2 AA batteries with total of 8.2 Wh energy. Then RPLSim mimics the decrease in battery capacities of each node until the next epoch. If all nodes are still alive, RPL is executed again on each node, and so forth. When at least one mote depletes all its battery, the simulation marks the end of the network lifetime. The discrete time resolution has been set as follows. The duration between epochs has been set to 6 months. Each two epochs, a small resolution epoch of 5 min is inserted to mimic network refresh.

3.3.2 Methodology

We compare the performance of Life-OF and MRHOF (previously presented in Section 2.5) in the same generated topologies. MRHOF is implemented based on its default configuration outlined in published RFCs [29], [54]. The definitions used for the RPL constants for each OF are listed in Table 3.3.

To compare both OFs, we run four simulation scenarios: we configure RPL with each OF in a single-PHY network and in a multi-PHY network. We choose FSK 868 MHz for single-PHY networks since we are interested in coverage for long range settings. Since FSK 868 MHz has the longest range among the three PHYs, it is guaranteed to

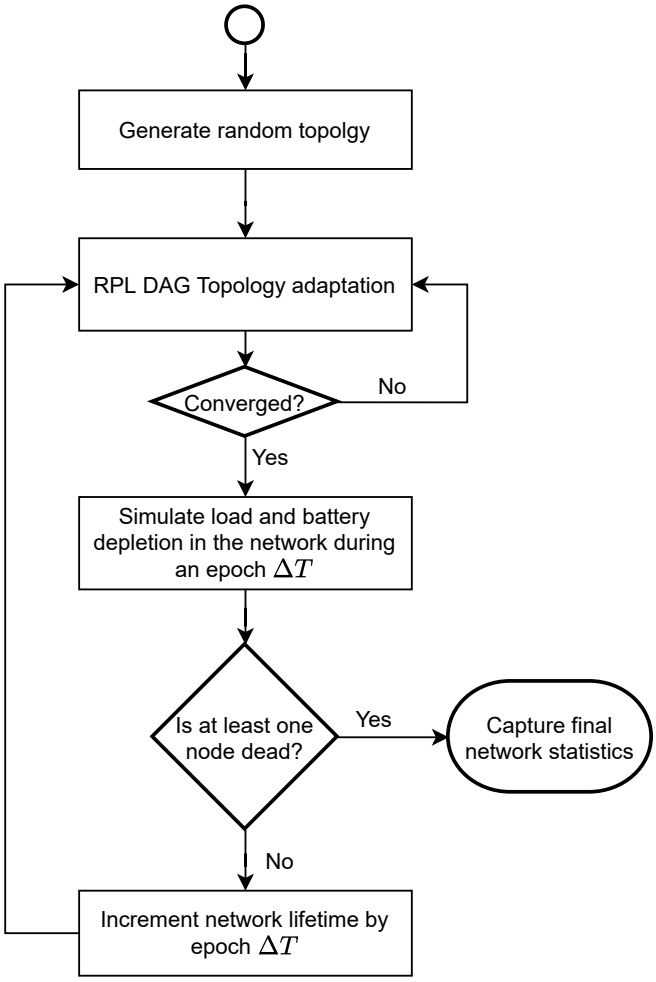

Figure 3.7: High level flow chart of RPLSim

provide the same coverage range as a multi-PHY network. This allows to have a fair comparison between both OFs since the resulting networks will cover the same territory. Each scenario is run 50 times with random topologies generated in each run. We use a topology configuration with the area size of 2×2 km^2, mimicking a typical industrial plant. We use a network size of 100 nodes which is an average size of an industrial network according to the IETF-defined use cases [71].

At the end of each run, two KPIs are captured: network lifetime and network ETX. Network lifetime is calculated based on the simulated duration until the first node depleted all its battery energy. This KPI is essential to estimate a real cost of operating the network in many industrial use cases. Network ETX is calculated for each node by summing the ETX of each link on the path from that node to the root. This KPI reflects the end-to-end latency which is necessary to observe how each OF impacts the upper bounds of latency in the network.

To report the results across runs for each KPI, we plot a statistical description of the distribution of measurements using box plots. Box boundaries represent the first and third quartiles of the distribution. A red horizontal line represents the median. Individual outliers are plotted as individual data point.

3.4 Summary

This chapter presents three experimental setups used for the research conducted in this thesis. First, the OpenTesbed, which consists of 42 nodes deployed across an office building, is used for network-wide evaluation of the protocol stack performance. We use the OpenTestbed in Chapters 4 and 5. Second, a local experimental setup for real-time performance demonstration using hardware probes, which we use in Chapter 6. Finally, RPLSim, a RPL simulator for high-level performance evaluation of RPL OFs, which we use in Chapter 7.

Chapter 4

6TiSCH Performance Evaluation using Different PHYs

Parts of this chapter were published as part of the following article: *No Free Lunch—Characterizing the Performance of 6TiSCH When Using Different Physical Layers*. Mina Rady, Quentin Lampin, Dominique Barthel, Thomas Watteyne. **MDPI Sensors**, vol. 20, no. 17, p. 4989, September **2020**.

Key Takeaways: Low-power wireless applications require different trade-off points between latency, reliability, data rate and power consumption. Given such a set of constraints, which physical layer should we be using? In this chapter, we study this question in the context of 6TiSCH, a state-of-the-art protocol stack developed for harsh industrial applications and recently standardized. Specifically, we augment OpenWSN, the reference 6TiSCH open-source implementation, to support one of three physical layers from the IEEE802.15.4g standard: FSK 868 MHz which offers long range, OFDM 868 MHz which offers high data rate, and O-QPSK 2.4 GHz which offers more balanced performance. We run the resulting firmware on the 42-mote OpenTestbed deployed in an office environment, once for each physical layer. Performance results show that, indeed, no physical layer outperforms the other for all metrics. The long range FSK 868 MHz radio yields the fastest network formation and lowest latency at the expense of battery lifetime. The short range O-QPSK 2.4 GHz radio yields the best network lifetime at the expense of latency, reliability, and network formation time. This chapter argues for combining the physical layers, rather than choosing one, in a generalized 6TiSCH architecture in which technology-agile radio chips (of which there are now many) are driven by a protocol stack which chooses the most appropriate physical layer on a link-by-link basis.

4.1 Introduction

The goal of this chapter is to provide a base for the vision of a generalized 6TiSCH protocol stack by comparing the performance of a 6TiSCH network for different PHY layers. Here, we try to address the question: *does multi-PHY integration make sense?* This is a necessary first step towards dynamically changing the PHY layer, the object of the thesis. Specifically, we augment the OpenWSN reference 6TiSCH implementation to support the following three PHYs: O-QPSK 2.4 GHz at 250 kbps, FSK 868 MHz option 1 at 50 kbps, OFDM 868 MHz option 1 Modulation and Coding Scheme (MCS) 3 at 800 kbps. The literature indicates that these three PHYs cover the range of possibilities of IEEE802.15.4g: very high data rate with OFDM 868 MHz, very long range with FSK 868 MHz, O-QPSK 2.4 GHz being a balance between range and data rate [16], [59], [72]. We then conduct a comprehensive experimental campaign, using the OpenTestbed which was introduced in Section 3.1. We compare the performance of the network in terms of network formation time, battery lifetime, end-to-end latency and end-to-end reliability.

The remainder of this chapter is organized as follows. Section 4.2 states the problems and lists the contributions of this chapter. Section 4.3 introduces the agile extension to the OpenWSN PHY-layer that enabled this research. Section 4.4 demonstrates the experiment results and KPI evaluations. Finally, Section 4.5 provides insights and conclusions based on the results.

4.2 Problem Statement and Contributions

While active research proposed various enhancements in 6TiSCH for achieving wire-like reliability and low power consumption, one common assumption is that it uses the IEEE802.15.4 O-QPSK at 2.4 GHz, as concluded in Section 2.2. While O-QPSK 2.4 GHz is appropriate for many applications, the increasing demand for long range (including for environmental monitoring and automated meter reading) has triggered the standardization of longer range PHYs [4]. A problem statement has been proposed within the IETF detailing the theoretical challenges or side-effects of augmenting 6TiSCH to include different PHYs [72]. Using a different PHY will cause the network to behave differently, leading to different overall performance. For example, a different energy consumption and link cost changes how links to neighbors are evaluated at the link-layer, hence which multi-hop paths are picked by the routing protocol. A different PHY also impacts the number of re-transmissions, the level of interference and the amount of contention in shared cells [73]. Changing the PHY layer triggers subtle changes in the behavior of the protocol stack, resulting in different performance. We believe measuring this difference is best done through a real-world system level evaluation [74]. We show that there are significant benefits for each of the radio options: FSK 868 MHz, OFDM 868 MHz, and O-QPSK 2.4 GHz, yet they all come at a certain cost.

The contribution of this chapter is three-fold:

- We augment the OpenWSN reference implementation of 6TiSCH to support the three PHY layers*.
- We conduct an experimental performance evaluation campaign of the resulting code on the 42-node OpenTestbed described in Chapter 3. For each PHY, we measure the network formation time, the end-to-end reliability, the end-to-end latency, the estimated battery lifetime of each node, and the memory footprint of the implementation.
- We highlight the advantages and disadvantages of each PHY layer, specifically:
  - Using FSK 868 MHz yields the fastest network formation, the highest end-to-end reliability, and the lowest end-to-end latency, at the cost of a 75% decrease in battery lifetime, on average, compared to O-QPSK 2.4 GHz.
  - Using O-QPSK 2.4 GHz yields the longest battery lifetime, at the cost of the slowest network formation, the lowest end-to-end reliability, and the highest end-to-end latency.
  - Using OFDM 868 MHz yields an intermediate network formation time end-to-end reliability, and end-to-end latency at the cost of a 30% decrease in battery lifetime compared to O-QPSK 2.4 GHz. In line with Muñoz et al. [4], a node using OFDM 868 MHz discovers a number of neighbors close to that of FSK 868 MHz despite having the highest data rate. This is because it is more robust against frequency selective interference than FSK 868 MHz [28] and more immune to WiFi interference than O-QPSK 2.4 GHz [5].

This shows there is no PHY among our candidates that is best across all metrics.

4.3 A PHY-layer Agile Extension of OpenWSN

As presented in Section 2.2, the IETF 6TiSCH working group has standardized how to combine TSCH and IPv6 [30]. The 6TiSCH protocol stack has been ported to all main open-source IoT protocol stacks: OpenWSN, Contiki-NG, RIOT and TinyOS [19].

Since it is the reference implementation, and since it is ported to the OpenMote B, we use the OpenWSN implementation in this thesis. Prior to this work, OpenWSN only supported the IEEE802.15.4 O-QPSK 2.4 GHz PHY. Although initial range measurements were conducted using the OpenMote's AT86RF215 radio [4], [5], the full 6TiSCH stack had never been ported. We therefore extend OpenWSN to support the following PHYs: FSK 868 MHz, OFDM 868 MHz, and O-QPSK 2.4 GHz. This extension consists of three steps: writing the low-level drivers to configure the radio chips appropriately, tuning the durations within the timeslots to each PHY, and providing a clean software abstraction to allow the TSCH implementation to switch between them.

*As an online addition to this chapter, these extensions have been merged into the main codebase of OpenWSN at `https://github.com/openwsn-berkeley` and published under an open-source license.

Table 4.1: Definition of timing variables that compose an IEEE 802.15.4e time-slot template

Radio-specific variables	
TsTxOffset	The time between slot start and data transmission
TsLongGT	The maximum duration for radio to listen for the beginning of data packet
TsTxAckDelay	The time between packet reception and acknowledgment start of transmission
TsShortGT	The maximum duration for radio to listen for the beginning of acknowledgment packet
wdRadioTx	The maximum time for a radio chip to start frame transmission
wdDataDuration	The maximum time to complete a transmission of a data frame
wdAckDuration	The maximum time to complete a transmission of an acknowledgment frame
Board-specific variables	
maxTxDataPrepare	The maximum time to retrieve and prepare a data frame on transmitter side.
maxRxAckPrepare	The maximum time to retrieve and prepare an acknowledgement frame on receiver side.
maxRxDataPrepare	The maximum time to prepare for data frame reception on receiver side.
maxTxAckPrepare	The maximum time to prepare for acknowledgement frame reception on transmitter side.
delayTx	The expected delay between issuing a transmit command by the micro-controller and its execution on the radio-chip
delayRx	The expected delay between issuing a receive command by the micro-controller and its execution on the radio-chip

We extend OpenWSN with a generic `openradio` interface. This interface driver implements the same set of functions called by the TSCH state machine, and maps them to that of the radio driver of the PHY being used. We further design a distinct time-slot template for each PHY. The concept of "time slot template" refers to the timings associated with each state of the IEEE802.15.4e state machine. It consists of the appropriate timing of the sequence of phases within a timeslot, which we fine tuned using a logic analyzer. These timings are affected by several factors, including the communication overhead for the SPI which is the connection between the micro-controller and the radio chip, as well as the PHY bitrate. The timings are defined in Table 4.1, and are divided in two categories: *(1)* board-specific timings, which depend on the performance of the firmware and the microcontroller and *(2)* radio-specific timings, which depend on the performance of the specific radio chips used. They are used to configure the state machine, which controls when a node switches state. Fig. 4.1 illustrates the different timeslot templates when transmitting a 100 B data payload with acknowledgment. Red markers highlight the approximate time for SPI communications from the micro-controller to the AT86rf215 radio (none for the CC2538 on-chip radio). A 40 ms slot template duration is used for all the options to accommodate for the slowest bit-rate PHY, FSK 868 MHz.

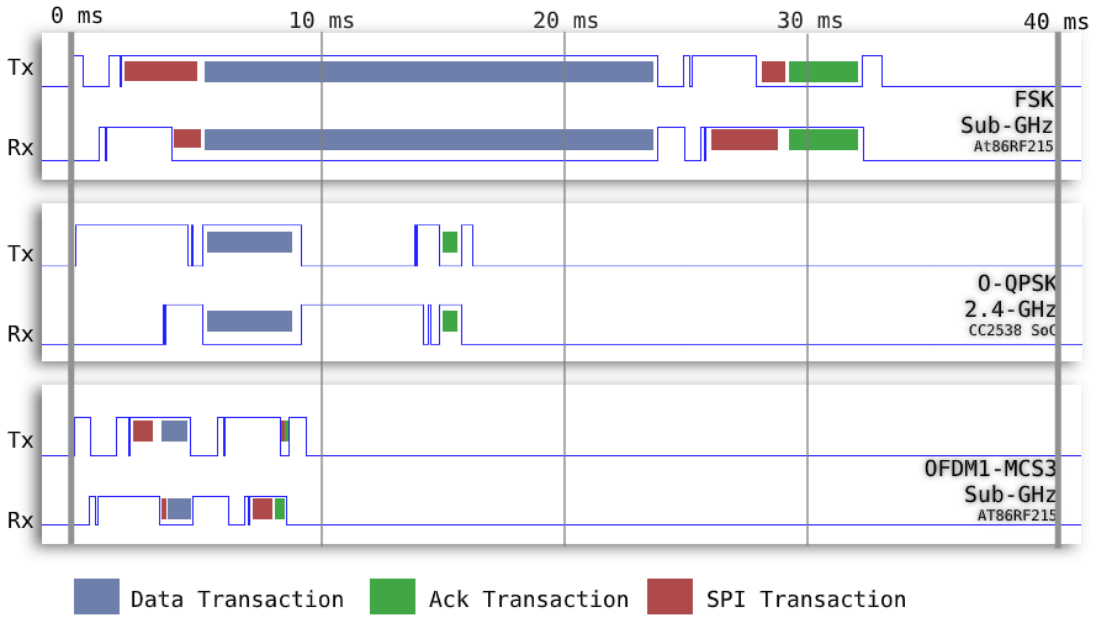

Figure 4.1: Timeslot templates for the three PHYs, for a 100 B data payload with acknowledgment. Red markers highlight when SPI transactions between the micro-controller and the AT86RF215 take place.

We use a slotframe length of 41 timeslots and we also use a 40 ms timeslot duration

for all the PHYs. Table 4.2 summarizes the parameters of the stack.

Table 4.2: Parameters of the OpenWSN protocol stack.

Parameter	**Value**
Application traffic period	60 s
RPL DIO period	10 s
RPL DAO period	60 s
neighbor table size	45
packet queue size	15
slotframe length	41
timeslot duration	40 ms
EB probability	10%
Number of radio channels	16
New neighbor RSSI threshold	-80 dBm
Max num. re-transmissions	15

Before this work, the flash memory footprint of the entire OpenWSN stack was 42 kB. This increases to 77 kB with the additions listed above, in particular with both the CC2538 and AT86RF215 drivers. This is a very small footprint which comfortably fits in modern SoC which all have 512 kB of flash, or more.

4.4 Experimental Results

To compare the performance of the 6TiSCH stack on top of each PHY, we use the OpenTestbed setup and experiment methodology introduced in Section 3.1. This section summarizes our key findings, focusing on network formation time (Section 4.4.1), end-to-end reliability (Section 4.4.2), end-to-end latency (Section 4.4.3), and battery lifetime (Section 4.4.4).

4.4.1 Network Formation Time

The network formation time is measured between the moment the DAG root is selected, and the moment the DAG root has received a data packet from each mote. The network formation process encompasses the time it takes for a mote to synchronize to the network, the time it takes for it to complete a security handshake and the time it takes for it to acquire a rank. It is the time a user would have to wait for their network to be fully functional.

This is a worst case setup, as we turn on all the motes first, and the gateway last. Per the 6TiSCH standard, traffic generated by the motes during their secure handshake uses shared cells. All motes trying to join approximately at the same time will cause a lot of contention of these shared cells, increasing the network formation time.

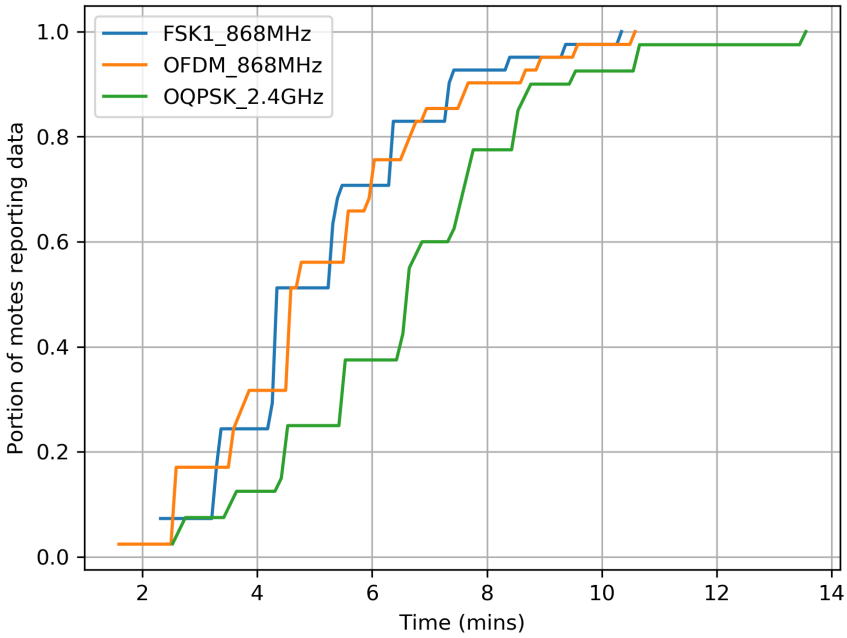

Figure 4.2: The network tends to form faster when using a longer-range PHY.

Fig. 4.2 shows that the FSK 868 MHz, OFDM 868 MHz, and O-QPSK 2.4 GHz network is 90%-formed in 7, 9, and 11 min, respectively. The higher the link budget (i.e. the longer the range), the faster the network forms.

To understand the impact of PHY on network formation time, we plot in Fig. 4.3 the number of neighbors evolving over time. Because of its long range, a mote using FSK 868 MHz tends to discover more nodes, faster than a node using O-QPSK 2.4 GHz. This observation exactly follows the link budget from Table 3.1. Discovering many neighbors is helpful in two ways. First, it allows a mote to quickly hear a node that is already part of the network, hence to synchronize quickly. Second, it gives a mote a higher probability of joining through a neighbor closer to the root; this decreases the number of hops necessary for joining.

However, having a longer range PHY increases the risk of interference between nodes and of worse hidden terminal problem. In addition, it increases the risk of neighbor table overflow. For example, if the neighbor table can hold up to 200 entries, *what is the appropriate behavior when a mote hears 100 other motes?* The challenge is that, without having another mote in its neighbor table, a mote cannot keep statistics to elect the "best" neighbors, and has to to make decisions on partial data, such as a single RSSI value. We note that none of the standards makes clear recommendation for neighbor table grooming.

Fig. 4.4 gives some insights into the network formation itself. It plots how the rank reported by the motes evolves over time. Per the RPL and Minimal Scheduling Function standards [32], [36], a mote's rank is computed using (4.1), where $numTx$ and $numAck$

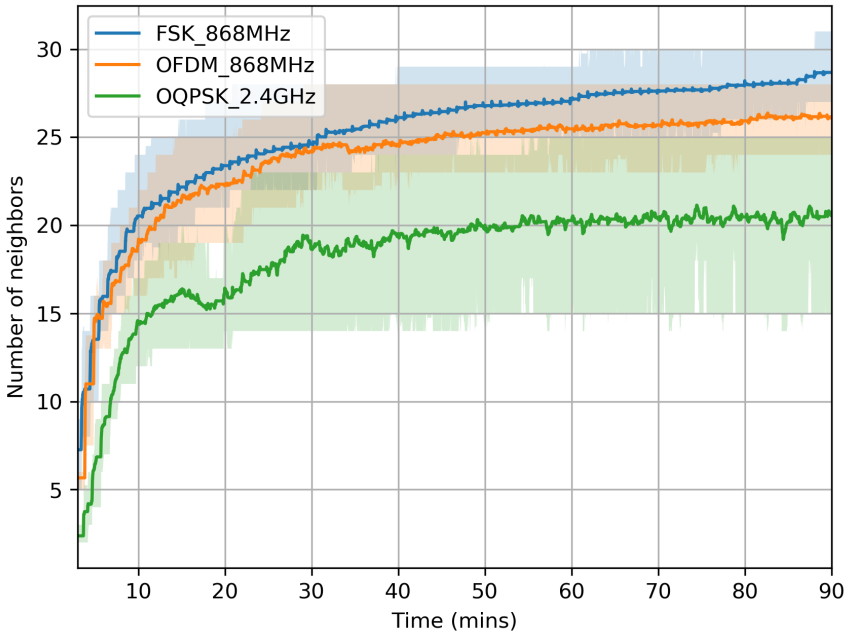

Figure 4.3: Motes discover more neighbors faster when using a longer-range PHY.

are counters of the number of transmission attempts and transmission successes to a neighbor, respectively. $minHopIncrease = 256$ is the rank increase if the link to the mote's routing parent is ideal. If that link becomes lossy (i.e. $numTx/numAck > 1$), the "cost" associated with the link increases, and the mote's rank increases accordingly.

$$\text{rank} = ((3 \cdot \frac{\text{numTx}}{\text{numAck}}) - 2) - \text{minHopIncrease}. \tag{4.1}$$

The first portion of Fig. 4.4 ($t < 50$ min) shows that the nodes start by having a very high rank. This is caused by two phenomena, combined. First, a mote may not discover its neighbor with the lowest rank immediately, and instead it me join with a artificially high rank; this resolves over time as the network stabilizes by becoming shallower. Second, all motes attempting to join create contention on the minimal cell, causing transmissions to fail, $numTx/numAck$ to increase, and the motes' rank to increase[†]. This, again, resolves as the network stabilizes by having less contention on the shared cells. These two phenomena compete: the longer the PHY range, the shallower the initial network, but the higher the contention. Fig. 4.4 shows that, once the network has stabilized, it tends to be shallower (smaller DAG rank) when using a longer-range PHY.

[†] In the OpenWSN implementation of the 6TiSCH stack, ETX is not captured for shared cells such as autonomous cells. However, poor ETX on shared cells may cause a node to select sub-optimal neighbors with less contention after repeated failures of join requests through its preferred neighbor. This leads to deteriorating the rank

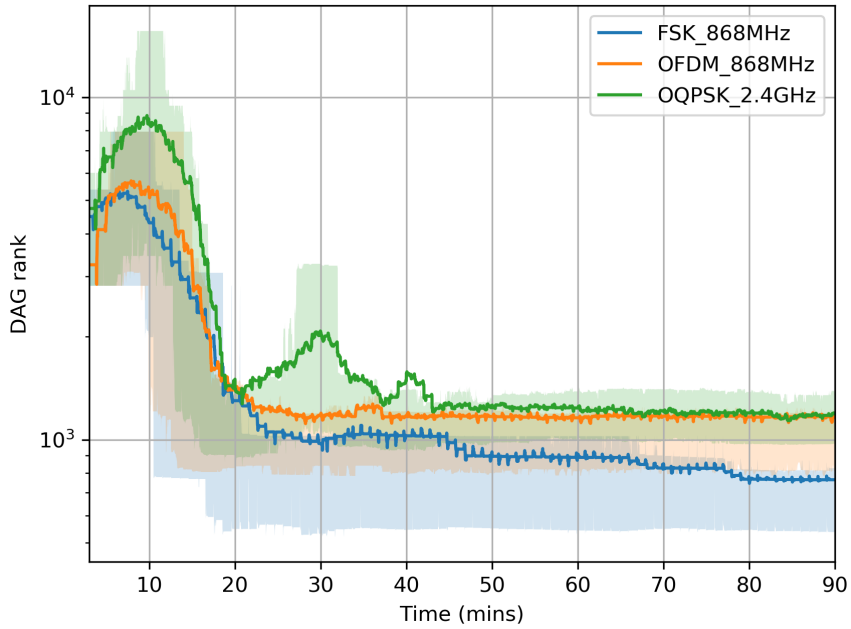

Figure 4.4: Contention and slow neighbor discovery cause the nodes' rank to be artificially high at the beginning of network formation.

4.4.2 End-to-End Reliability

We call end-to-end reliability the portion of UDP datagrams of each mote that reach the root, and use the counter in the datagrams to compute it. Table 4.3 shows PDR statistics over the last 15 min of the experiments, computed for all motes in the network. We expect close to 100% PDR in all cases (commercial TSCH implementation offer >99.999% PDR [42]).

One possible reason for end-to-end packet loss is that packet drop might be happening because of queue overflow. As shown in Section 4.4.1, a lower link budget leads to higher DAG rank, and more relaying, which increases the likelihood of filling up the packet buffer and dropping packets. Fig. 4.5 show the Cumulative Density Function (CDF) of the queue occupancy values reported by the motes, in the same period corresponding to Table 4.3. Even though Table 4.2 correctly indicates the buffer can hold up to 15 packets, 5 additional buffer entries are reserved for control frames such as Enhanced Beacons and acknowledgments. When the number of occupied entries in the buffer exceeds 15, more data packets cannot be admitted into the buffer and are dropped. Motes running O-QPSK 2.4 GHz and OFDM 868 MHz drop packets 3% and 1% of the time, respectively. FSK 868 MHz does not suffer buffer overflow, as the network is much shallower.

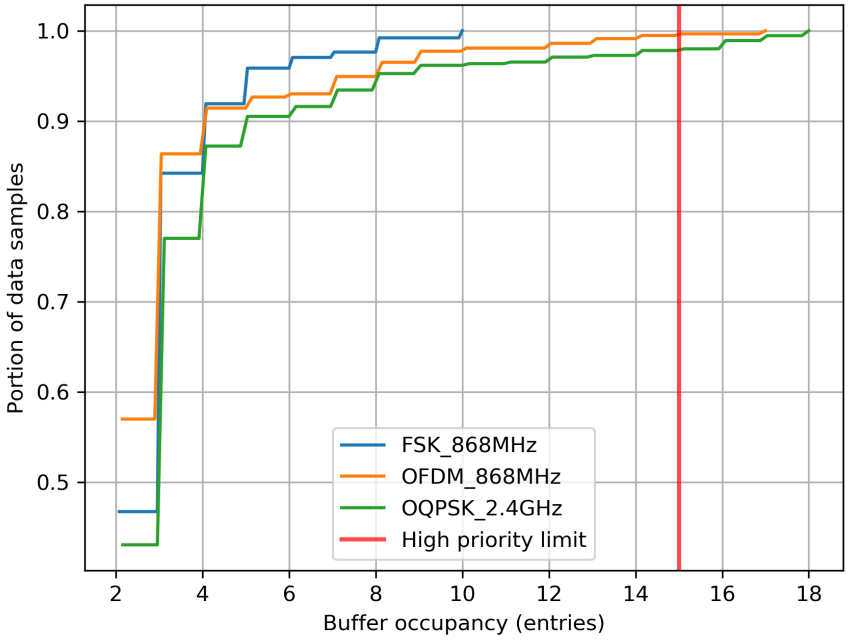

Figure 4.5: Cumulative Density Function (CDF) of buffer occupancy over the last 15 mins of the experiment. Having more than 15 entries occupied in the buffer (the red line) leads to data packet drops.

Table 4.3: End-to-end Packet Delivery Ratio (PDR) statistics over all motes in the network, computed over the last 15 min of the experiments.

	Min	**Average**	**Median**	**Max**	**StDev**
FSK 868 MHz	100.0%	100.0%	100.0%	100.0%	0.0%
OFDM 868 MHz	93.8%	99.8%	100.0%	100.0%	0.9%
O-QPSK 2.4 GHz	73.3%	98.1%	100.0%	100.0%	6.0%

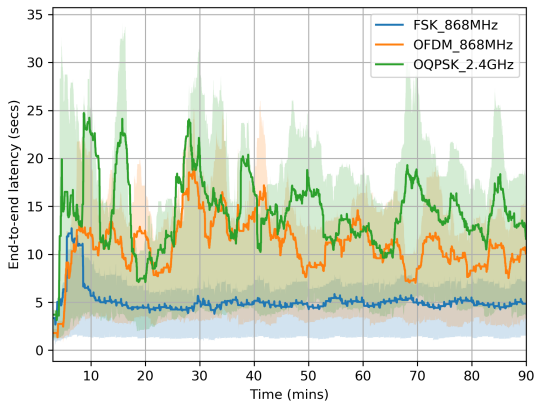

(a) Time series

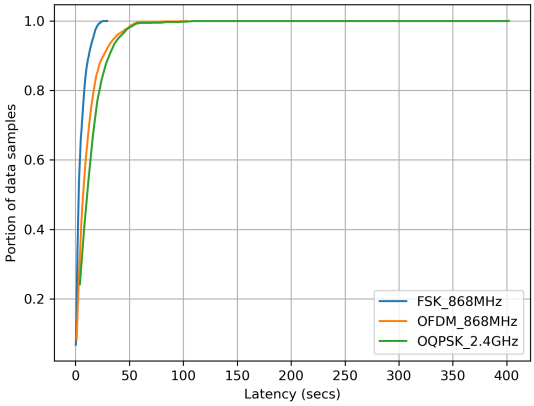

(b) Cumulative Density Function (CDF)

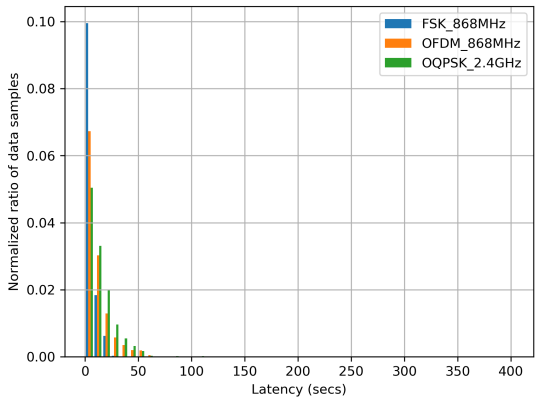

(c) Probability Density Function (PDF)

Figure 4.6: End-to-end latency in the network recorded over the entire 90 min experiments. The longer the PHY range, the lower the latency.

4.4.3 End-to-End Latency

We call end-to-end latency the amount of time between the moment a mote generates a new UDP datagram, and the moment the latter reaches the root. It is calculated based on the difference between the ASN when the UDP packet is generated and the ASN when it arrives at the root. It is affected by several factors including number of hops between the mote and the root and number of re-transmissions at each hop.

Fig. 4.6a plots the evolution of latency over time. As shown in Fig. 4.6b, 90% of the data reaches the root after 10, 25, and 35 s for FSK 868 MHz, OFDM 868 MHz and O-QPSK 2.4 GHz, respectively. Fig. 4.6c shows a long-tailed distribution of latency for shorter range PHYs.

With 41 slots per slotframe and 40 ms timeslot, each mote on average gets one transmission opportunity every 1.68 s. Given the increased number of hops for lower range PHYs, the higher latency of O-QPSK 2.4 GHz, compared to that of FSK 868 MHz, was to be expected.

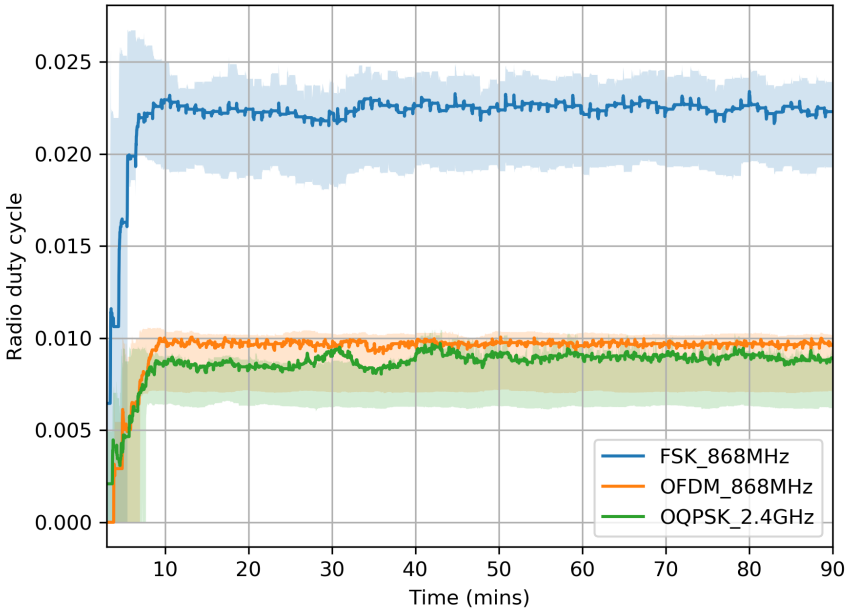

Figure 4.7: Evolution of the mote's radio duty cycle over time.

4.4.4 Battery Lifetime

We have the motes report what portion of the time their radio is active ("radio duty cycle"), and what portion of the time the radio is transmitting ("transmit duty cycle"). We then combine that with the current draw of the radio in transmit and receive states, the supply voltage and the energy contained in a battery to compute a battery lifetime. This computation does not take into account the possible current draw of other electronics, and assumes the battery is a perfect bucket of charge (i.e. ideal battery). Even though this is not an accurate prediction of the lifetime of the mote on a real battery, it is good enough to compare the effect on lifetime of the different PHYs. We are aware that current peaks shorten the effective mote lifetime compared to the "ideal battery" lifetime. The PHYs leading to the shorter "ideal battery" lifetime in our survey also have the higher peak current. This reinforces our conclusions.

We compute a mote's radio duty cycle as T_{on}/T_{total} (see Section 3.1.2). Fig. 4.7 shows the evolution of the duty cycle over time. We expect the duty cycle to decrease with data rate. This does *not* hold for OFDM 868 MHz because of the time to issue SPI commands to the AT86RF215, which can take up to 1 ms, as explained in Section 4.3 and shown in Fig. 4.1.

Given T_{TX} and T_{on}, we use (4.2) to compute reception time T_{RX}, the transmit duty cycle DC_{TX} and the receive duty cycle DC_{RX}.

Table 4.4: "Ideal battery" lifetime for each configuration.

	FSK 868 MHz	OFDM 868 MHz	O-QPSK 2.4 GHz
DC	2.100%	0.750%	0.650%
DC_{TX}	0.250%	0.038%	0.050%
DC_{RX}	1.850%	0.713%	0.600%
I_{TX}	62 mA	62 mA	24 mA
I_{RX}	28 mA	28 mA	20 mA
Supply voltage	2.5 V	2.5 V	3.0 V
energy per day	0.0141 Wh	0.0033 Wh	0.0015 Wh
battery lifetime	0.6 years	1.7 years	2.4 years

Table 4.5: Summary of the Key Performance Indicator (KPI) measured in our testing. The best values are shown in bold.

	network formation	end-to-end reliability	end-to-end latency	battery lifetime
	(Section 4.4.1)	(Section 4.4.2)	(Section 4.4.3)	(Section 4.4.4)
FSK 868 MHz	**7 min**	**100.00%**	**10 s**	0.6 years
OFDM 868 MHz	9 min	99.84%	25 s	1.7 years
O-QPSK 2.4 GHz	11 min	98.08%	35 s	**2.4 years**

$$\begin{cases} \mathrm{T_{RX}} &= \mathrm{T_{on}} - \mathrm{T_{TX}}\,, \\ \mathrm{DC_{TX}} &= \frac{\mathrm{T_{TX}}}{\mathrm{T_{total}}}\,, \\ \mathrm{DC_{RX}} &= \frac{\mathrm{T_{RX}}}{\mathrm{T_{total}}}. \end{cases} \tag{4.2}$$

Table 4.4 details the calculation of battery lifetime, assuming a mote is powered by a pair of AA batteries holding 8.2 Wh of energy. O-QPSK 2.4 GHz exhibits a battery lifetime 40% larger than OFDM 868 MHz and 300% larger than FSK 868 MHz. Despite the advantages of FSK 868 MHz and OFDM 868 MHz in range, reliability and latency, their utilization leads to more frequent battery replacement.

4.5 Conclusions

Table 4.5 summarizes the key performance indicators of our network measured in the experimental campaign. FSK 868 MHz exhibits the best network formation time, end-to-end reliability and end-to-end latency, at the cost of a battery lifetime roughly 10 times lower than O-QPSK 2.4 GHz. OFDM 868 MHz shows balanced results, between FSK 868 MHz and O-QPSK 2.4 GHz. There is no single PHY layer that exhibits the best performance over all KPIs.

So which PHY should I use? If choosing a single PHY, which to pick depends

on the application. If it is acceptable to change batteries every half a year or so, FSK 868 MHz appears to be the most appropriate. If battery lifetime is of utmost importance, Table 4.5 suggests O-QPSK 2.4 GHz is the most appropriate. Finally, for an "in between" performance, choose OFDM 868 MHz.

Of course, it is important to note that the results depend on the use case and the KPIs and their respective importance. This can lead to a different answer to this question and we develop a rationale to illustrate this claim. First, the results presented in this chapter, while conducted and presented in a rigorous fashion, only hold for use cases very similar to the deployment shown in Fig. 3.1. There are undoubtedly cases (deeply sparse network, heavily unbalanced deployment, ...) where our results do not hold, and where the "ranking" of the different PHYs is different. Second, even if every precaution is taken to pick the right PHY during the design phase of the network, it is entirely possible that conditions or requirements change during the operation of the network. This could lead to operating with the "wrong" PHY layer, leading to sub-optimal performance.

It is interesting for future work to revisit the KPIs used as reference points in these experiments and to see the tradeoffs could look like if different KPIs are used. To confirm this view: network deployment cost as a KPI can create interest in long range PHYs (since lower densities are favored by industrialists). However, if we introduce another KPI such as network operation costs (including the cost of battery replacement), then the having short range PHYs can allow improved battery lifetime and therefore lower operational costs.

The real outcome of this paper is not the absolute numbers presented in Table 4.5. What that table does indicate is that no PHY is the best for all metrics, and that best performance is achieved when *combining* the PHY layers, rather than *picking* one. This result holds when contemplating additional PHY layer, one obvious candidate being LoRa [12]. As alluded to in Section 4.1, we are at an exciting stage where we have both radio chips which are able to switch PHY on a frame-by-frame basis, and we have the scheduling technology to orchestrate this PHY-layer agility. We argue for a technology-agile network, in which each mote keeps track of the quality of its link to its neighbors *for each PHY layer*, and uses the PHY layer most appropriate for each frame. This means a mote may use a different PHY to communicate with different neighbors or to send frames belonging to different classes of traffic. This also means that, in a multi-hop scenario, a packet can travel from source to destination using a different PHY at each hop. In that context, energy efficient neighbor discovery and network consistency are the main challenges, elements we addressed in this research.

Chapter 5

Generalizing 6TiSCH for an Agile Multi-PHY Networking

Parts of this chapter were published as part of the following article: *g6TiSCH: Generalized 6TiSCH for Agile Multi-PHY Wireless Networking.* Mina Rady, Quentin Lampin, Dominique Barthel, Thomas Watteyne. **IEEE Access**, vol. 9, pp. 84465-84479, **2021**.

Key Takeaways: Wireless networks traditionally use a single physical layer for communication: some use high bit-rate short-range radios, others low bit-rate long-range radios. This chapter introduces g6TiSCH, a generalization of the standards-based IETF 6TiSCH protocol stack. g6TiSCH allows nodes equipped with multiple radios to dynamically switch between them on a link-by-link basis, as a function of link-quality. This approach results in a dynamic trade-off between latency and power consumption. We evaluate the performance of the approach experimentally on the OpenTestBed. Each OpenMote B can communicate using FSK 868 MHz, O-QPSK 2.4 GHz or OFDM 868 MHz, a combination of long-range and short-range physical layers. We measure network formation time, end-to-end reliability, end-to-end latency, and battery lifetime. We compare the performance of g6TiSCH against that of a traditional 6TiSCH stack running on each of the three physical layers. Results show that g6TiSCH yields lower latency and network formation time than any of the individual PHYs, while maintaining a similar battery lifetime.

In Chapter 4, we demonstrated that no single PHY performs best across all KPIs. The main contribution of this chapter is generalizing 6TiSCH to support a multi-PHY approach; we call this "g6TiSCH". In g6TiSCH, nodes dynamically switch between using low bit-rate and high bit-rate PHYs, based on the link quality to each

neighbor. We implement g6TiSCH in OpenWSN*, the reference 6TiSCH open-source implementation [75]. In this implementation, we use three PHYs: FSK 868 MHz option 1 at 50 kbps (offering the lowest bit-rate), OFDM 868 MHz option 1 MCS 3 at 800 kbps (offering the highest bit-rate), and O-QPSK 2.4 GHz at 250 kbps as an intermediate option. We experimentally compare the performance of g6TiSCH against the performance of the 6TiSCH architecture with each PHY individually (as previously studied [68]). The comparison is based on the KPIs recommended by Vucinic et al. [42]: network formation time, end-to-end latency, end-to-end reliability, and battery lifetime.

The remainder of this chapter is organized as follows. Section 5.1 presents the problem statement and lists the specific contributions of this chapter. Section 5.2 shows how the 6TiSCH stack is adapted to provide multi-PHY support. Section 5.3 introduces the experimental testbed we used and the methodology we followed to generate the KPIs. Section 5.4 discusses experimental results. Finally, Section 4.5 concludes this chapter.

5.1 Problem Statement and Contributions

As noted in Section 2.6, several studies have explored comparing and integrating multiple PHYs in hybrid architectures [59]–[62]. These studies indicate the significance of hybrid networks. However, the challenge remains for a fully wireless, single-stack architecture that can accommodate a set of PHYs and yet offer wire-like reliability, especially for low-power and lossy applications.

The 6TiSCH protocol stack combines low-power operation and high reliability but it only uses one PHY, which is IEEE802.15.4 O-QPSK 2.4 GHz. Muñoz et al.have outlined the challenges and opportunities for a generalized 6TiSCH architecture [72]. One challenge is that the difference in energy consumption between the PHYs changes how the cost of communication to different neighbors is measured at the link-layer. This also affects how multi-hop paths are formed by the routing protocol. PHYs differ in their expected number of re-transmissions, resulting level of interference and resulting contention in shared cells [73]. Furthermore, previous experiments in [68] show system-level side-effects of each PHY. That is, a short-range PHY such as O-QPSK 2.4 GHz leads to a higher probability of packet queue overflow for increased re-transmissions and forwarding, which leads to packet drop. A long-range PHY such as FSK 868 MHz increases the risk of interference between nodes and of worsening the hidden terminal problem. In addition, it leads to a higher probability of neighbor table overflow due to an increased number of discovered neighbors, which leads to denial of service to possibly good neighbors.

This chapter goes one step further by demonstrating a generalized 6TiSCH stack for multi-PHY wireless networking. The contributions of this chapter are three-fold:

- We detail the minimal adaptations we had to do on some layers of the 6TiSCH protocol stack to support the g6TiCH architecture.

* As an online addition to this chapter, the source code is available under an open-source license at `http://github.com/openwsn-berkeley/`.

- We augment the OpenWSN reference implementation of 6TiSCH with g6TiSCH support, and compare its performance to single-PHY networks using O-QPSK 2.4 GHz, OFDM 868 MHz, and FSK 868 MHz.
- We evaluate end-to-end performance using industrial KPIs, and show how g6TiSCH provides a more balanced performance compared to single-PHY networks.

The following section gives an overview of the 6TiSCH adaptation to g6TiSCH for a generalized multi-PHY support.

5.2 Adapting 6TiSCH for a Generalized Multi-PHY Support

In our generalized architecture, the following adaptations have been introduced to the 6iTSCH protocol stack:

- In Section 5.2.1, we show how TSCH is combined with Time-Slotted Physical-layer Hopping. This allows a mote to choose a different physical layer at each slot: radio channel, frequency band, radio modulation and the radio chip used (in case of multiple radio interfaces).
- In Section 5.2.2, we show how minimal cells are used to broadcast EBs and DIOs on each PHY. This enables nodes to synchronize and then discover neighbors on each PHY.
- In Section 5.2.3, we show how the objective function used by the routing algorithm is adapted to favor parents with energy efficient PHYs. The 6P is then adapted so that nodes can determine the type of PHY they need in their requested cells. The longest range radio, FSK 868 MHz, is also used as a default for autonomous cells.

The remainder of this section will go over each adaptation in more detail.

5.2.1 Time Slotted Physical-layer Hopping

The IEEE802.15.4 (2015) standard defines the notion of a "PHY" as the combination of "the radio frequency (RF) transceiver and its low-level control mechanisms" (see [20], Section 5.6). It also defines the "channel" as the RF used by the transceiver for transmissions and receptions (Sections 10.1 and 11.3). The IEEE802.15.4e MAC layer of 6TiSCH uses channel hopping over 16 channels for O-QPSK 2.4 GHz.

In g6TiSCH, we introduce Time Slotted PHY Hopping for medium access: for a mote, time is divided into slots and in each time slot, the mote selects a specific PHY layer independent from the one used in the previous slot. The mote selects the most appropriate PHY at each slot depending on the negotiated links and protocol stack configuration. In our implementation, we use the OpenMote which features two radio chips: Atmel AT86RF215 which implements FSK 868 MHz and OFDM 868 MHz in the

sub-GHz band, Texas Instruments CC2538 which implements O-QPSK in the 2.4 GHz band. FSK 868 MHz offers the lowest bit-rate at 50 kbps, OFDM 868 MHz offers the highest bit-rate at 800 kbps, and O-QPSK 2.4 GHz offers an intermediate bit-rate at 250 kbps. Their physical properties are outlined in Table 3.1 [21], [27].

To use a different PHY at each slot, we extend the OpenWSN implementation with the `openradio` extension that allows a generic interface to the drivers of different chips from the MAC layer, as described in Section 4.3.

Timings are tuned with a logic analyzer; resulting templates are depicted in Fig. 4.1. We use a 40 ms timeslot duration in all slot templates in g6TiSCH to accommodate for the lowest bit-rate PHY, FSK 868 MHz. This decision is to allow for comparison with the results from the single-PHY networks previous research in Chapter 4.

5.2.2 Generalized Neighbor Discovery and Network Join

In a traditional 6TiSCH network, when a new node is switched on, it keeps its radio on in receive mode, on the O-QPSK 2.4 GHz PHY. The radio switches from channel to channel, "scanning" the medium until it receives an EB broadcast from a synchronized node [18]. All synchronized motes transmit an EB with a given probability in the minimal shared cell. The EB contains details on the source mote, in addition to the specification of the slot-frame and the offset(s) of minimal cells that are used for EB broadcasts [29]. Once the new mote receives an EB, it synchronizes to the common slotframe shared by the network and starts aggressively duty-cycling its radio for energy-saving. The node keeps listening on minimal cells for more neighbors and then chooses one neighbor as a proxy for joining the network. It establishes a secure join procedure using Constrained Join Protocol (CoJP) [76] with the proxy mote using its autonomous cell.

In this g6TiSCH amendment, a minimal cell is allocated for *each* PHY for EB transmission. In this architecture, un-synchronized motes need to know which cells to use for EB broadcast and which PHY to use in each cell. To address this, we use the most significant byte in the `linkOptions` field to determine the PHY used for each minimal cell (Appendix A.1 in RFC8180 [29]). This way, when an un-synchronized mote processes an EB, it populates its schedule accordingly. As demonstrated in the sequence diagram in Fig. 5.1, the root transmits EBs on the 3 minimal cells. Mote B uses FSK 868 MHz for medium scanning since previous experiments in [59], [68] show that it leads to fastest synchronization (thanks to its longest range). Fast synchronization is important because it allows the mote to turn its radio off and save energy. When new mote B receives the EB transmitted from the root on the FSK 868 MHz minimal cell, it synchronizes to the network and registers the root in its neighbor table.

Other approaches could be used for neighbor discovery; for example, only one minimal cell can be allocated using the longest range PHY (e.g., FSK 868 MHz). This may lead to saving the energy for the two extra minimal cells. The benefit of using one minimal cell for each PHY is its simplicity as motes do not have to agree on a pre-specified PHY to synchronize into the network. Furthermore, increased contention is expected on the sub-GHz band because of its long range and on the 2.4 GHz band due to common Wi-Fi interference. Therefore, combining both bands improves discovery performance.

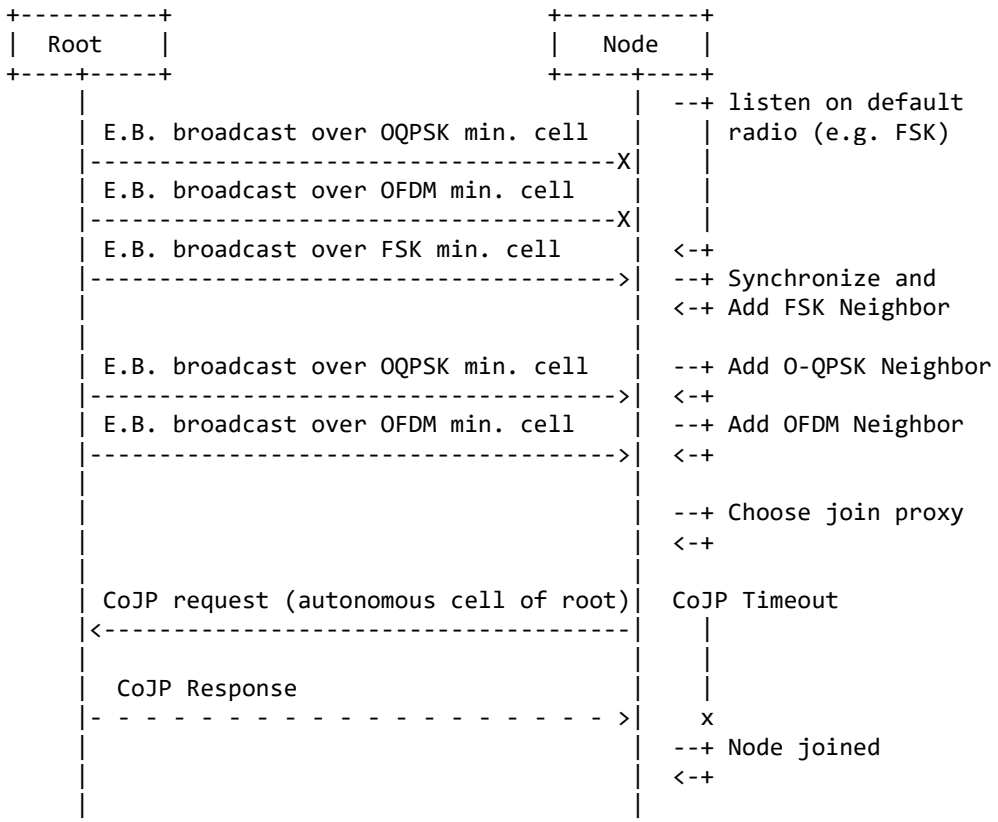

Figure 5.1: Neighbor discovery is adapted to listen on different PHYs for new neighbors. Use of hybrid PHYs on minimal cells enable faster neighbor discovery and Constrained Join Protocol handshake. Adapted from IETF draft [76].

Then node B starts the neighbor discovery as it begins scanning the medium on the *minimal cell of each PHY* for more EBs from the neighboring PHYs. The use of multiple minimal cells allows the mote to discover available neighbors on each PHY. In this adaptation, PHYs of a neighboring mote are considered as different neighbors. In classical 6TiSCH, the minimal cells are used in either transmit or receive modes; that is, in case there are no packets queued for transmission, the mote goes to receive mode *by default*. Since g6TiSCH uses n times more PHYs than classical 6TiSCH, it also uses n times more minimal cells for neighbor discovery. This can cause it to consume, roughly, n times more power for broadcast cells. One way to mitigate this is as follows. In case there are no packets queued for transmission, each cell goes to receive mode with a given probability; otherwise, the PHY remains powered off for energy saving. We use $P_{rx} = \frac{1}{n}$, where P_{rx} is the probability to go in receive mode. This allows the mote to balance the energy spent in listening according to the number of used PHYs. For example, a network that uses three PHYs would consume approximately 200% more power in minimal cells than a single-PHY network if the radios were never switched off in any of these cells. So, in a configuration with three PHYs, we use $P_{rx} = \frac{1}{3}$. Therefore, if there are no packets queued for transmission, the radio will turn on for reception in all cells approximately 100% instead of 300% of the time compared to single-PHY network. This way, the multi-PHY network will remain approximately at the same power consumption at minimal cells as the single-PHY network.

Node B starts the procedure to join the network according to the join protocol [76]. The procedure selects the neighbor with the best join priority as proxy (the closer to the root, the lower the energy cost of the join procedure). It then sends the join request on the autonomous cell of the proxy (e.g. the root in this case). In this g6TiSCH amendment, FSK 868 MHz is used for communication on autonomous cells since it is the most robust PHY. When the request is authenticated and acknowledged by the root, the join procedure is successful, and B can proceed with parent selection and cell negotiation.

We note that security is an integral part of the 6TiSCH framework as defined in IEEE 802.15.4e (Section 7) [18] and the IETF 6TiSCH Minimal Security draft [76]. All the security features 6TiSCH carry over to g6TiSCH, including packet encryption and secure join.

5.2.3 Generalized Parent Selection and Link Negotiation

The IETF RPL-related standards define mechanisms for neighbor evaluation and parent selection [32], [34]. In the IPv6 RPL routing layer of 6TiSCH, a node selects a parent mote by evaluating the expected path cost through each neighbor to the root and it chooses the parent with the least expected path cost. The cost of a single link is estimated based on the expected transmission count (ETX) ratio as in (5.1), where: $numTx$ is the number of transmissions on the link and $numAck$ is the number of acknowledgments received. This full path cost through neighbor i to the root is evaluated by the objective function based on (5.2) (as defined in the 6TiSCH minimal configuration [29]), where: $Rank_i$ is the advertised rank of the neighbor, $minHopIncrease$ is the minimal cost to use for a one

hop link. For example, the root has a default rank of 256. If a mote has a link to the root with perfect ETX ratio of 1, the expected path cost is 512. After a parent is selected, the routing algorithm can later decide to change the parent to new neighbor i if the condition in (5.3) evaluates to *true*. The factor P is the parent switch threshold so that the mote does not change parent unless it expects significant improvement (i.e. hysteresis). This way, the network avoids too frequent parent changes, which would lead to instability. The recommended configuration for this threshold is $2 \times minHopIncrease$, as proposed in the minimal 6TiSCH configuration [29].

$$\mathrm{ETX_i} = \frac{\mathrm{numTx_i}}{\mathrm{numAck_i}} \tag{5.1}$$

$$\mathrm{Cost(Neighbor_i)} = \mathrm{Rank_i} + ((3 \cdot \mathrm{ETX_i}) - 2) \times \mathrm{minHopIncrease}. \tag{5.2}$$

$$\mathrm{f(Parent, Neighbor_i)} = \begin{cases} \text{true}, & \text{if Cost(Parent)} - \mathrm{Cost(Neighbor_i)} \geq \mathrm{P} \\ \text{false}, & \text{otherwise} \end{cases} \tag{5.3}$$

In g6TiSCH, a combination of neighbor IPv6 address and a PHY link is considered an independent neighbor. The use of multiple PHYs poses the need for a metric to evaluate and compare different PHYs. There can be different ways to build this metric; for example, based on power consumption, latency, or time-on-air. We use a simple configuration for the routing layer that is sufficient to demonstrate the advantage of the g6TiSCH architecture.

Therefore, for the purposes of the experiment, we choose to evaluate the different PHYs based on energy consumption in order to extend the battery lifetime as much as possible. The objective function is adapted as in (5.4) to compute the link cost of a certain "neighbor" by giving weight to the expected energy per bit E_{bit} for the PHY of that neighbor. Therefore, in case neighboring links have similar ETX ratios, the mote would favor PHYs with lower E_{bit} for energy saving.

$$\begin{aligned} \mathrm{Cost(Neighbor_i)} = \mathrm{Rank_i} + ((3 \cdot \mathrm{ETX_i}) - 2) \\ \times \mathrm{minHopIncrease} \times \mathrm{Factor(PHY_i)}. \end{aligned} \tag{5.4}$$

To derive an ordering of the PHYs based on power consumption, we estimate the E_{bit} for each PHY as a function of its power consumption for transmission and reception and its bitrate. The function is expressed in (5.5), where I^i_{tx} and I^i_{rx} are the current draw for transmission and reception for PHY_i, V^i_s is the voltage supply for the radio chip of PHY_i, and R^i_b is the bit rate. Table 5.1 shows the E_{bit} for each PHY. Therefore, the least power consuming PHY is OFDM 868 MHz, followed by O-QPSK 2.4 GHz and FSK 868 MHz. We assign $Factor(OFDM) = 1$, and $Factor(OQPSK) = 2$. However, we assign $Factor(FSK) = 5$ just to make the switch to an FSK 868 MHz PHY harder than the switch to O-QPSK 2.4 GHz PHY, to account for its energy hungry footprint. Different configurations of the OF can be used to tune the performance depending on the application criteria, exercising different tradeoffs between datarate and range. Chapter 7

Table 5.1: PHY layers energy per bit estimations. OFDM 868 MHz is the lowest energy footprint per bit transmission/reception followed by O-QPSK 2.4 GHz and FSK 868 MHz.

	FSK 868 MHz	**OFDM 868 MHz**	**O-QPSK 2.4 GHz**
Radio chip	AT86RF215	AT86RF215	CC2538
Data rate	50 kbps	800 kbps	250 kbps
I_{TX}	62 mA	62 mA	24 mA
I_{RX}	28 mA	28 mA	20 mA
Supply voltage	2.5 V	2.5 V	3.0 V
Energy per bit	4.50 μJ	0.28 μJ	0.53 μJ

focuses in more detail on how an OF can operate a multi-PHY network in a more generic manner.

$$\mathrm{E_{bit}(PHY_i)} = \frac{(\mathrm{I^i_{tx}} + \mathrm{I^i_{rx}}) \cdot \mathrm{V^i_s}}{\mathrm{R^i_b}} \tag{5.5}$$

After the objective function converges on a given combination of neighbor IPv6 and PHY setting, the node initiates the request to allocate cells with the selected parent. In the standard 6TiSCH stack, cells are identified by a combination of slot offset and channel offset. The Minimal Scheduling Function (MSF) [36] initiates a 6top request for the parent to allocate a dedicated cell for uplink traffic [35]. This 6top request is sent within a maximum period from the moment the routing algorithm decides on switching parents (whether switching between different PHYs or completely different nodes). This maximum period is called the "housekeeping" period which is part of the current draft of the Minimal Scheduling Function. This way, the latency of the parent-switching has an upper-bound duration for a more deterministic performance. When the parent approves the request, the cell is allocated on both motes.

In g6TiSCH, the definition of a cell is extended to include the used PHY as well. The 6top request to add cells is extended to define what type of PHY it needs for that cell. A sequence diagram of the transaction is outlined in Fig. 5.2. We use two unused bits of the `linkOptions` byte to encode the PHY type of the requested cell. When the parent acknowledges the request, the cells are added on both sides and the uplink negotiation is complete.

An example of a complete g6TiSCH slotframe is shown in Fig. 5.3 for a network of three motes: A is the root, B is a relay node, and C is a leaf node. Three minimal cells are allocated at the beginning of the slotframe, one for each PHY. EB and DIO broadcasts are transmitted within these slots for network synchronization and neighbor discovery.

Each mote allocates an autonomous cell using its FSK 868 MHz radio for 6top negotiation transactions. Mote B has up-link cells to A in slot 6 with OFDM 868 MHz PHY and Mote C also established an O-QPSK 2.4 GHz link to B in slot 5. Therefore, from a forwarding perspective, node B uses O-QPSK 2.4 GHz with its CC2538 radio chip

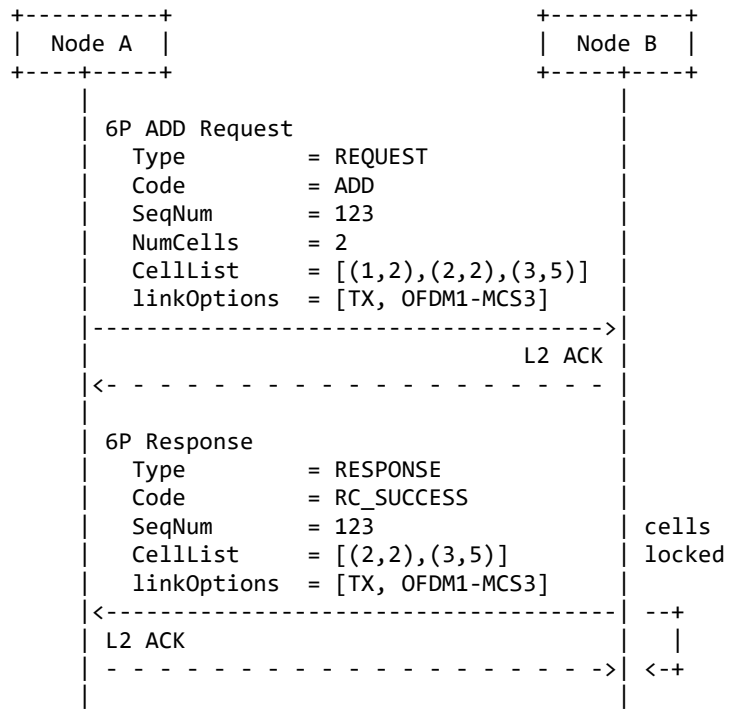

Figure 5.2: 6top protocol transaction to allocate a cell specifying its PHY layer radio setting. Adapted from IETF RFC8480 [35].

Table 5.2: Parameters of the OpenWSN protocol stack.

Parameter	**Value**
Application traffic period	60 s
RPL DIO period	10 s
RPL DIO probability	10%
RPL DAO period	60 s
Packet queue size *	15
Slotframe length	41
Timeslot duration	40 ms
EB probability	10%
O-QPSK 2.4 GHz channels	16
FSK 868 MHz channels	16
OFDM 868 MHz channels†	5
New neighbor RSSI threshold	−80 dBm
Max num. re-transmissions	15

* The buffer can hold up to 15 data packets (in addition to 5 reserved entries for network control packets).

† We restrict the number of OFDM 868 MHz channels in this experiment to 5 channels which is the maximum allowed in the European 868 MHz band.

to listen for data packets from C in slot 5 and channel 1. It then uses OFDM 868 MHz with its AT86RF215 radio chip to send up-link frames to A in slot 6 and channel 7.

5.3 Experimental Setup and Methodology

To examine the performance of the g6TiSCH architecture, we use the OpenTestbed setup presented in Section 3.1 for experimental evaluation. Network performance is compared to 6TiSCH deployments with each PHY individually. This section gives an overview of the experimental setup and the methodology for the performance evaluation for g6TiSCH and the single-PHY networks.

We extended the OpenWSN 6TiSCH reference implementation with g6TiSCH. Before this update, the memory footprint of the full OpenWSN stack was 42 kB of flash. The size of the updated implementation is 79 kB, including the drivers for both the CC2538 and the AT86RF215 radio chips. This fits comfortably in modern micro-controllers, which typically feature 512 kB of flash memory. We use a slotframe duration of 41 slots, as previously used in [68] for comparison. The configuration of the protocol stack is detailed in Table 5.2.

For experimentation, we use the OpenTestbed setup † The network is run three times

†The testbed setting used for this chapter has 36 motes instead of 42 motes as in the previous setup. This is because 6 motes went down during the COVID-19 pandemic and it was not possible to visit the

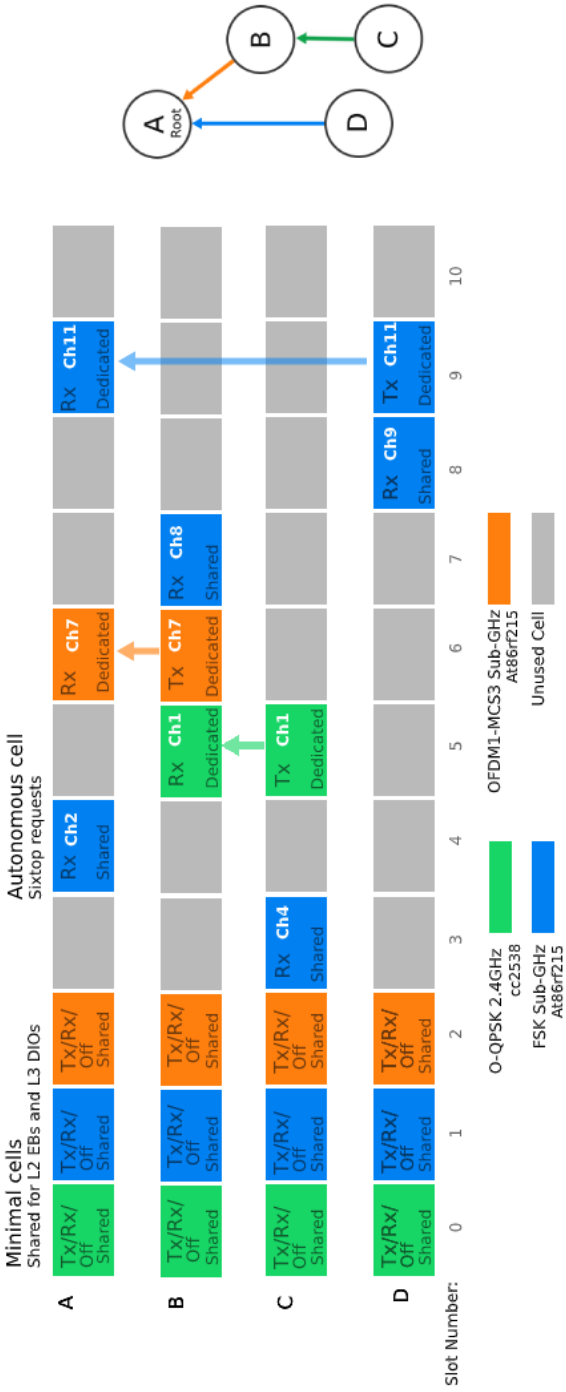

Figure 5.3: Example of a multi-PHY slot frame in the resulting generalized 6TiSCH architecture. A minimal cell for each PHY-layer enables discovery of different radios. FSK 868 MHz is used for autonomous cells. Node C allocates dedicated O-QPSK 2.4 GHz cells for its parent B. Node B allocates dedicated OFDM 868 MHz cells for its parent A. Node C allocates dedicated FSK 868 MHz cells for its parent A.

with each PHY individually. For short, the single PHY networks will be referred to by their PHY names hereafter (i.e. O-QPSK 2.4 GHz, FSK 868 MHz, and OFDM 868 MHz). It is then run a fourth time with the generalized multi-PHY architecture. This is to demonstrate that the generalized architecture is capable of providing a more balanced performance than each PHY individually. For each experiment, a mote placed in the middle of the floor is set as the DAG root (see Fig. 3.1) and the network is run for 90 min.

The following measurements are captured and sent every 60 s from each mote:

- a counter, that is used to detect loss of data packets.
- the time at which the data packet was created (expressed as ASN),
- the DAG rank of the sender,
- T_{on}: how long the sender's radio has been on since the previous data packet transmission,
- T_{TX}: how long the sender's radio has been on and transmitting since the previous data packet transmission,
- T_{on}^{FSK}, T_{on}^{OFDM}, and T_{on}^{OQPSK}: the breakdown of T_{on} for each PHY ,
- T_{TX}^{FSK}, T_{TX}^{OFDM}, and T_{TX}^{OQPSK}: the breakdown of T_{TX} for each PHY,
- T_{total}: the amount of time since the previous data packet transmission,
- the maximum and minimum number of packets in the packet buffer since the previous packet.

As previously described, we use the logged data to compute Network Formation Time, End-to-End Reliability, End-to-End latency, and Network lifetime.

We are aware that end-to-end latency for OFDM 868 MHz and O-QPSK 2.4 GHz can be improved by using smaller slot durations (instead of the 40 ms timeslot). However, to maintain consistency across experiments, we choose to change one parameter only, the network PHY, in order to measure its impact on end-to-end KPIs. Therefore, we fix the slot-duration at 40 ms for all networks in order to isolate any possible effects of smaller slot durations (such as increased duty cycle). This way, we can ensure that our observations are strictly due to change of PHYs. We are also aware that use of different slot durations in the same slotframe for g6TiSCH can improve latency performance. However, we are interested in demonstrating the baseline performance of g6TiSCH in this study. Furthermore, we address this in a separate study in Chapter 6 since it touches on a separate research context of "Schedule Compactness" in TSCH networks.

We display the results in Time Series form and CDF form (as introduced in Section 3.1.2.

center physically to resolve the problem due to confinement conditions.

5.4 Experimental Results

This section details the findings from the experimental campaigns. We show the performance of the networks in terms of: Network formation time (Section 5.4.1), end-to-end latency (Section 5.4.2), end-to-end reliability (Section 5.4.3), and battery lifetime (Section 5.4.4).

5.4.1 Network Formation

Network formation time is influenced by the duration of a *full join* process, which includes the time a mote needs to synchronize to the network, establish a secure join hand-shake, and successfully negotiate a link to a parent (as outlined in Sections 5.2.2 and 5.2.3). As in the previous chapter, we assume a worst-case scenario as all motes are flashed at once and begin the network join procedure at the same time. This increases contention since neighbor discovery and link negotiations occur on shared cells. So this helps us observe the behavior of the network under stress.

We plot in Fig. 5.4 the cumulative density of the time-to-first-data-packet from each of the 36 motes in the network. For 90% of the motes, network formation time is 5, 5, 7, and 18 min for g6TiSCH, FSK 868 MHz, O-QPSK 2.4 GHz, and OFDM 868 MHz, respectively. Among the single PHY networks, the OFDM 868 MHz network is the slowest to form. This is because the low number of available channels (5) for OFDM 868 MHz Option 1 increases the probability of collision in shared cells, slowing down neighbor discovery. The g6TiSCH formation time is in the same order of magnitude as FSK 868 MHz and O-QPSK 2.4 GHz networks in spite of the larger number of available links. This is because the g6TiSCH network dynamically improves its selected PHYs, its formation time remains within the same efficiency.

This can be observed in Fig. 5.5, which shows the number of PHYs selected for routing as the g6TiSCH network is forming. The multi-PHY neighbor discovery enables the network to combine the advantages of each PHY. On minimal cells of long-range PHYs such as FSK 868 MHz, a mote can hear a larger portion of the network with an increased risk of contention. On minimal cells of short-range PHYs such as O-QPSK 2.4 GHz, a mote can hear a smaller portion of the network with less risk of contention. Therefore, this leads to an overall robust network formation.

5.4.2 End-to-end Latency

We show in Fig. 5.6 a time-domain plot of the end-to-end latency in the network. The cumulative density of all the packets, during the steady state phase, is shown in Fig. 5.7. The longer range of OFDM 868 MHz and FSK 868 MHz (due to the sub-GHz band) leads to lower latency because of decreased re-transmissions and decreased number of hops. This is because motes are able to reach closer to the root thanks to the low ETX.

The g6TiSCH architecture exhibits a lower latency than each single-PHY network, although the best PHY for up-link is selected with respect to power consumption. Interestingly, it even demonstrates better latency than both the OFDM 868 MHz and

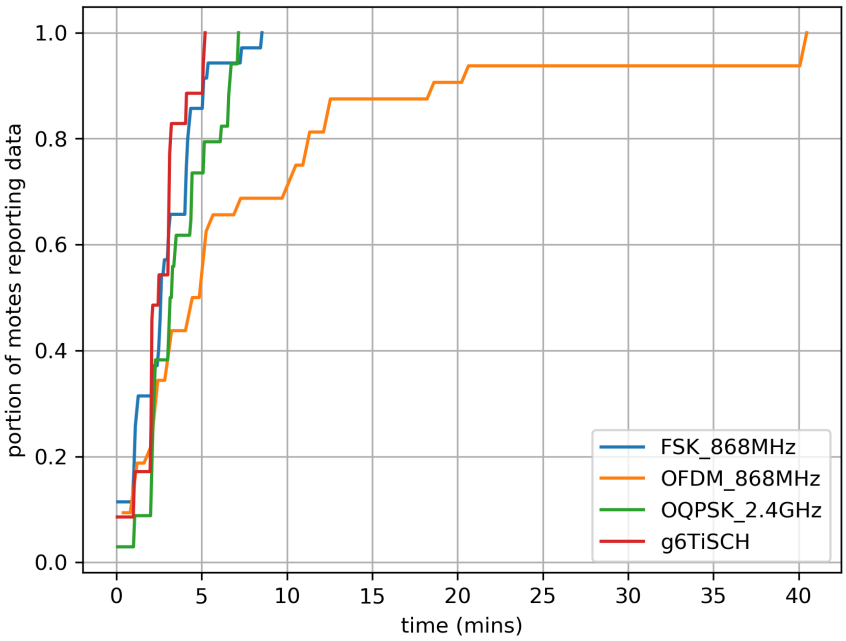

Figure 5.4: Dynamic selection among multiple radios allows a robust network formation, within the same order of magnitude as the long range FSK 868 MHz network.

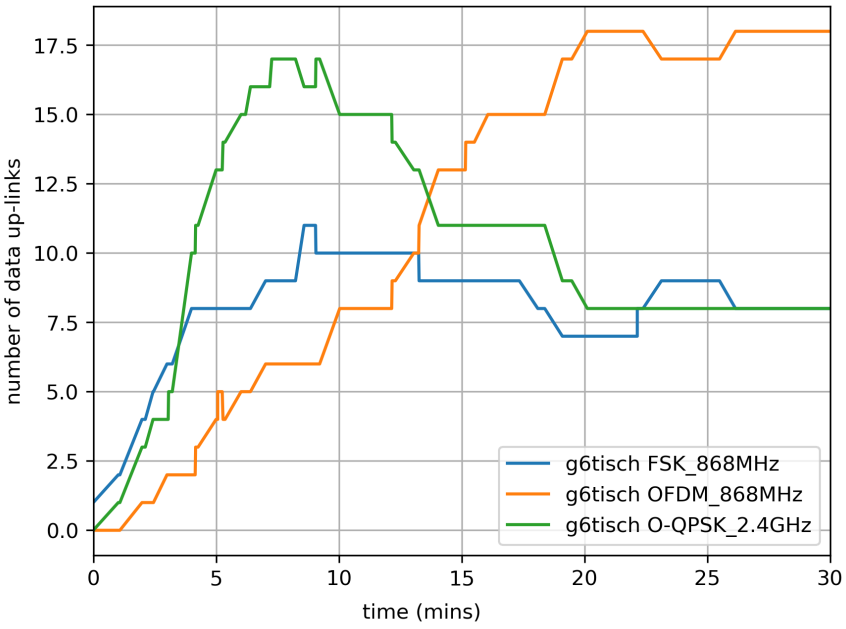

Figure 5.5: As the g6TiSCH data collection tree is forming, it routes up-link traffic over diverse PHYs.

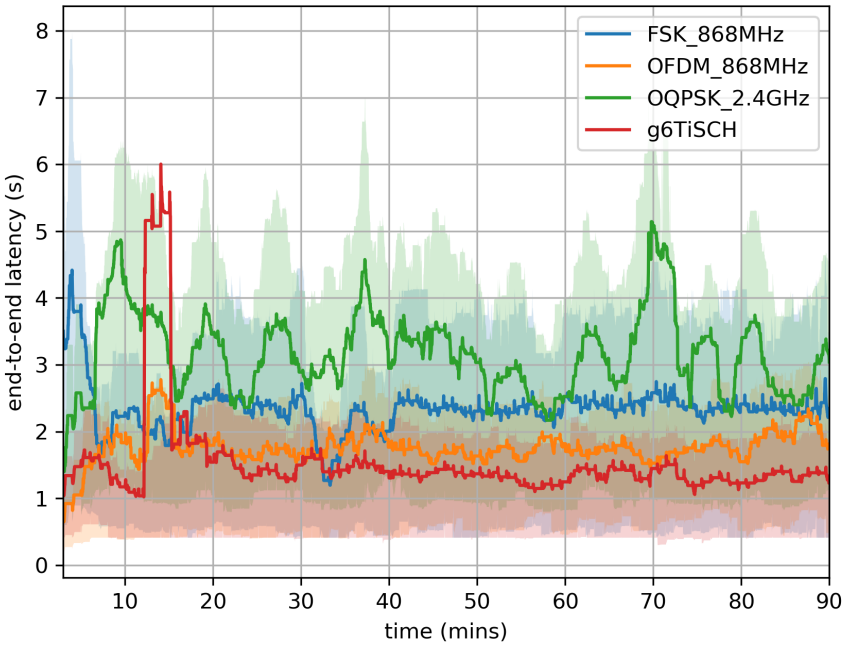

Figure 5.6: Using multiple radios at the same time yields lower end-to-end latency than using a single radio.

FSK 868 MHz networks. This is because the routing layer favors a parent switch only if the rank difference is more than 2 $\cdot$ $minHopIncrease$ as expressed in (5.3) (i.e. hysteresis), which is equivalent to two hops with perfect links. Therefore, in a single-PHY network, if a mote is two hops away from the root, it will still not pick the root as its parent since the cost improvement is not high enough to motivate the change of parent. This leads to sub-optimal latency for the benefit of network stability. However, in g6TiSCH, the $Factor(PHY_i)$ coefficient in the OF in (5.4) increases the cost of both FSK 868 MHz and O-QPSK 2.4 GHz links by a factor of 2 and 5, respectively. This is equal to or larger than the hysteresis threshold and therefore, it creates more incentive to find paths with lower ranks when possible, effectively leading to lower latency.

5.4.3 End-to-end reliability

End-to-end reliability is measured using the packet counter in the UDP packet to identify lost packets. End-to-end PDR is the ratio of received packets to total packets sent from a mote. Table 5.3 shows a statistical summary for the PDR for all motes in the last 30 min for each network. We note that the FSK 868 MHz network outperforms O-QPSK 2.4 GHz, which is consistent with the previous observation in [68]. g6TiSCH offers 100% reliability, the same as FSK 868 MHz, even though only 20% of the links used for routing use FSK 868 MHz (in steady state). The remaining links are 51% OFDM 868 MHz and 29% O-QPSK 2.4 GHz.

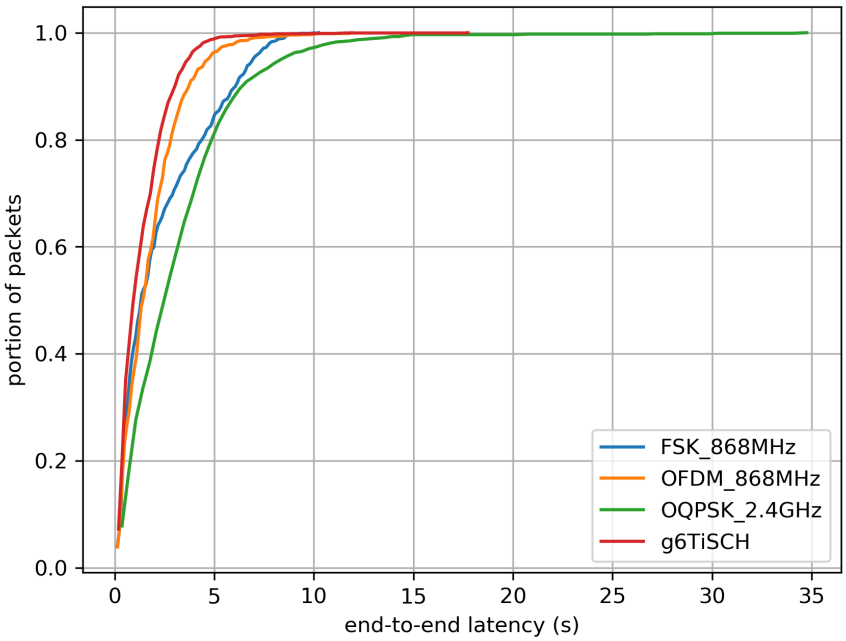

Figure 5.7: Cumulative distribution function of end-to-end latency, at steady state.

Table 5.3: End-to-end Packet Delivery Ratio (PDR) statistics over all motes in the network, computed over the last 30 min of the experiments.

	Min	**Average**	**Median**	**Max**	**StDev**
FSK 868 MHz	100.0%	100.0%	100.0%	100.0%	0.00%
OFDM 868 MHz	100.0%	100.0%	100.0%	100.0%	0.00%
O-QPSK 2.4 GHz	96.7%	99.7%	100.0%	100.0%	0.96%
g6TiSCH	100.0%	100.0%	100.0%	100.0%	0.00%

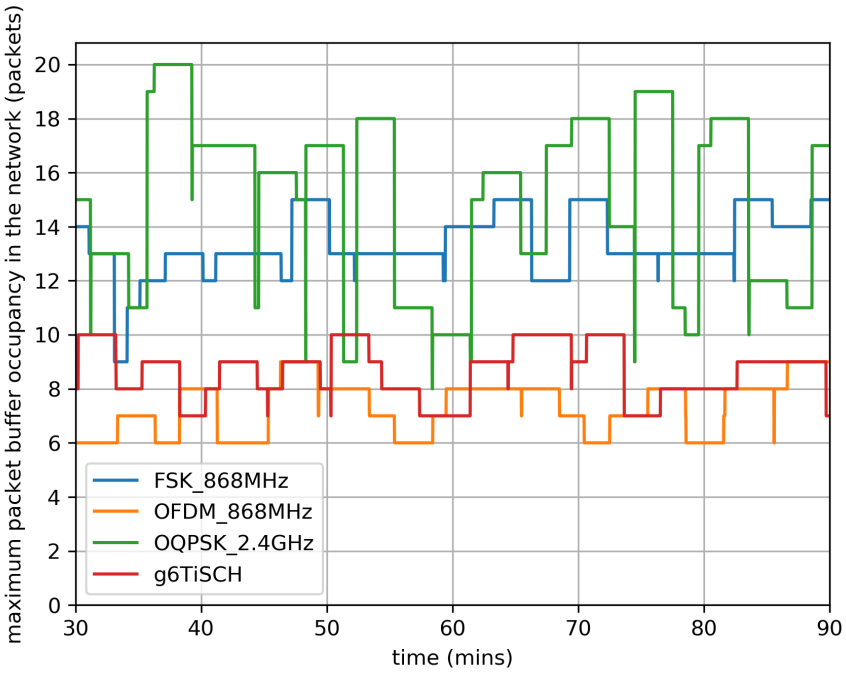

Figure 5.8: Improved overall link quality in g6TiSCH leads to efficient buffer usage due to less re-transmissions and forwarding. Packet buffer is efficiently used and packets are not dropped due to buffer overflow.

Packet loss can occur from packets being dropped because of buffer overflow. We show in Fig. 5.8 the maximum buffer size captured in the network. Both g6TiSCH and FSK 868 MHz show lower memory footprint than O-QPSK 2.4 GHz after 30 min into the experiment. This is because of decreased re-transmissions and forwarding as explained in Section 5.4.2.

This demonstrates an advantage of the generalized architecture: it achieves reliability comparable to that of a full FSK 868 MHz network, yet with only 20% of FSK 868 MHz links.

5.4.4 Battery lifetime

The battery lifetime is estimated based on the measured radio duty cycle during the experiment. We measure the duration the radio spends transmitting and the total duration the radio is on (including the time the radio spends in receive mode). While this is not a precise predictor of the battery lifetime, it is an indicator of the order of magnitude of lifetime for each network. Therefore it is sufficient for the purpose of comparing the networks. Fig. 5.9 shows the evolution of the transmit duty cycle in the network over the experiment duration. g6TiSCH shows an overall lower radio duty cycle than FSK by nearly 30%. This is attributed to it using OFDM 868 MHz and O-QPSK 2.4 GHz extensively, benefiting from their higher bit-rates.

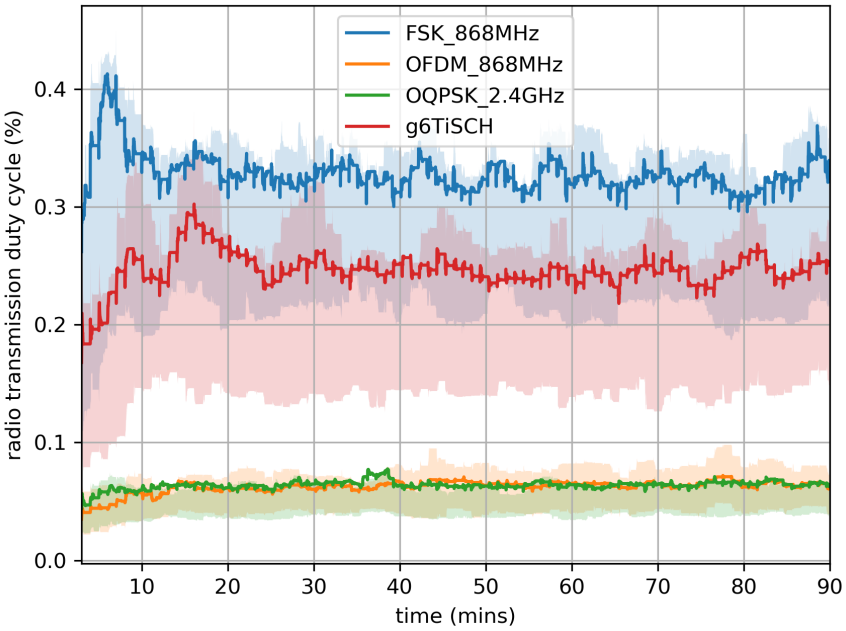

Figure 5.9: Diversity of radios allows overall lower radio duty cycle compared to a pure long range FSK 868 MHz network.

It is interesting to see the benefit g6TiSCH brings to RPL as it dynamically switches to parents with faster bit rates when possible (Section 5.2.3). This is measured by looking at how the duty cycle of each PHY evolves over time inside the g6TiSCH network. The impact can be seen in Fig. 5.10 as we observe that the duty cycles of FSK 868 MHz keep decreasing over time, along with a slight increase in OFDM 868 MHz duty cycle. This is because the g6TiSCH objective function ((5.4)) switches to parents with faster bit rates as the topology converges (based on the $Factor(PHY_i)$ parameter).

The battery lifetime of the single-PHY networks is estimated based on the power consumption of each PHY. We assume two 4.1 Wh "ideal batteries" in series, acting as a perfect voltage source (as previously assumed in Chapter 4). Since we are only interested in the overall orders of magnitude of power consumption for each PHY, this simple battery model is sufficient for this purpose. For a given T_{TX} and T_{on} for a specific PHY, we use (4.2) to compute the duty cycle of transmission DC_{TX} and the duty cycle in receive mode DC_{RX}.

From the data series of the DC measurements, we compute the global DC for the steady state (last 60 min in the network). Fig. 5.11 shows the expected battery lifetime at steady state for g6TiSCH compared to each single-PHY network. FSK 868 MHz has the shortest lifetime (compared to O-QPSK 2.4 GHz and OFDM 868 MHz), which was expected as it has the lowest bit-rate.

The battery-lifetime of g6TiSCH is estimated based on the duty cycle breakdown between the three PHYs. It demonstrates a distribution of battery lifetime for the

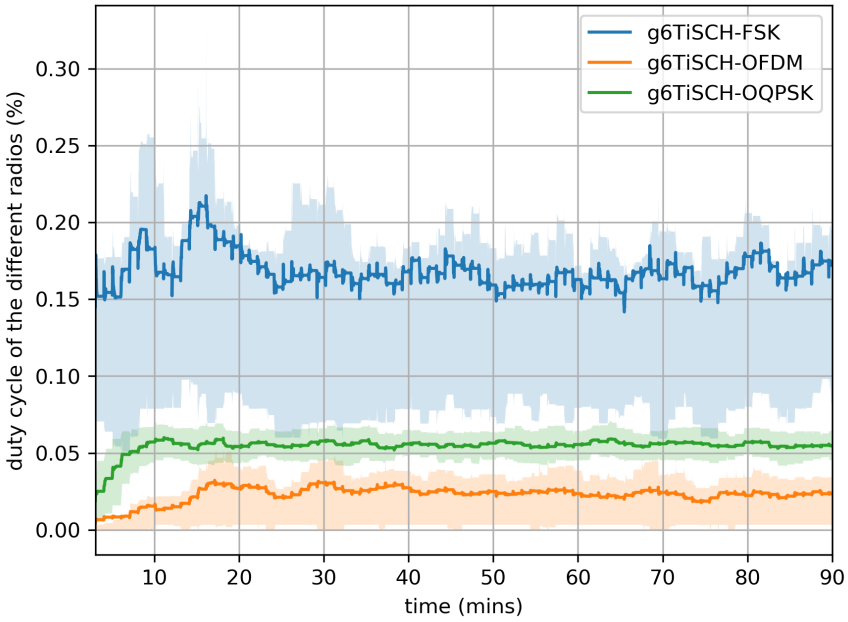

Figure 5.10: Over time, the objective function favors the use of OFDM 868 MHz over FSK 868 MHz and O-QPSK 2.4 GHz, saving on the transmission radio duty cycle.

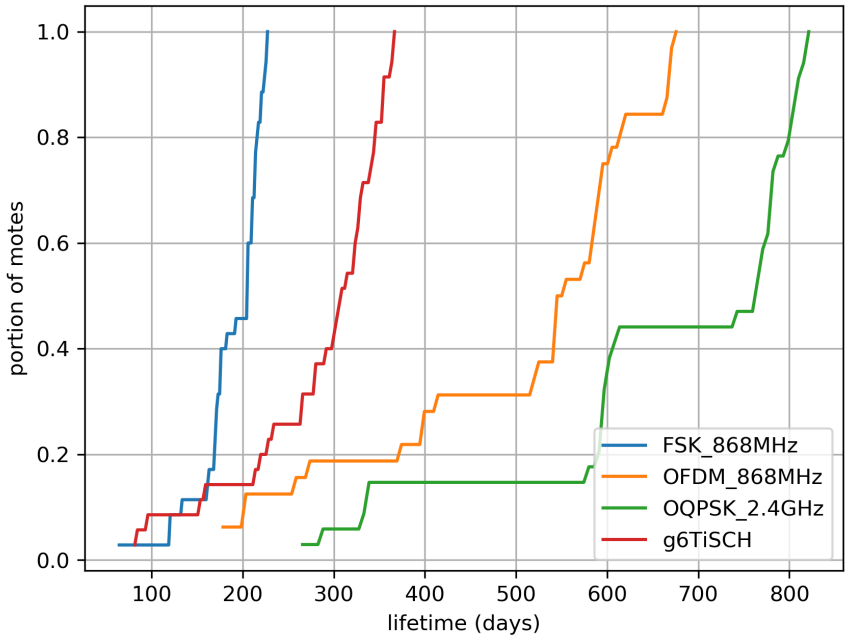

Figure 5.11: Cumulative distribution function of battery lifetime in the network demonstrates the g6TiSCH improving the energy footprint of the network compared to a pure long range FSK 868 MHz network.

nodes with a median that is 100 day higher than the FSK 868 MHz network thanks to the overall lower duty cycle. However, it has on overall the same network lifetime as FSK 868 MHz (i.e. time to first battery depletion). Therefore, there is an interesting room for improvement on this aspect by exploring a routing algorithm to optimize for network lifetime (which is a key focus of Chapter 7).

5.5 Conclusions

This chapter presents g6TiSCH, a generalized 6TiSCH architecture for multi-PHY wireless networking. g6TiSCH adds agility to the protocol stack: nodes can use diverse physical layers within the same network and adapt their links depending on their conditions, while maintaining wire-like reliability.

To introduce this agility, we augment the 6TiSCH protocol stack in different ways. At the MAC layer, we add the physical layer to use for each timeslot. At the 6LoWPAN adaptation layer, we demonstrate a generalized neighbor discovery mechanism where motes discover the network over different PHYs. At the RPL layer, we adapt the routing objective function with weighted link costs.

The resulting architecture is evaluated experimentally on the OpenTestbed to prove the soundness of the approach on a real-life scenario. We extract KPIs important for industrial applications. Experiments with g6TiSCH show fastest network formation, lowest latency, wire-like end-to-end reliability, and improved energy footprint compared to a pure long-range network. Furthermore, our proposed objective function for IPv6 RPL successfully steers the network topology, over time, towards energy efficiency. This is achieved by dynamically switching to faster bit-rates when possible, while maintaining latency and reliability performance.

While the quantitative results are specific to this experiment, the key findings hold. First, g6TiSCH provides more controls that help achieving a more balanced performance than single-PHY networks. Second, by combining long-range and short-range radios, g6TiSCH yields lower latency and network formation time than any of the individual PHYs, while maintaining a similar battery lifetime. Third, the routing layer in g6TiSCH improves the network's energy footprint over time by selecting faster links for routing. This balances performance and energy consumption of the network for deployments where there are both long and short distances between nodes. This provides an incentive to exploit the characteristics specific to each PHY and drive the network to build up trade-offs between energy consumption and performance in diverse use cases instead of having to choose one PHY over the other ones.

Chapter 6 introduces extending g6TiSCH with the use of slots with variable duration in the same slot frame in order to further lower latency. This way, a faster PHY can use a slot with smaller duration. This enables the network to have more compact schedule with both long and short duration slots. Furthermore, Chapter 7 explores, using RPL simulations, how to improve the battery lifetime of the network using multi-PHY routing. The RPL objective function relies on different metrics to improve the battery lifetime.

Chapter 6

Heterogeneous Slot Frames in 6TiSCH

Parts of this chapter were published as part of the following article: *6DYN: 6TiSCH with Heterogeneous Slot Durations*. Mina Rady, Quentin Lampin, Dominique Barthel, Thomas Watteyne. **MDPI Sensors**, special issue on Dependable IoT Networking vol. 21, no. 5, p. 1611, February **2021**.

Key Takeaways: In the previous chapters, we demonstrated that new radio chips implement different physical layers, allowing firmware to change modulation, datarate and frequency dynamically. This technological development is an opportunity for industrial low-power wireless networks to offer even higher determinism, including latency predictability. This chapter introduces 6DYN, an extension to the IETF 6TiSCH standards-based protocol stack. In a 6DYN network, nodes switch physical layer dynamically on a link-by-link basis, in order to exploit the diversity offered by this new technology agility. To offer low latency and high network capacity, 6DYN uses heterogeneous slot durations: the length of a slot in the 6TiSCH schedule depends on the physical layer used. This chapter shows how reserved bits in 6TiSCH headers can be used to standardize 6DYN and details its implementation in OpenWSN, a reference implementation of 6TiSCH.

In Chapter 5 we introduced a generalization of the 6TiSCH protocol for agile multi-PHY networking but using a slot-frame with the same slot duration. This chapter goes a step further by introducing 6DYN, a g6TiSCH extension in which a node dynamically changes its PHY *and* the slot duration at each time slot, depending on the bitrate of the used PHY.

Since 6TiSCH was designed on a fixed PHY, in today's 6TiSCH standard, all slots are of the same duration. The slot duration is tuned so there is time to transmit the longest supported frame and receive an acknowledgment. When using the IEEE802.15.4 2.4 GHz

PHY at 250 kbps, a slot is typically 10 ms long. When using multiple PHYs, we can have two approaches. The first is to settle for using the longest slot duration among all PHYs. This is the approach we previously took in Chapter 5. While this makes scheduling simple, it makes most slots artificially long, wasting latency and network capacity. A more complete approach is to vary the slot duration on a slot-by-slot basis, based on the PHY used. This is the approach 6DYN uses.

This chapter answers the following questions:

- *How can we build a g6TiSCH schedule with different slot durations?*
- *What are the minimal changes we need to make to the 6TiSCH standard to achieve this network agility?*
- *What are the benefits of 6DYN over using the longest duration?*

The remainder of this chapter is organized as follows. Section 6.1 states the problem and lists this chapter's contributions. Section 6.2 presents the design of 6DYN, including slot duration management, neighbor discovery and timeslot allocation. Section 6.3 lists the two small changes needed to the 6TiSCH standard to support 6DYN. Section 6.4 describes our implementation of 6DYN in OpenWSN, the reference implementation of 6TiSCH. Finally, Section 4.5 concludes this chapter.

6.1 Problem Statement and Contributions

In their IETF problem statement, Muñoz et al.discuss the challenges of integrating heterogeneous PHYs in 6TiSCH [72], including multi-PHY discovery of neighbors and routing.

6DYN is one answer to those challenges, with a particular focus on schedule compactness. In a 6TiSCH network today, a communication opportunity between neighbor nodes is identified by a timeslot and a channel offset. 6DYN adds one dimension to this, the PHY, as illustrated in Fig. 6.1. The result is that, when neighbor nodes communicate, they previously agree on the frequency band, modulation and bit-rate that make their communication most efficient.

The contribution of this chapter is three-fold:

1. 6DYN, a TSCH approach in which nodes use multiple PHYs in an efficient manner by managing a communication schedule with multiple slot durations
2. A draft standardization of 6DYN by crafting it as an extension of 6TiSCH
3. An implementation of 6DYN in OpenWSN, a reference open-source implementation of 6TiSCH

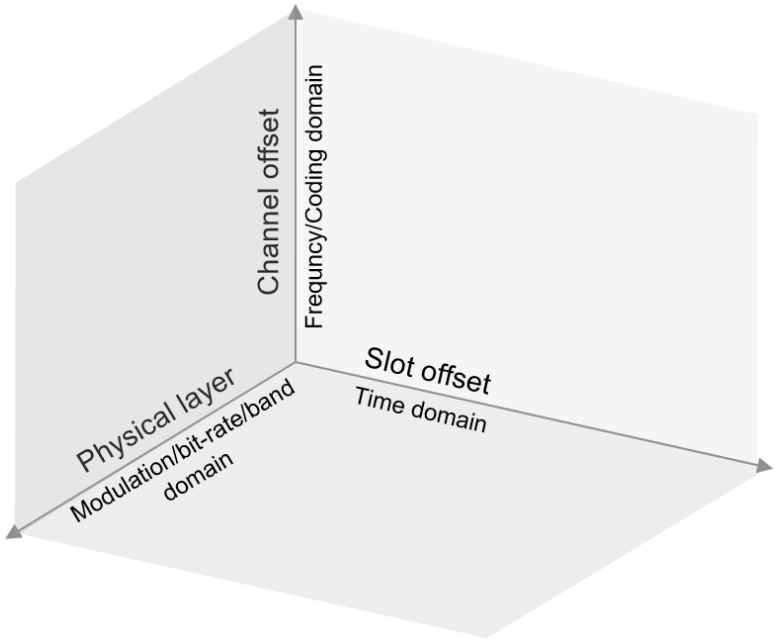

Figure 6.1: 6DYN assigns a PHY to each communication opportunity, on top of a timeslot and a channel offset.

6.2 6DYN: A TSCH Network with Heterogeneous Slot Durations

A typical TSCH slotframe is depicted in Fig. 1.3. In this example, each node in the network allocates a dedicated cell for its parent for uplink traffic. All nodes in the network use a uniform slot duration to construct their schedules, since all nodes only use a single PHY, O-QPSK 2.4 GHz at 250 kbps. In IEEE802.15.4, which 6TiSCH is based on, the maximum MAC payload is 127 B, which takes 4 ms to transmit. Taking into account the time-on-air of both the data frame and the acknowledgement that follows, as well as the turn-around and processing times, a slot duration of 10 or 20 ms is typical.

With the integration of the IEEE802.15.4g amendment, the IEEE802.15.4 standard comprises a wide range of PHYs. At sub-GHz, the PHY with the extreme bitrates are FSK 868 MHz at 50 kbps and OFDM 868 MHz at 800 kbps. At 2.4 GHz, O-QPSK 2.4 GHz offers a middle ground at 250 kbps, on a different frequency band. We showed that these three PHYs are complementary to one another, and being able to dynamically switch between them on a link-by-link basis offers diversity, which increases network performance (Chapter 4). Table 3.1 lists the PHYs.

Our previous proposal, g6TiSCH (Chapter 5), uses those three PHYs, but with a uniform slot duration, 40 ms. 6DYN is an extension of g6TiSCH where slots have different durations, as a mechanism to lower latency and increase network capacity.

The rest of this chapter is organized as follows. Section 6.2.1 focuses on the timeslot

templates for each PHY. Section 6.2.2 describes how slots with different durations can be combined in a single schedule. Section 6.2.3 details how neighbor nodes discover one another, on each PHY. Section 6.2.4 details how cells of different durations are allocated.

6.2.1 Timeslot Templates

To support each PHY in the same schedule, we first need to design their timeslot templates in accordance with IEEE 802.15.4e standard. We refer to the templates designed in Section 4.3. A full list of the factors that are considered in the design of a time-slot template is presented in Table 4.1. Fig. 4.1 is a capture of the logic analyzer, showing when the motes exchange a 127 B data frame (the maximum length), exchange an acknowledgment frame and communicate over SPI. As much as possible, we condense the activity at the beginning of the slot, in order to terminate the sequence as soon as possible within a slot.

We note that the FSK 868 MHz and OFDM 868 MHz PHYs require time for SPI transactions between the radio chip (AT86RF215) and the micro-controller (CC2538). For O-QPSK 2.4 GHz, the radio front-end is part of the CC2538 in a system-on-chip design. Fig. 4.1 shows that OFDM 868 MHz, O-QPSK 2.4 GHz and FSK 868 MHz transactions are over in roughly 10, 20 and 40 ms, respectively. We choose these "round" numbers because they make the slot lengths multiples of one another, significantly simplifying scheduling, as demonstrated in the following section.

6.2.2 Heterogeneous Slot Durations

How then can the different slot durations be integrated in the same slotframe? The approach by Brachmann et al. [59], inspired by IEEE802.11 WiFi networks, is to use the slowest bit rate PHY with a specific slot duration for control packets, and the highest bitrate PHY for data packets and grouping multiple slots for it. While this approach improves schedule compactness, it does not give the node the flexibility to use lower bit-rates for data transmissions in case the quality is poor.

Another approach in g6TiSCH is to use a uniform slot duration based on the slowest PHY (40 ms) as presented in Chapter 5, while allowing the node to switch between the three PHYs for data packet depending on link quality. This gives the mote flexibility to tune its performance by switching to faster bit-rates when possible or to slower bit-rates when necessary. It is also easier to manage the schedule using the existing scheduling policies that are designed to manage slots with a uniform slot duration. This does lead to schedule compactness and capacity problems: in each OFDM 868 MHz and O-QPSK 2.4 GHz slot, the mote wastes 30 or 20 ms, respectively.

We extend the approach of g6TiSCH by allowing for slots of different durations. We set the slot duration to that of the *fastest* PHY, 10 ms, and *group consecutive slots* when using slower PHYs, resulting in some longer "virtual" slots. Given the durations listed in Section 6.2.1, an O-QPSK 2.4 GHz slot occupies two consecutive slots, while an FSK 868 MHz slot occupies four consecutive slots. We use this approach for any dedicated cell that is dynamically negotiated between neighbors and use the slowest

bit-rate (FSK 868 MHz) for autonomous cells. Autonomous cells are used to "bootstrap" the negotiation.

Fig. 6.2 depicts the resulting heterogeneous slotframe for a multi-hop network of three motes and one root. On top of the 16 frequencies for O-QPSK 2.4 GHz, this schedule also includes 16 FSK 868 MHz frequencies with 200 kHz channel spacing and 5 OFDM 868 MHz frequencies with 1.2 MHz channel spacing. We use a slotframe length of 163 timeslots, resulting in a duration of 1.63 s, comparable to the 1.64 s used in g6TiSCH. A separate minimal cell is allocated at the beginning of the slotframe for each of the PHYs, for network-wide communication. Autonomous cells are allocated using the longest range FSK 868 MHz PHY.

6.2.3 Neighbor Discovery

Given that 6TiSCH is a multi-hop mesh network, nodes need to discover one another, on different PHYs. Among other things, this allows each node to pick the most suitable neighbor and the most suitable PHY, for up-link communication. In traditional 6TiSCH, all nodes that are part of a network send enhanced beacons on the schedule's minimal cell at a slow rate. By listening on that cell when not sending, a node eventually builds up a list of all the other nodes it can hear, i.e. its neighbors.

We adapt this discovery mechanism to multi-PHY discovery by having three distinct minimal cells, one for each PHY. Fig. 6.2 shows these cells. Since 6DYN is based on g6TiSCH, it follows the same generalized neighbor discovery mechanism introduced in Section 5.2.2 If a node has not joined the network yet, it listens for beacons using its FSK 868 MHz radio. After it hears an enhanced beacon, the node synchronizes to the network and continues listening for enhanced beacons only on the minimal cell. A mote's neighbor table contains one row per tuple (MAC address, PHY). This allows keeping the upper layers unchanged, notably the routing layer.

6.2.4 Timeslot Allocation

In a distributed network, neighbor nodes negotiate with one another to add/delete dedicated cells in their schedule to communicate. This mechanism is augmented to support multi-PHY operation: schedule a single cell to add an OFDM 868 MHz cell, schedule two consecutive cells to add an O-QPSK 2.4 GHz cell and schedule four consecutive cells to add an FSK 868 MHz cell. The node issuing the transaction proposes groups of contiguous cells that are unused in its schedule; the other node selects a group it is not using itself.

6.3 Extending 6TiSCH with 6DYN

As a path towards standardization, this section details how the 6TiSCH standard can be amended to support 6DYN. The goal is to make only small adjustments to the standard to simplify implementation and favor adoption. Implementing 6DYN does not require more adjustments to the frame formats other than what was already proposed for g6TiSCH

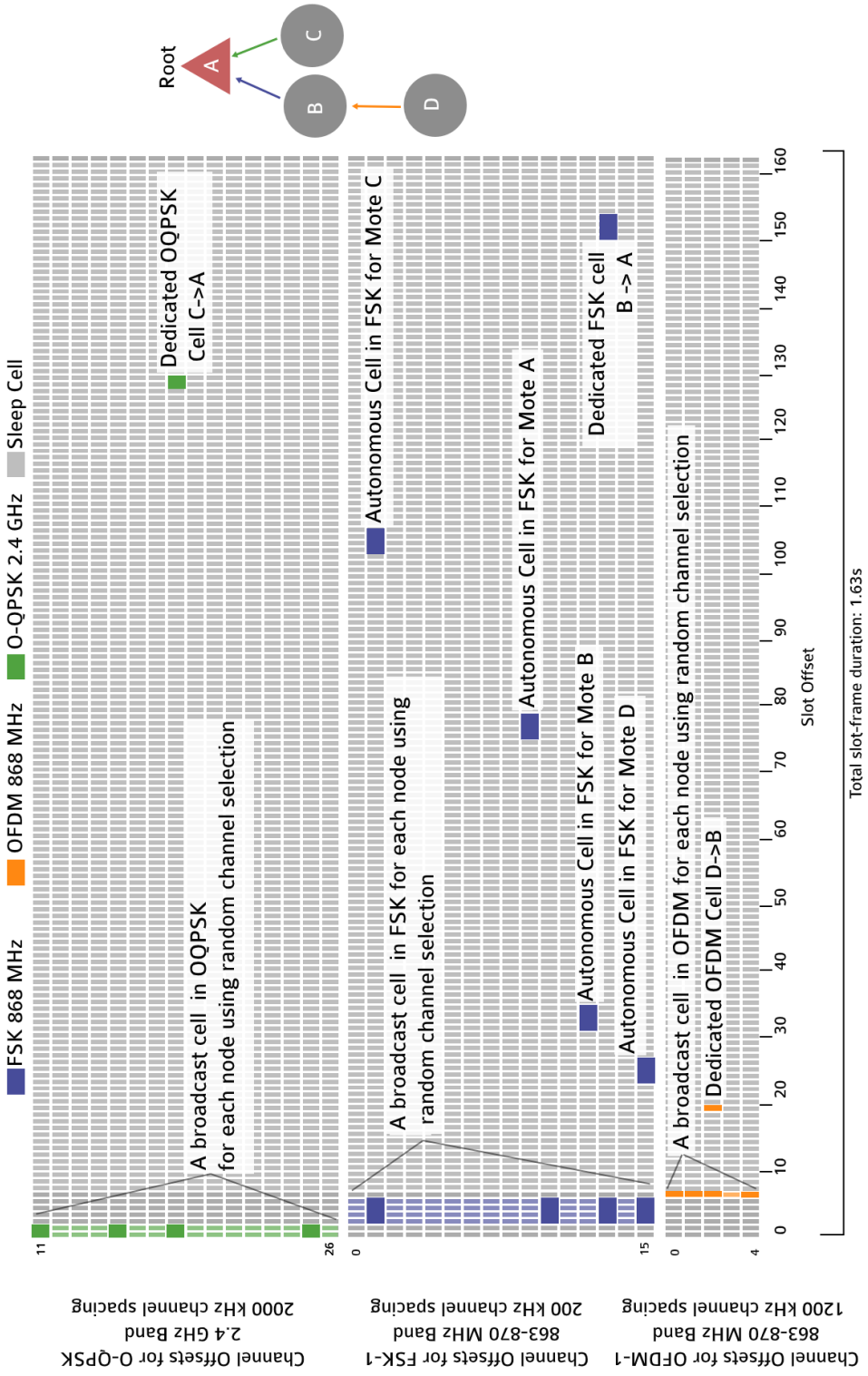

Figure 6.2: A heterogeneous slotframe for an example multihop topology, including broadcast cells for multi-PHY network discovery.

outlined in Section 5.2. However, the cell reservation algorithm is adapted to detect partial conflicts between cells that consist of slot groups as detailed in Section6.4

The first change is to encode the PHYs used in the network in the Enhanced Beacon (EB) [29]. Per the IEEE802.15.4 standard, the EB encodes the slot offsets of each minimal cell in the TSCH slot frame, and Link Information Elements [29]. In the Link Information Elements for each minimal cell, we use the left-most 3 bits of the Link Options byte to encode the type of PHY associated with each minimal cell. These bits are currently "reserved for future use" in the IEEE802.15.4 standard. This allows a mote that hears an EB during the joining process to bootstrap its schedule correctly. This mechanism further allows a network to use only a subset of the PHYs listed in Table 3.1. The remaining steps of the secure joining procedure of a node is carried out by the Constrained Join Protocol (CoJP) [76] and is unmodified. The resulting join process is illustrated in Fig. 5.1.

6P is used by neighbor nodes to negotiate when adding/deleting cells with one another [35]. The second change is to extend 6P for an ADD request to indicate which PHY to use. We use the left-most 3 bits of the Cell Options byte in the 6P header to encode the PHY index of the requested cells. These bits are currently "reserved for future use" in the 6P standard. The resulting 6P ADD transaction is illustrated in Fig. 5.2.

These two changes, while requiring a rigorous definition through an official standard, remain small changes to the standard. The remaining of the 6TiSCH standard remains unmodified.

6.4 Implementing 6DYN in OpenWSN

We extend OpenWSN, the 6TiSCH reference open-source implementation, with 6DYN. We demonstrate the running stack in the local hardware setup detailed in Section 3.2, including the debugging infrastructure. Section 6.4.1 highlights the key elements in the implementation of 6DYN. Section 6.4.2 shows 6DYN running on the OpenMote B board.

6.4.1 Implementing 6DYN

We implemented 6DYN in OpenWSN*, following the architecture indicated in Section 6.2 and the frame defined in Section 6.3. The implementation extends the `openradio` interface introduced in Section 5.2.1, by allowing variable slot durations for a slot-template. While the implementation is relatively straightforward, we believe the following details to be particularly important.

In our implementation, we encode the communication schedule as a circular linked list of cells, in increasing slot offset order. We only use a single entry in that linked list to represent a cell, regardless of the PHY used. This means that an FSK 868 MHz timeslot, which spans 40 ms (i.e. four cells), occupies the same memory footprint as a 10 ms OFDM 868 MHz timeslot. The fact that timeslots are ordered in a circular linked

* As an online addition to this chapter, all of the source code used is available at `https://github.com/openwsn-berkeley/`

list allows the implementation to iterate to the next slot without a time-consuming search operation.

The default implementation of MSF in OpenWSN allocates multiple entries in the same timeslot (i.e. backup slots). This is done so that, if there are no packets associated with this timeslot, the MAC layer executes a lower-priority slot entry [36], [77]. This implementation does not carry over directly to 6DYN, as slots can be partially overlapping. In our implementation, backup slots are allowed only for slots of the same size.

The flash memory footprint of g6TiSCH without the 6DYN extension is 79 kB. Implementing 6DYN increases that footprint to 84 kB, still very far from filling up the 512 kB of flash memory available on the OpenMote B.

6.4.2 Running 6DYN

To "witness" the execution of 6DYN, we use OpenMote B boards to form a link between two motes and a multi-hop network of four motes. On top of the 6DYN-enabled 6TiSCH protocol stack, on each mote, we run an application which periodically reports an incrementing counter (used to compute end-to-end reliability) and the radio duty cycle of each PHYs.

Fig. 6.3 shows the resulting real-time capture of MAC-layer events on both nodes (left) during a ping session from the root to the node (right) using 6DYN.

Fig. 6.4 shows the annotated activity of both nodes. Slot are 10 ms long, the slotframe is 163 slots long. On the left, per the neighbor discovery detailed in Section 6.3, we see the three minimal cells: a 20 ms O-QPSK 2.4 GHz cell, a 40 ms FSK 868 MHz cell and a 10 ms OFDM 868 MHz cell. Fig. 6.4 shows a dedicated cell using FSK 868 MHz, which the nodes negotiated using 6P, as detailed in Section 6.3. Finally, we see each node switching on its radio during its autonomous cell; each node listens for a short period and turns off its radio as no frame is received.

Fig. 6.5 shows the activity of four motes implementing 6DYN and forming a multi-hop network. It shows how different pairs of nodes establish different links (`D`→`B`, `B`→`A` and `C`→`A`), incidentally each using a different PHY.

6.5 Conclusions

New radio chips implement multiple PHY layers, offering different trade-offs between range, data rate and power consumption. Because a low-power wireless network is composed of many links, each with different characteristics, being able to dynamically change between PHYs on a link-by-link basis yields higher network performance than locking the entire network to a single PHY. Recent proposals, such as a g6TiSCH (Chapter 5), propose a networking approach which allows for this technology agility, in a time slotted and scheduled manner. They do so, however, by aligning the duration of a timeslot to the slowest PHY layer. While this simplifies the implementation, the

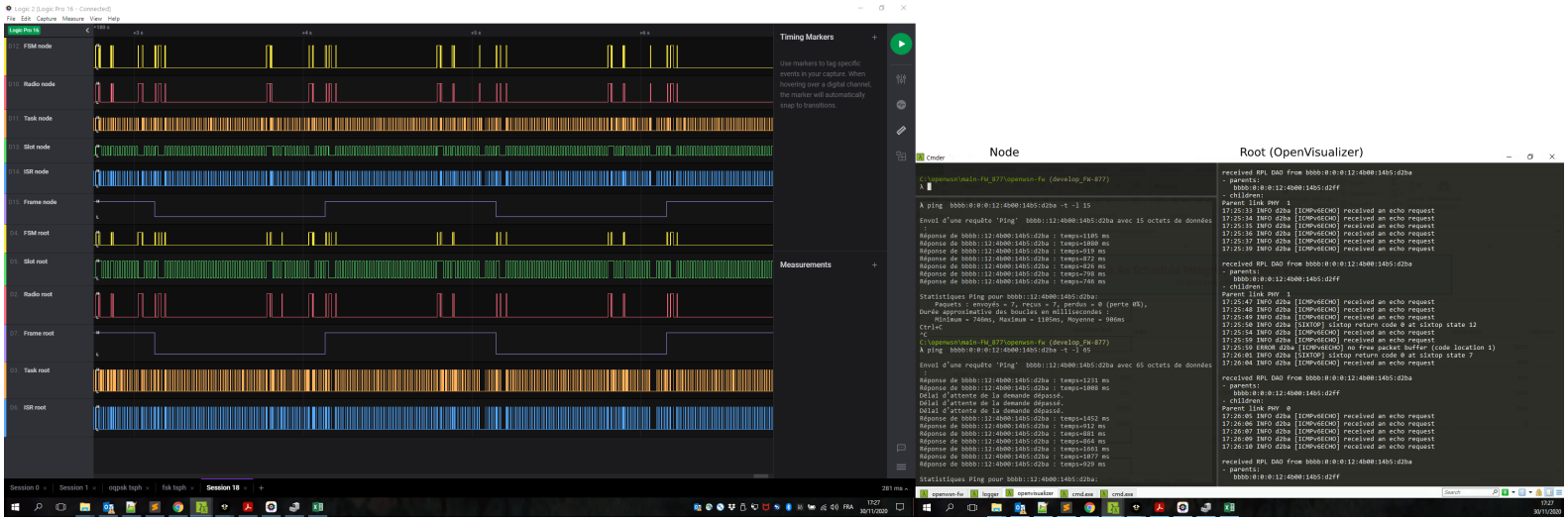

Figure 6.3: Logic Analyzer capture (left) showing the activity between root and node while a pinging session is open (right) using 6DYN.

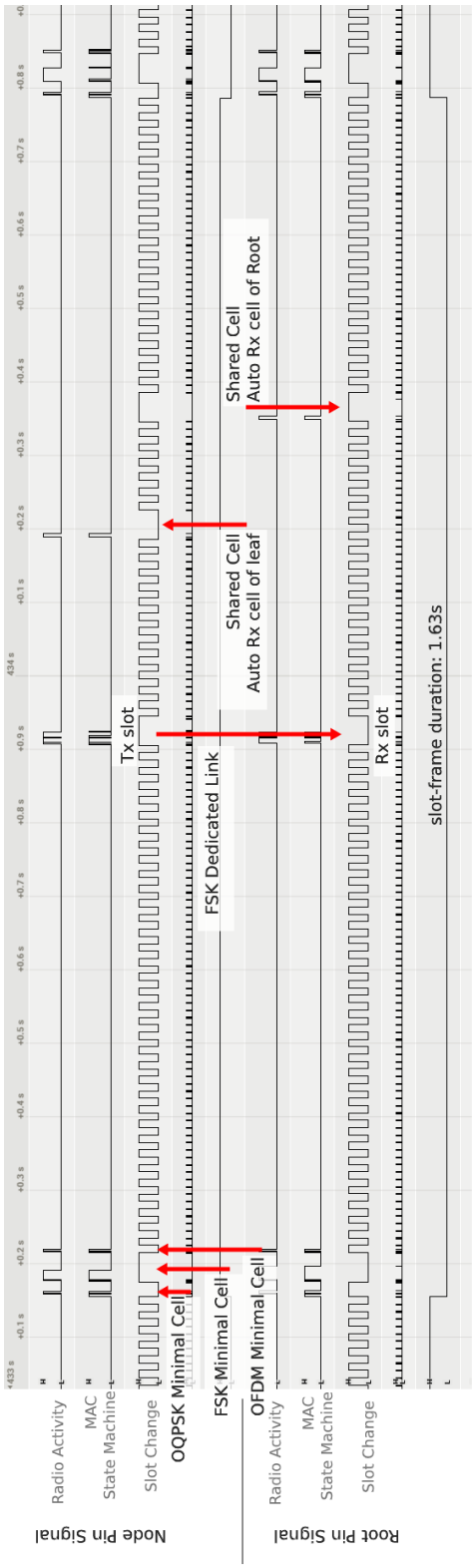

Figure 6.4: Logic analyzer trace showing the activity of two neighbors nodes communicating using 6DYN.

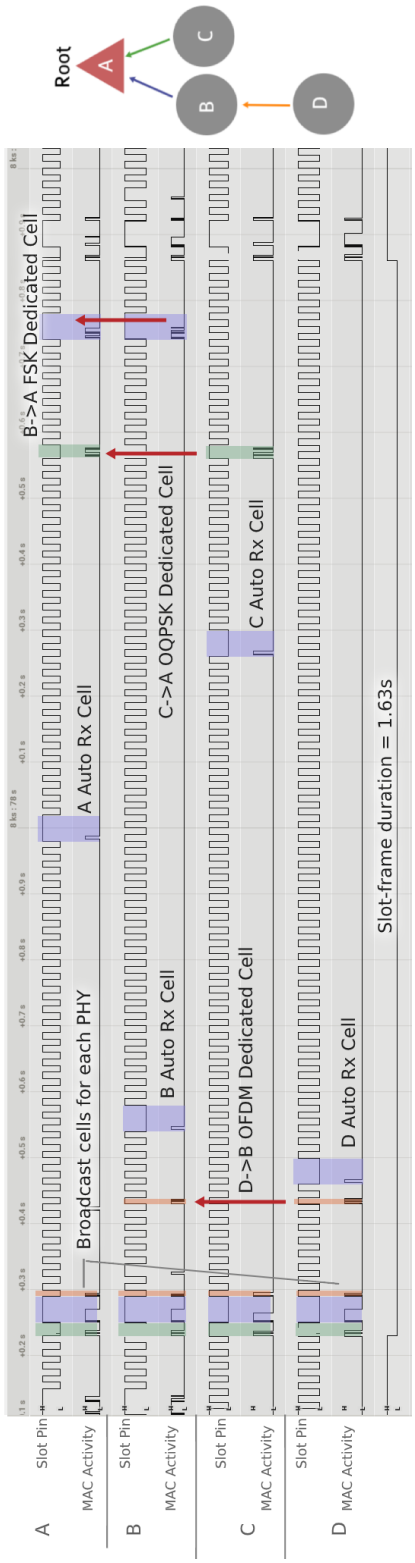

Figure 6.5: Logic analyzer trace showing the activity of four motes implementing 6DYN and forming a multi-hop network. The resulting schedule corresponds to Fig. 6.2.

time “wasted” when using faster PHYs results in increase latency and reduces network capacity.

This chapter introduces 6DYN, a time-synchronized channel hopping protocol which uses heterogeneous timeslot durations. 6DYN defines different timeslot durations: 10 ms when using OFDM 868 MHz, 20 ms when using O-QPSK 2.4 GHz and 40 ms when using FSK 868 MHz. 6DYN offers diversity across modulations, data rate and frequency bands. We detail how 6DYN achieves multi-PHY neighbor discovery and how timeslots are allocated. We also show how reusing two sets of reserved bits in packet headers makes 6DYN easy to standardize as an extension to 6TiSCH. We implemented 6DYN in OpenWSN, the reference implementation of 6TiSCH, an extension that is available to the community.

We see 6DYN as a step towards deterministic networks in industrial applications (e.g., control loops), made possible by multi-PHY chips. In the next chapter, we move up to the routing layer. We address how routing metrics can be adapted to improve the network lifetime by making good use of diverse PHYs in the network.

Chapter 7

Multi-PHY Routing in RPL for Extending Network Lifetime

Parts of this chapter were published as part of the following article: *Bringing Life out of Diversity: Boosting Network Lifetime using Multi-PHY Routing in RPL.* Mina Rady, Quentin Lampin, Dominique Barthel, Thomas Watteyne. **Wiley Transactions on Emerging Telecommunications (ETT)**, *under review.*

Key Takeaways: In this chapter, we propose a routing mechanism based on the RPL protocol in a wireless network that is equipped with a mix of short-range and long-range radios. We introduce Life-OF, an objective function for RPL which uses a combination of metrics and the diverse physical layers to boost the network's lifetime. We evaluate the performance of Life-OF compared to the classical MRHOF objective function through simulation. Two Key Performance Indicators (KPIs) are reported: network lifetime, network latency. Results demonstrate that MRHOF tends to converge to a pure long-range network, leading to short network lifetime. In contrast, Life-OF improves network lifetime by continuously adapting the routing topology to favor routing over nodes with longest remaining lifetime. Life-OF combines diverse radios and balances power consumption in the network. This way, nodes switch between using their short-range radio to improve their own battery lifetime and using their long-range radio to avoid routers that are close to depletion. Results show that using Life-OF improves the lifetime of the network by up to 300% compared to MRHOF, while maintaining similar latency.

In the previous chapters we demonstrated mechanisms for multi-PHY integration under a generalized 6TiSCH protocol stack. This chapter goes a step further by exploring how can multi-PHY integration improve network lifetime.

Why, then, does it make sense to optimize for network lifetime as opposed to simply selecting links with the least power consumption? The reason is that, in many cases,

optimizing for energy saving alone does not necessarily mean optimizing for network cost [78]. Network cost can be defined by the hours spent by employees for replacing the batteries and the salaries involved. In those cases, network devices are maintained by dispatching employees, either to nearby or to remote locations, to replace the depleted batteries of nodes. This leads to a situation where the cost of the actual batteries is negligible compared to the cost of battery replacement. In this case, the real cost of running the network can be expressed as the number of times employees are mobilized to replace a battery (regardless whether it is for one device or all the devices). For instance, a network can have 90% of its motes living for 5 years with 10% of the motes that die after 6 months. In this case, the real cost of running the network is the cost of one battery replacement mission per *six months*. However, if 100% of the nodes have a 2-year battery lifetime, the effective cost of running the network is one battery replacement mission every *two years*. The latter scenario is more budget-efficient, even if it has an overall lower average battery lifetime. Therefore, it becomes desirable to improve the time for the first battery to deplete and have all nodes reach the end of their batteries at approximately the same time.

In this chapter, we propose an OF that improves network lifetime using dynamically calculated metrics and using a heterogeneous physical layer. We call it the Lifetime Objective Function, "Life-OF". When using this OF, the network alternates between two kinds of connectivity are: (1) a node uses short-range PHYs to save its own energy (while having its neighbors consume more energy); (2) it uses long-range PHYs, thereby saving the energy of its neighbors. The result is that the network re-routes traffic to avoid relay nodes that are close to full depletion. We demonstrate the performance of this OF by simulating nodes that are equipped with radios that vary in link-budget, bit-rate, frequency band, and power consumption. Specifically, we use the following PHYs: FSK 868 MHz as a the slowest bit-rate PHY, OFDM 868 MHz as the fastest bit-rate PHY, the canonical O-QPSK 2.4 GHz as an in-between option.

The remainder of this chapter is organized as follows. Section 7.1 defines the problem statement and presents the specific contributions of the chapter. Section 7.2 outlines the components of the routing algorithm for Life-OF. Section 7.3 presents the simulation results. Finally, Section 7.4 presents the conclusions of the chapter.

7.1 Problem Statement and Contributions

Previous research on the optimization of LPWAN architectures has demonstrated that optimizing for energy consumption in the network may *not* necessarily result in lower network costs [78]. An example of this is the case where the cost of battery replacement is fixed whether it is for one mote or for the entire network. This cost reflects the paid-time of staff members to collect all the nodes and have all their batteries replaced. Therefore, this cost is incurred once the first mote has died, regardless how much energy was still remaining in the other motes.

Availability of radio chips that support changing PHYs on a frame by frame basis can offer a chance to improve network lifetime. First, if a node has remaining lifetime

less than its surrounding routers, it can extend its own lifetime by switching to route its traffic using a more energy efficient PHY (i.e. a short-range PHY). Second, if a node has remaining lifetime that is higher than its surrounding routers, it can relieve the routers by using a longer range PHY to bypass them and reach the root directly (or to reach the closest point to the root).

Achieving this multi-PHY integration in RPL was identified in an IETF problem statement by Muñoz et al. [72]. We demonstrate in the g6TiSCH architecture in Chapter 5 how a simple adaptation to RPL for multi-PHY integration can provide a balanced network performance. This research aims at going one step further by proposing an OF that optimizes for network lifetime while harnessing the advantages of heterogeneous PHYs.

Specifically, the contribution of this chapter is three-fold:

- We propose Life-OF: an OF for RPL that improves network lifetime using a heterogeneous physical layer.
- We evaluate the performance of Life-OF by simulation in long-range industrial scenarios, and compare its performance against MRHOF in a single-PHY setting and in a multi-PHY setting.
- We demonstrate that using Life-OF in a multi-PHY network leads to the best network lifetime at the expense of increasing latency of only 10% of the nodes by up to 300%.

7.2 The Routing Algorithm

This section outlines the adaptations necessary for RPL to optimize for network lifetime. The adaptations to RPL to integrate Life-OF consist of four main components:

- Path evaluation and selection (i.e. the objective function).
- Calculation of remaining battery lifetime by each node.
- Calculation of the node's new rank.
- Identifying the RPL protocol elements required by Life-OF.

Fig. 7.1 is a high-level diagram that shows how the components interact with each other in a closed loop. The component for evaluating the node's remaining lifetime keeps track of the duty cycles for the different PHYs for a certain period.

The "path evaluation and selection" component keeps track of the current node's rank and the advertised ranks of each neighbor. Based on Life-OF, it selects the path with the best estimated path metric. At the beginning of a defined period (i.e. an epoch), the "Node remaining lifetime evaluation" component estimates the node's lifetime based on the usage of each PHY, its power consumption, and the remaining battery energy.

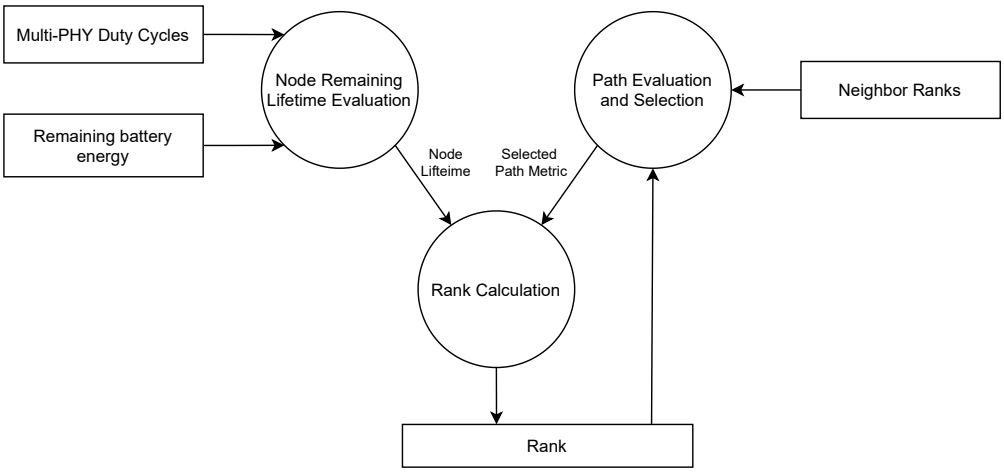

Figure 7.1: A logical diagram of interaction between the components of the Life-OF.

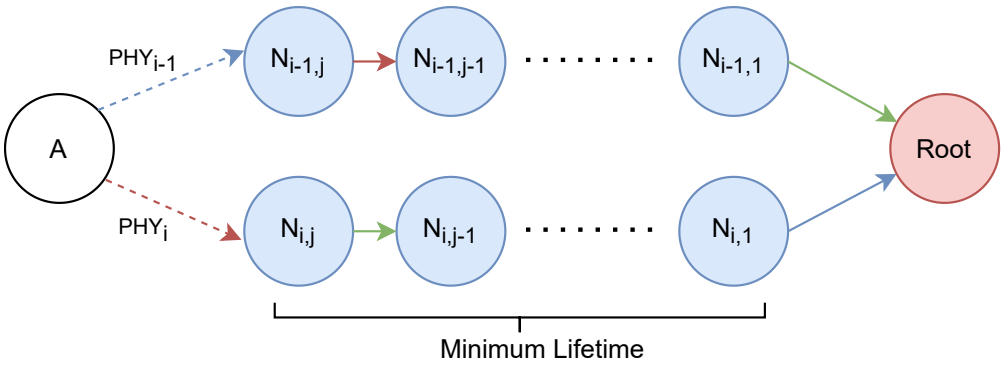

Figure 7.2: Example topology to illustrate the behavior of Life-OF for path selection in a multi-PHY topology

Whenever there is a new lifetime estimation or a newly selected path, the node's rank is calculated by the "rank calculation" component.

The remainder of this section describes the behavior of each component.

7.2.1 Path Evaluation

This section describes how a node evaluates a cost for each neighbor and the path selection criteria. We consider a neighbor to be a combination of node and PHY layer. Each neighbor i has a designated rank: $Rank_i$. Each PHY_i has a designated weight that corresponds to its expected power consumption and ETX. We refer to this as weighted ETX $\text{WETX}(\text{PHY}_\text{i})$.

We define a function that estimates a cost for each neighbor i based on the $Rank_i$ and $\text{WETX}(\text{PHY}_\text{i})$. The objective is to select the neighbor with the *lowest* cost among available neighbors. We illustrate in Fig. 7.2 a scenario where node A is making a routing

decision between paths through N_i and N_{i-1}. Let the whole network agree on a common set of PHYs: $\Phi = \{PHY^1, \ldots, PHY^L\}$. Let node A have K neighbors and use $\mathrm{PHY_i}$ with neighbor i, with $\mathrm{PHY_i} \in \Phi$.

To obtain the cost, $\mathrm{WETX(PHY_i)}$ has to be derived at first as follows:

- Energy per bit (E_b) for all PHYs is obtained through (7.1), where I_i is the current consumption of the radio chip of $\mathrm{PHY_i}$ in amps, V_i is the voltage in volts, and the bitrate is in bps.
- $\mathrm{EnergyWeight(PHY_i)}$ is obtained by normalizing the E_b of all the PHYs with respect to the PHY with the lowest E_b according to (7.2).
- $\mathrm{ETX(PHY_i)}$ is obtained using (7.3) where $\mathrm{numTx_i}$ is the number of transmissions to neighbor i, $\mathrm{numAck_i}$ is the number of received acknowledgments.
- $\mathrm{WETX(PHY_i)}$ is obtained as a function of $\mathrm{EnergyWeight(PHY_i)}$ and $\mathrm{ETX(PHY_i)}$, per (7.4)

$$\text{Energy Per Bit}(\mathrm{PHY_i}) = \frac{\mathrm{I_i} \times \mathrm{V_i}}{\mathrm{Bitrate_i}} \tag{7.1}$$

$$\text{Energy Weight}(\mathrm{PHY_i}) = \frac{\text{Energy Per Bit}(\mathrm{PHY_i})}{\mathrm{Min}(\text{Energy Per Bit}(\mathrm{PHY_1}, \ldots, \mathrm{PHY_L}))} \tag{7.2}$$

$$\mathrm{ETX_i} = \frac{\mathrm{numTx_i}}{\mathrm{numAck_i}} \tag{7.3}$$

$$\mathrm{WETX(PHY_i)} = \mathrm{EnergyWeight(PHY_i)} \times \mathrm{ETX(PHY_i)} \tag{7.4}$$

The cost of the path through a neighbor N_i is per (7.5).

$$\mathrm{Cost(N_i)} = \frac{\mathrm{Rank(i)}}{\mathrm{WETX(PHY_i)}} + \mathrm{MinHopRankIncrease} \tag{7.5}$$

Where:

- We define $Rank_i$ using a range of values from $[-50, -10^5]$, where -50 is the highest possible rank (i.e. least preferable), and -10^5 is the best possible rank (i.e. the advertised rank of the root)
- `MinHopRankIncrease` is a constant value to guarantee loop avoidance by ensuring that the rank decreases monotonically across a given path.

The reasoning behind the formulation in (7.5) is as follows. $Rank_i$ expresses the rank of the neighbor, and therefore, the lower, the better. If both neighbor N_i and N_{i-1} have the same rank, then the neighbor with the PHY of lower energy weight will result into a lower rank, and therefore will be favored as per (7.4), (7.2), and (7.1). If both neighbors share the same rank and the same PHY, then the neighbor with the lower ETX – as per (7.4) and (7.3) – will be favored.

7.2.2 Node Lifetime Estimation

Estimating the lifetime of a node is key as a node metric and as a path metric as well. If a node has a low lifetime, it should favor higher bit-rate PHYs for up-link and it should also be avoided by other nodes to be used as a router.

The remaining lifetime of a node can be estimated in two ways, depending on the available hardware. Some boards are equipped with circuits that allow measuring the remaining battery charge. This allows keeping track of charge withdraw and subsequently estimating the remaining lifetime of the node. However, other boards may not have that circuitry in place and therefore cannot have that necessary information from the hardware. In our approach, we assume the scenario where this circuitry is not available and we demonstrate how a node can estimate its energy consumption and remaining battery energy. Therefore, the node's remaining lifetime is estimated *(1)* by monitoring the average power consumption of each PHY and *(2)* by estimating its remaining lifetime.

To estimate the average power consumption of L available PHYs, the node keeps track of the duty cycle of each PHY j in receive mode and in transmission. Based on the power characteristics of each PHY, the node can estimate the overall power consumption of the different PHYs. The average power consumption of node A can be estimated as $Power(A)$ as per (7.6). After a certain duration ΔT, the node re-computes its remaining battery energy according to (7.7). The remaining node lifetime can be estimated based on the remaining battery energy according to (7.8)

$$\begin{aligned}\text{Power Consumption(A)} = \\ \sum_{\text{j=0}}^{\text{L}} \text{Duty Cycle}_{\text{rx}}(\text{PHY}_\text{j}) \times \text{I}_{\text{rx}}(\text{PHY}_\text{j}) \times \text{V}(\text{PHY}_\text{j}) + \\ \sum_{\text{j=0}}^{\text{L}} \text{Duty Cycle}_{\text{tx}}(\text{PHY}_\text{j}) \times \text{I}_{\text{tx}}(\text{PHY}_\text{j}) \times \text{V}(\text{PHY}_\text{j})\end{aligned} \tag{7.6}$$

$$\text{Remaining Battery Energy} = \text{Latest Battery Energy} - (\text{Power Consumption(A)} \times \Delta\text{T}) \tag{7.7}$$

$$\text{Lifetime} = \frac{\text{Remaining Battery Energy}}{\text{Power Consumption}} \tag{7.8}$$

We are aware that there are different internal activities that can consume significant power compared to radio activities such as certain kinds of sensors or extensions to the node. Since this chapter focuses on the routing protocol on top of heterogeneous radios, we choose to assume that the power consumption of non-radio components is the same across all nodes.

The energy weights are calculated for the used PHYs based on their power characteristics (Table 3.2). The resulting energy weights are outlined in Table 7.1

In the following sub-section, we describe how a node calculates its new rank.

Table 7.1: Derived energy weights of the simulated PHYs

	FSK 868 MHz	**OFDM 868 MHz**	**O-QPSK 2.4 GHz**
Radio chip	AT86RF215	AT86RF215	CC2538
Energy per bit	4.50 μJ	0.28 μJ	0.53 μJ
Energy weight*	16.00	1.00	1.89

(*) Normalized as ratio to the PHY with the lowest energy per bit (i.e. OFDM 868 MHz)

7.2.3 Node Rank Calculation

In a classical RPL OF such as MRHOF, the rank can be influenced by only one dynamic metric: path ETX. In Life-OF, the rank of the node is influenced by three dynamic metrics: path lifetime, path hop-count, and path ETX. As illustrated in Fig. 7.1, in Life-OF, the rank of a node is re-calculated when one of two following events take place: *(1)* there is new estimation of the lifetime of the node, *(2)* the node changes parent.

In the first case, when there is new estimation of the lifetime of a node, the new rank $Rank'$ is calculated as follows. Let node A (Fig. 7.2) have a route through N_{i-1}. Assume the lifetime of node A (Fig. 7.2) changes at an epoch, it obtains the following metrics:

- The path lifetime (years): the minimum of the lifetimes of all the nodes in the path *except* the root *and* the node itself. We call this Lifetime($\overrightarrow{N_{i-1}}$).
- The path hop-count (hops): the number of hops to the root. We call this Hop Count($\overrightarrow{N_{i-1}}$)
- The energy weight of PHY_{i-1}, calculated as WETX($\mathrm{PHY_{i-1}}$) according to (7.4).

Subsequently, the new rank $Rank'$ is calculated using these metrics according to (7.9).

$$\begin{aligned}\mathrm{Rank'(A)} = &\frac{-1 \times \mathrm{Lifetime}(\overrightarrow{N_{i-1}}) \times 10^5}{\mathrm{WETX}(\mathrm{PHY_{i-1}})} \\ &+ \mathrm{Hop\ Count}(\overrightarrow{N_{i-1}}) \times \mathrm{MinHopRankIncrease}\end{aligned} \tag{7.9}$$

The reasoning behind this formulation is as follows. A lower rank indicates better position in the network and a better candidate for routing. Therefore, higher lifetime leads to lower rank as it is converted to a negative value. A scaling factor of 10^5 is used to increase sensitivity to path lifetime. Using this value for scaling factor allows the rank to remain below -1 when the path lifetime goes down to one day and the node is two FSK hops away from the root. If the node is routing over a PHY with higher WETX, its advertised rank will be lower accordingly. This way, its attractiveness as a router decreases by a factor of WETX. Finally, adding the number of path hops makes nodes closer to the root (along the same path) more attractive as routers.

Table 7.2: Specification of the DAG Metric Container

	Metric Type	`R-Flag`	`A-Field`
Node Lifetime	Node State and Attribute Object	0 (Aggregate)	2 (Minimum)
Hop Count	Hop Count Object	0 (Aggregate)	0 (Additive)
ETX	Link Reliability Object	0 (Aggregate)	0 (Additive)

In the second case, if node A switches to a new path through neighbor N_i (while its own remaining lifetime has not changed), it calculates its new rank $Rank'$ according to (7.10). $Rank'$ is then the new advertised rank for node A.

$$\begin{aligned} \mathrm{Rank'(A)} = \mathrm{Max}\left(\mathrm{Rank(A)}, \frac{\mathrm{Rank(N_i)}}{\mathrm{WETX(PHY_i)}}\right) \\ + \mathrm{WETX(PHY_i)} \times \mathrm{MinHopRankIncrease} \end{aligned} \tag{7.10}$$

The reasoning behind this formulation is similar to the previous formulation. We note that the worse rank between the node and its parent is identified using the expression $Max(Rank(A), Rank(N_i))$. This way, the node advertises the worst case scenario along its path. Finally, we add $\mathrm{WETX(PHY_i)} \times \mathrm{MinHopRankIncrease}$ to increase the attractiveness of nodes higher up the same path.

In the following sub-section, we describe a specification within the RPL protocol to implement Life-OF.

7.2.4 RPL Protocol Elements

We want to understand what changes to RPL are needed to enable Life-OF.

First, we propose that the RPL DMCs contain three different metrics derived from the standard [33]: node lifetime, path hop-count, and link ETX. A DMC is an option within RPL DAO and DIO control messages that is used to express metrics used for the DODAG. The DMC "may contain a number of discrete node, link, and aggregate path metrics and constraints specified in [33] as chosen by the implementer" [32]. Table 7.2 outlines how each metric can be specified within the RPL standard and the relevant settings in DMC flag field (as introduced in Section 2.5.1). Life-OF only uses the link-level ETX metric and does not need a path-level ETX metric. We propose to keep ETX as a path metric in the DMC for performance comparison with MRHOF.

Second, execution of Life-OF should be triggered when the estimated node lifetime changes (in addition to normal triggers such as reception of DIOs). This additional trigger conforms to the Objective Function guidelines in RFC 6550. It is important to choose a balanced duration of sampling the node's power consumption and remaining battery energy. On the one hand, the sampling duration should be long enough to provide reliable lifetime estimations and therefore stable routing decisions. On the other hand, it should not be too long that it prevents nodes from reacting fast enough when they are undergoing heavy power consumption.

7.3 Results

To evaluate the performance of Life-OF, we use the simulation setup and methodology outlined in Section 3.3.2. This section presents the results of the simulation runs. The section is organized in four parts. First, we give an example of a network topology and show the behavior of Life-OF in comparison with MRHOF in a multi-PHY network. Second, we evaluate the performance of both OFs through a comprehensive simulation campaign in a single-PHY context. Third, we repeat this performance evaluation to a multi-PHY context. Fourth, we present the combined results in aggregate plots, side-by-side, for a global view of the results from all simulations.

7.3.1 Example Topology

This section presents an example topology to illustrate how Life-OF improves network lifetime in comparison to MRHOF by harnessing the benefits of diverse PHYs.

Fig. 7.3 shows the resulting topology when using MRHOF in a multi-PHY network. Using MRHOF results in a network that is purely based on FSK 868 MHz. As MRHOF optimizes exclusively for ETX, it ends up selecting FSK 868 MHz throughout the network, irrespective of its energy hungry footprint. This causes the network to ignore high bit-rate links with ETX lower than FSK 868 MHz despite their energy efficiency. It also causes the network to maintain the same routing topology over time without adapting to avoid paths close to the end of their lifetime.

Applying Life-OF to the same topology as Fig. 7.3 results in a different routing topology; this is plotted in Fig. 7.4. As observed in the plot, Life-OF results in a routing topology that combines the low bit-rate FSK 868 MHz radio with high bit-rate OFDM 868 MHz radio. It uses FSK 868 MHz links to communicate directly with the gateway, thus saving energy of routers. It uses multi-hop OFDM 868 MHz links, where it makes sense, in order to save energy of leaf nodes.

We note that, as the network is aging, Life-OF re-computes its routing topology by detecting nodes that are closest to death and establishing new routes with improved lifetime. This is different from MRHOF, which converges to a given topology that remains the same for the entire simulated period, since the optimization is considering ETX only, without consideration to dying nodes. This is illustrated in Fig. 7.5, which shows the evolution of estimated network lifetime for both OFs within the simulated durations. We observe that MRHOF starts with an already low network lifetime that keeps decreasing linearly until death at 0.8 years. By contrast, Life-OF is able to find a new network topology in each epoch that avoids nodes close to death, thus "pumping" life into the network in each epoch. This results in a network lifetime of 3 years, or 275% more than the lifetime achieved with MRHOF.

7.3.2 Single PHY networks

This section presents the results of simulating a single-PHY network with Life-OF routing, comparing it to MRHOF. We observe in Fig. 7.6 that using Life-OF yields

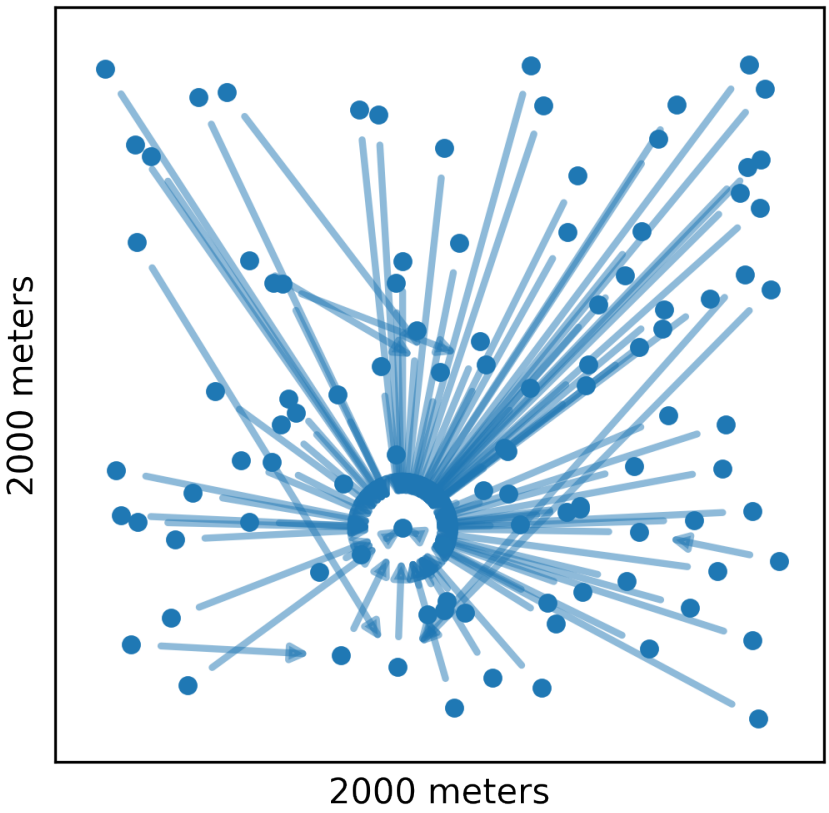

Figure 7.3: Example of a resulting routing topology when using MRHOF. The latter selects FSK 868 MHz links throughout, as a result of optimizing for ETX only.

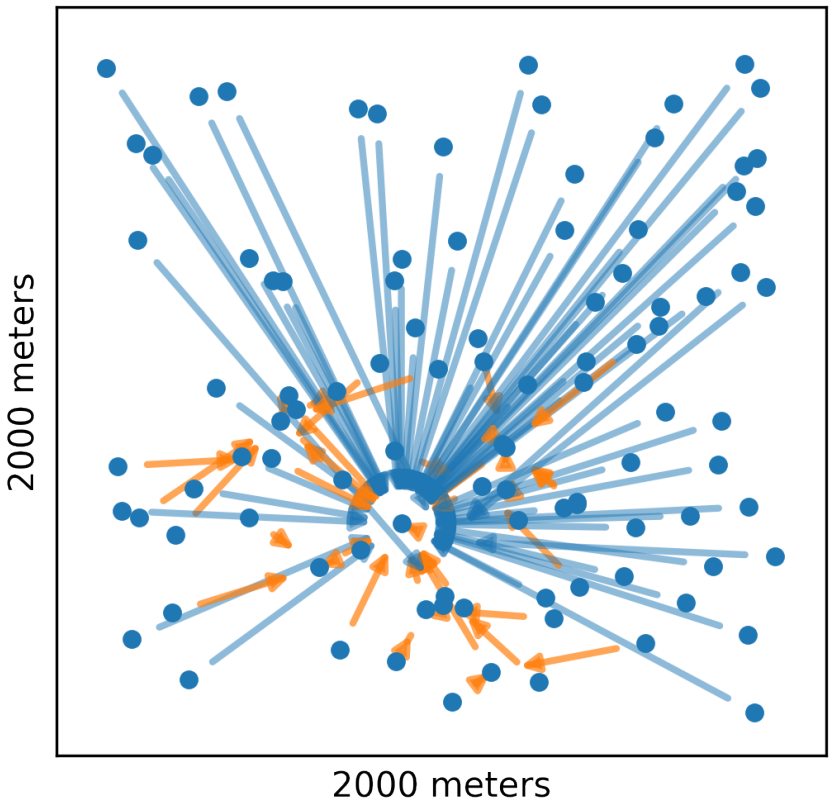

Figure 7.4: Example of a resulting topology using Life-OF that makes use of diverse PHYs to improve network lifetime.

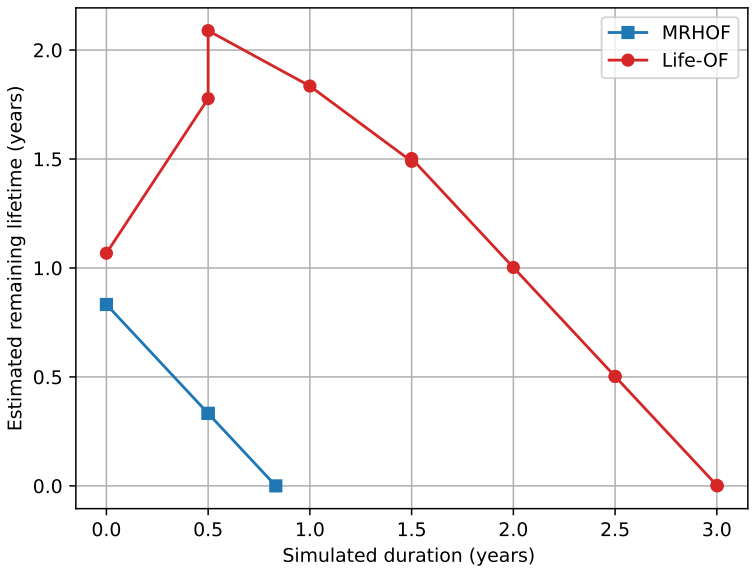

Figure 7.5: In the network demonstrated in Fig. 7.4, Life-OF adapts the network at each epoch by finding a topology that improves the network lifetime. This results in a lifetime 275% higher than MRHOF.

nearly 400% the network lifetime of MRHOF. Even though this is a single-PHY network, using Life-OF still leads to adapting the routing topology at each epoch by selecting paths with higher lifetime. This way, the network is able to achieve an improved lifetime, even with the highest power consuming PHY. This demonstrates the benefit of using Life-OF even when the network is physically equipped with one PHY only.

We show in Fig. 7.7 the distribution of the resulting end-to-end ETX in the network. We observe that most of the ETX of the network using Life-OF is still at 1, same as MRHOF. Interestingly, MRHOF leads to more exceptions with higher end-to-end ETX than Life-OF, even though MRHOF optimizes for ETX alone. This happens because the hysteresis of MRHOF can cause it to ignore paths with small rank improvements (compared to the hysteresis of Life-OF, see Table 3.3).

7.3.3 Multi-PHY networks

This section presents the results of simulating a multi-PHY network with Life-OF routing, in comparison to MRHOF. This is to demonstrate how both OFs perform when there are diverse PHYs available for routing. The distribution of network lifetime for both OFs is presented in Fig. 7.8. We observe that using Life-OF results in improving the lifetime of the network by 370% compared to MRHOF. This is consistent with the pattern observed in Fig. 7.5 that demonstrates the performance of routing with Life-OF, which keeps adapting the topology at each epoch to improve lifetime.

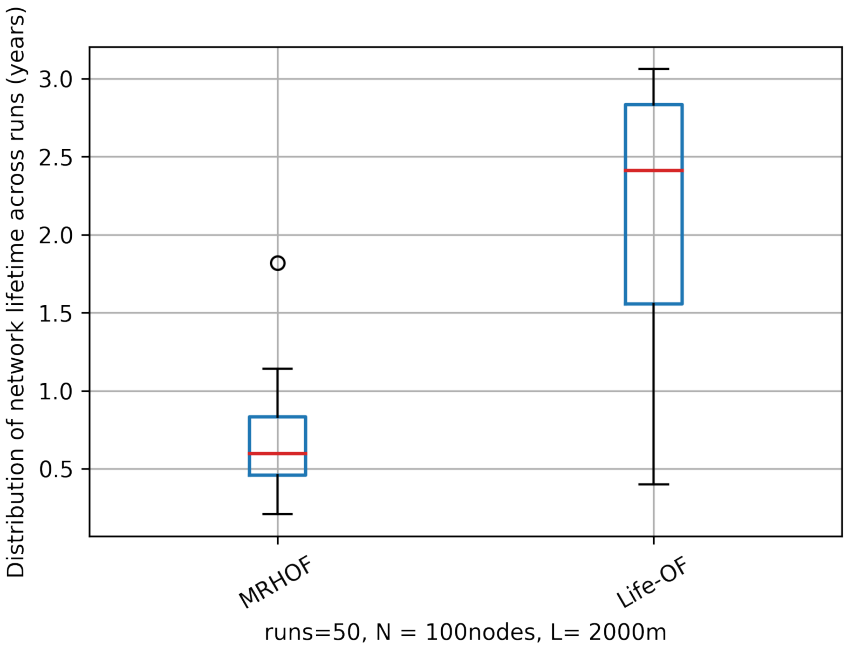

Figure 7.6: Life-OF yields 400% the network lifetime of MRHOF in single-PHY FSK 868 MHz setting

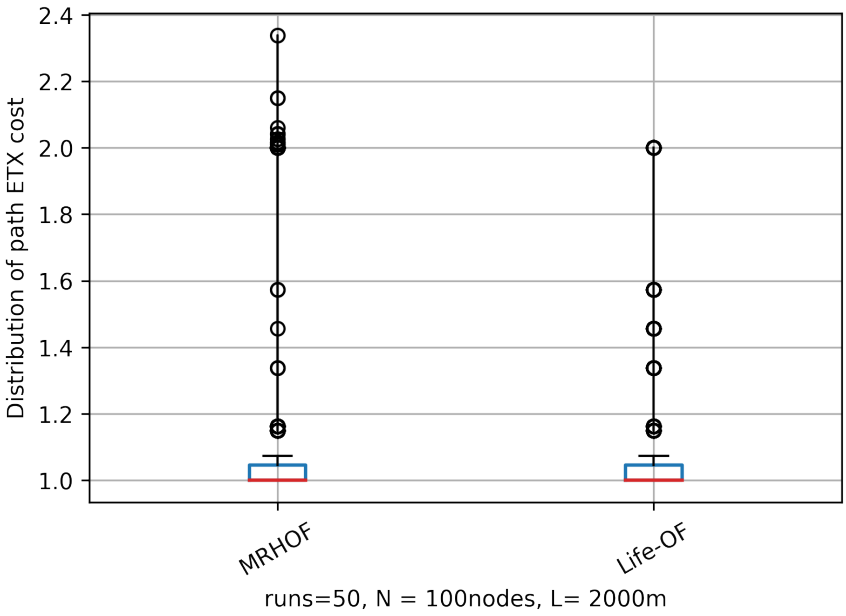

Figure 7.7: Most ETX of the network is still at 1, similar to MRHOF in single-PHY networks.

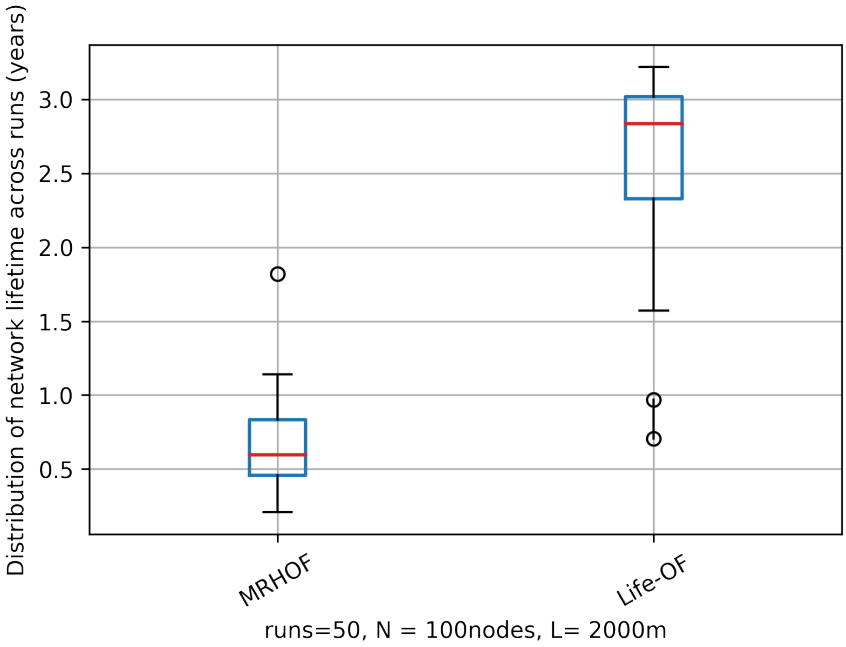

Figure 7.8: Life-OF yields 470% the network lifetime of MRHOF in multi-PHY setting

We show the distribution of the resulting end-to-end ETX in the network in Fig. 7.9. We observe that most of the ETX of the network using Life-OF is still at 1, same as MRHOF. As previously observed in the single-PHY networks, the rare cases where Life-OF leads to higher end-to-end ETX are more numerous. This is an expected side-effect of the use of multi-hopping with faster radios as illustrated in the topology in Fig. 7.4. This way, Life-OF is able to save energy of the nodes in the network that are closest to the end of their lifetime.

7.3.4 Combined Results

This section presents the aggregate simulation results for all scenarios in combined plots for a global comparison. The distribution of network lifetime for the four scenarios is plotted in Fig. 7.10. Using Life-OF in combination with heterogeneous PHYs results in the highest network lifetime, with a median of nearly 2.8 years. It is followed by using Life-OF in a single-PHY and multi-PHY networks where it shows the lowest network lifetime performance.

We observe that the ETX of most of the networks are still at 1 as shown in Fig. 7.11. As previously observed, Life-OF shows more exceptional topologies with higher ETX than MRHOF.

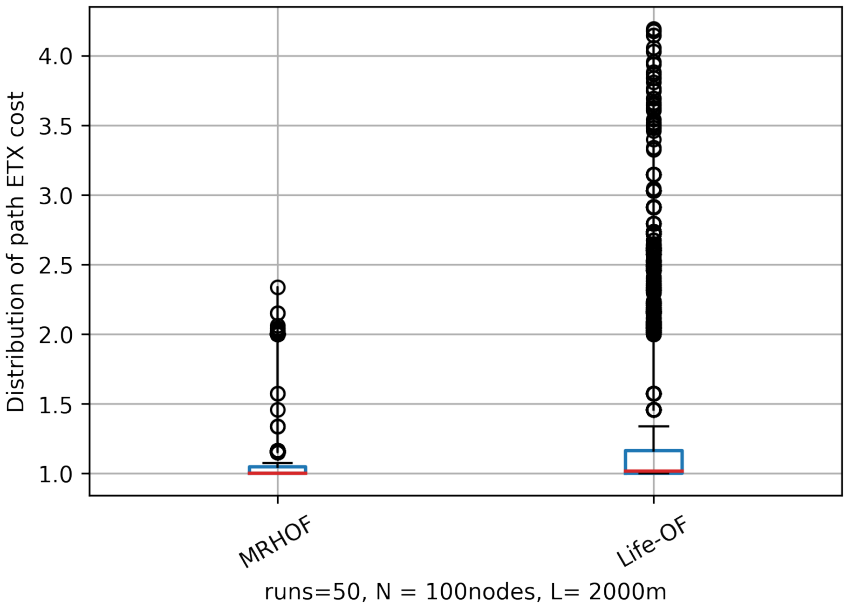

Figure 7.9: Most ETX of the network is still at 1, similar to MRHOF in the hybrid network

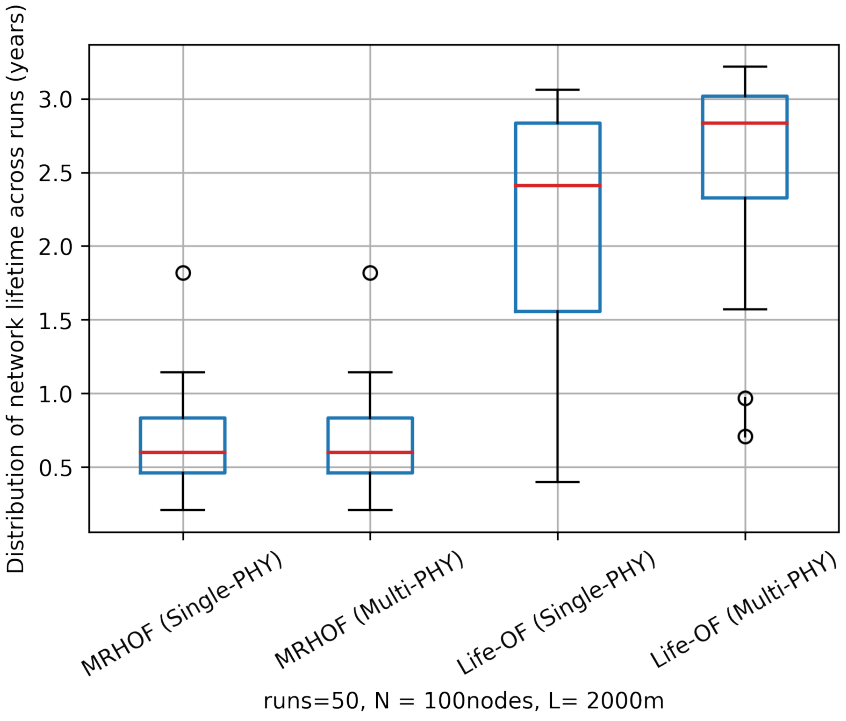

Figure 7.10: Best lifetime performance is achieved by using the hybrid network with Life-OF

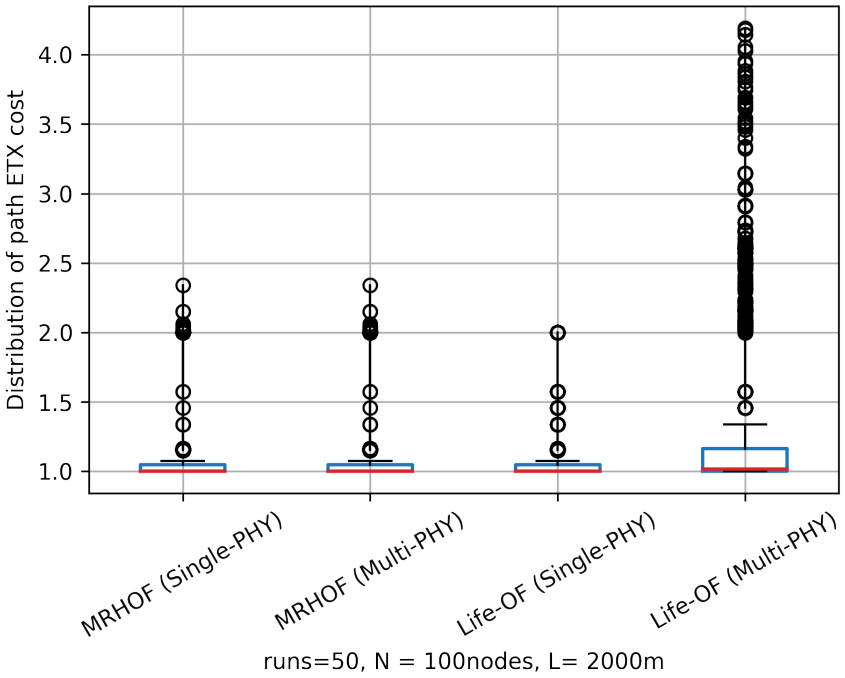

Figure 7.11: Most ETX of Life-OF using the hybrid network is still at 1, similar to other energy expensive settings

7.4 Conclusion

In this chapter, we propose Life-OF, an OF that uses a combination of metrics in order to improve network lifetime using diverse PHYs. We demonstrated how the routing layer can consider the link quality, node's remaining lifetime, hop-count, and the characteristics of each available PHY to make routing decisions that improve the network's lifetime. We demonstrate how Life-OF can be defined using RPL protocol specifications.

The performance of Life-OF is compared to classical MRHOF using simulations in single-PHY and multi-PHY settings. The simulations consider a scenario in a $2 \times 2\ km^2$ area. Simulation results demonstrate that MRHOF converges to a pure long-range FSK 868 MHz network, leading to lowest network lifetime. However, Life-OF is able to improve network lifetime by continuously adapting the routing topology to favor routing over nodes with relatively high remaining lifetime. It combines diverse PHYs in a way that balances power consumption in the network. This way, nodes can switch between using short-range PHYs to improve their own battery lifetime or using long-range PHYs to avoid routers that are close to depletion. Results show that using Life-OF yields 400% the network lifetime of MRHOF in a single-PHY setting. Furthermore, using Life-OF yields 470% the network lifetime of MRHOF in a multi-PHY setting.

Chapter 8

Conclusions and Future Work

This chapter concludes this manuscript by summarizing the work and listing its main contributions (Section 8.1), and discussing the avenues for future research that this work opens (Section 8.2).

8.1 Conclusions

This thesis contributes to the research field of low power IoT. Such networks are characterized by the use of battery-powered sensor nodes which relay their readings using wireless PHYs. The IoT use cases cover a wide range of applications, including predictive industrial maintenance, precision agriculture, environmental monitoring, and smart utility metering. Early IoT technologies that were introduced in the market rely on short-range PHYs that operate in the 2.4 GHz band. Examples of these technologies are BLE, Zigbee, SmartMesh IP, and WirelessHART; they can create indoor coverage or reach for tens of meters. Longer range connectivity could only be achieved via multi-hopping. A later family of technologies was introduced in the market that rely on long-range PHYs, which rely on lower bitrates, sub-GHz frequencies, and/or narrow band channels, to improve link robustness. Some examples of such technologies are LoRaWAN, Sigfox, and NB-IoT; their coverage span anywhere from hundreds of meters to several kilometers. Many of these technologies rely on proprietary PHYs. In 2012, the IEEE adopted a standard set of 31 PHYs serving both long-range and short-range applications under the IEEE802.015.4g amendment.

Both short-range and long-range PHYs have different physical characteristics. For example, long-range PHYs offer link robustness at the expense of higher energy consumption per bit and increased interference in dense networks. Short-range PHYs, however, offer lower energy consumption per bit at the expense of link robustness. Therefore, this leads to the first question we address in this thesis: *does it make sense to integrate multiple PHYs in a network for improved QoS?* Second, *how can we generalize the standard IETF 6TiSCH protocol stack to support multi-PHY networking* (i.e. g6TiSCH), and *how does it compare to a single-PHY 6TiSCH network with respect to QoS?* Third, *how can the g6TiSCH protocol stack support variable-duration slots to*

improve schedule compactness by using shorter slots for fast bitrate PHYs? Finally, *how can a routing protocol make use of multi-PHY integration to improve network lifetime?*

We organize this manuscript in seven core chapters, including four with technical contributions.

Chapter 1 provides a historical perspective on the concept of agility in computer systems. It gives background on emergent families of IoT technologies prevailing the market and the research: short-range multi-hop networks and long-range star networks. Then we discuss why multi-hop topologies are still relevant even with long-range PHYs before we conclude with the organization of this manuscript.

Chapter 2 presents related work in several research and standardization tracks. We outline related work on the evaluation of IEEE 802.15.4g PHYs and we conclude with the need for an end-to-end evaluation of 6TiSCH protocol stack using different IEEE 802.15.4g PHYs. We introduce an overview of the 6TiSCH protocol stack and related research on its performance improvement. We discuss challenges in operating networks in the unlicensed bands. We then discuss related work on improving TSCH schedule compactness. This is followed by an overview of RPL and related work in multi-PHY routing and network lifetime optimization. Finally, we present the state of the art on multi-PHY integration.

Chapter 3 introduces the three technical setups used for the experiments conducted throughout this thesis. We introduce the OpenTestbed of 42 OpenMote B nodes deployed in a real office setting at Inria-Paris, which we use for the experiments in Chapters 4 and 5. We then introduce the local setup of four OpenMote B nodes using hardware probes. This is used to demonstrate the real-time performance of 6TiSCH with a heterogeneous slot-frame in Chapter 6. Finally, we introduce the RPLSim, a high-level discrete-time RPL simulator that we use for the multi-PHY routing simulations in Chapter 7.

Chapter 4 discusses the question of whether multi-PHY integration makes sense. We argue for a positive answer: instead of finding the best PHY for a network, we argue for a "no free lunch" principle. That is, no single PHY can offer best performance across all end-to-end network KPIs.

Chapter 5 adapts the 6TiSCH protocol stack for multi-PHY networking. It demonstrates how a set of short-range and long-range radios can be integrated under one generalized 6TiSCH architecture using Time Slotted PHY Hopping for medium access. The performance of g6TiSCH is evaluated experimentally on the OpenTestbed.

Chapter 6 demonstrates how to enable compact scheduling in a TSCH slot-frame in a decentralized multi-PHY network. The schedule can adapt slot-duration on a slot-by-slot basis depending on the bit-rate of the used PHY ("6DYN") and we show how this can help mitigate the unlicensed band limitations. Finally we demonstrate the real-time behavior of 6DYN using local hardware probes.

Chapter 7 introduces how multi-PHY networking can improve network lifetime. We propose"Life-OF", a RPL OF that optimizes for network lifetime and we describe how to adapt RPL control messages to support this OF. Finally, both Life-OF and the standard MRHOF are evaluated using RPLSim and we demonstrate how Life-OF combines diverse PHYs to boost network lifetime.

In summary, this works makes the following three contributions to the field of low power IoT:

- On a conceptual front, the thesis argues for a "no free lunch" principle: no single PHYs outperforms other PHYs across all industrial KPIs. We advance how multi-PHY radio chips can be used to enable multi-PHY integration, so that a node can change PHYs on a link-by-link basis using Time Slotted PHY Hopping. We introduce compact scheduling for industrial multi-PHY networking and we further make the case for boosting network lifetime using multi-PHY routing.
- We propose a generalization of the standard IETF 6TiSCH protocol stack for multi-PHY networking. We show how to adapt the 6TiSCH architecture for multi-PHY integration: IEEE 802.154e MAC layer, Sixtop sub-layer, MSF sub-layer, 6LoWPAN layer, and RPL routing layer. We demonstrate how RPL can improve network lifetime by proposing an OF that combines different PHYs to achieve this objective.
- This thesis has resulted in technical developments in embedded firmware, software, and simulation to evaluate our proposals for multi-PHY integration. We extend OpenWSN – an RTOS and a reference implementation of 6TiSCH – with multi-PHY support with the OpenMote B board, and develop a KPI monitor to extract industrial KPIs out of our experiments on the OpenTestbed. We further develop a high level discrete-time RPL simulator that mimics the evolution of network lifetime as a function of RPL configuration.

8.2 Future Work

This work has opened up several avenues for future work on agile multi-PHY networking. Section 8.2.1 discusses building open and flexible multi-PHY network architectures. Section 8.2.2 discusses challenges for scheduling in multi-PHY networks.

Section 8.2.3 discusses open challenges on multi-PHY gateways. Section 8.2.4 discusses the possibility to extend this multi-PHY approach to cellular networks. Section 8.2.5 discusses open research challenges related to security in multi-PHY networks. Section 8.2.6 discusses the QoS degradation in the unlicensed band and how multi-band support can yield improved QoS. Section 8.2.7 discusses future work on routing metrics for reducing network costs.

8.2.1 Open Multi-PHY Architectures

Throughout this thesis, we used only three PHYs from the IEEE 802.15.4g amendment, where each PHY has a specifically interesting feature: FSK 868 MHz as a long range PHY, OFDM 868 MHz as a fast bit-rate PHY, and O-QPSK 2.4 GHz as a canonical in-between option. But, as noted in Section 2.1, there is a total of 31 available PHYs in the IEEE802.15.4g amendment. Furthermore, there are other proprietary PHYs with

different characteristics such as the LoRa PHY which is used for long-range coverage. It is configurable with 6 spreading factor indexes and tunable bandwidth ranging from 7.8 kHz up to 500 kHz (subject to regional regulation) [79].

Therefore, future work can explore how to keep an open network architecture that allows flexible additions of new PHYs to improve the QoS for different use cases. This can be illustrated by two examples.

The first example is of an industrial site that spans tens of square kilometers. In that case, the network may combine a LoRa PHY with high spreading factor index for long-range hops (e.g. $SF = 12$), a faster bitrate LoRa configuration for nearby nodes such as (e.g. $SF = 7$), and an in-between option (e.g. $SF = 10$)

The second example is of a network deployed in deep-indoor environment such as inside a residential complex. In that case, the network may benefit from a configuration that is fully based on an OFDM family of PHYs such as OFDM Option 1 which offers a bitrate from 100 kbps up to 800 kbps depending on the MCS. This can be interesting because OFDM is particularly robust against multi-path fading in indoor or urban settings [5].

Future work can therefore explore how the architecture of the network can accept new PHYs. One challenge is how slot-templates can be conceived quickly (if not automatically) for each PHY. Slot-templates were designed manually for this thesis with the aid of hardware probes which can be impractical to do every time a PHY is introduced.

8.2.2 Scheduling in Multi-PHY networks

Future work can compare the performance of 6DYN to g6TiSCH using same slot durations in large scale networks. This could be interesting when adaptive MSF is used by allowing motes with high bit-rate up-links to increase their throughput by allocating more slots. Moreover, there is a whole diversity of different combinations that would be interesting to evaluate. For instance a network can use a combination of PHYs on the 5kbps-250kbps range to fit more sparse deployment or 250kbps to 800kbps to fit more dense deployments.

It can also be interesting to explore how parallel transmissions can take place within 6DYN to improve reliability. At this point, g6TiSCH and 6DYN are designed to use only one transmission per slot. Since the mote has two different chips, it seems feasible that multiple chips can be sent commands at the same time. However, this requires more careful design of time slot templates since the time for each state in the radio varies by the design of each chip and how it is connected to the micro-controller (e.g., in an SoC or through SPI).

8.2.3 Multi-PHY Gateways

There is growing industrial interest in efficient use of the fixed infrastructure by minimizing wasted RF resources. For example, recent development in cellular 5G networks have focused on “network slicing” which is the ability to divide

the infrastructure among different use cases (e.g. human-type communications and machine-type communications) [80].

The g6TiSCH architecture put forward in this thesis can be used to provision multi-PHY GWs where each connecting end device can negotiate a PHY depending on its own configuration. This does not come at extra cost for the GWs if they are equipped with PHY-agile radio chips which support PHY changing on a frame-by-frame basis.

A challenge for this research is *how to define an upper limit for the resources allocated for each PHY?* Assuming the GW is using 6DYN to improve schedule compactness, should the upper limit on each PHY be expressed in number of slots or total time on air? Furthermore, *can the GW dynamically expand the slot-frame to admit more flows? or is it better to request some devices to use faster bitrates when possible?* In addition, *how does increasing the number of supported PHYs impact the network performance in terms of signaling overhead?* Finally, this track can address the different scheduling strategies to improve network QoS. For example, if a poorly covered end device is generating high packet rate, should it resort to use slower bit-rate or reserving more slots with higher bit-rate?. One way to address these challenges is by using heuristic search methods at run-time to find better slot-frame configuration for improved QoS for connecting devices.

8.2.4 Multi-PHY Cellular Networks

Future work can consider the potential for deployment of multi-PHY base stations (Section 8.2.3) in a cellular topology. This can lower the Total Cost of Ownership (TCO) of the network infrastructure in three ways. First, since cellular base stations are major cost elements because of the cost of manual labor to maintain them, it is not feasible to add stations to improve coverage in remote areas with few users. Using a g6TiSCH architecture enables end users to deploy cheap, possibly battery-powered, routers for coverage extension in hard to reach areas. This way, network QoS may be improved for extensive coverage for the users at no additional cost to the operators. Second, since base stations costs are fixed, using a multi-PHY gateway allows a device to switch to faster bitrates when possible. Although existing cellular architectures such as NB-IoT [15] use different PHYs for different activities, the set of used PHYs is pre-determined by the relevant standard. However, use of an open multi-PHY architecture allows admitting more diverse use cases at the same cost. Therefore, it allows more efficient use of the base station resources. Third, since the g6TiSCH architecture is fully wireless, it is possible to have a cellular-like network spanning dozens of kilometers without the need for wired infrastructure. This can enable low-cost and pervasive coverage in challenging wide areas such as mountains or hilly landscapes.

We identify three challenges for this research focus. The first challenge is how to measure the monetary cost of multi-PHY management (resulting from energy spent on signaling overhead) and the possible side-effects on other performance aspects of the network. This way, we can explore the possible side-effects of increasing the number of supported PHYs in the network and weigh them against the benefits in reducing TCO or QoS improvement.

The second challenge is to explore how the network can support human-type

communications that are significantly different in their requirements from IoT (e.g. voice calls). g6TiSCH uses low power radios that are designed to fit LLNs in general (assumed to be stationary and with low per device packet rates). However, the concepts developed in 6DYN (specially use of Time Slotted PHY Hopping) can be applied to higher throughput radios, such as commonly used for human-type communications.

For example:

- a high bitrate PHY can be sufficient for a nearby stationary device and vice versa,
- a node can negotiate slots to nearby stations during mobility for a smooth handoff, and
- a node can negotiate cells with different PHYs to use for different applications (e.g. low bitrate PHY for alarms and high-bitrate PHY for applications with regular non-critical transmission).

Finally, how can multi-PHY base stations be deployed in complex terrain for improved coverage? One way to address this is by referring to existing machine learning methods that use Light Detection and Ranging (LIDAR) data for coverage improvement in complex terrain [81], [82] and adapting them for multi-PHY architectures.

8.2.5 Security in Multi-PHY Networks

Security is a fundamental aspect of networked computer systems and it is an integral element of the 6TiSCH protocol stack [76]. Future work can explore how multi-PHY capabilities can be used to enhance network security against different threat models. We present two examples for this track.

First, a network that is deployed in a hostile zone can possibly increase the difficulty of jamming or sniffing of its communication channels by adopting what can be called "PHY-Anonymity". The network can use two sets of PHYs: a statically defined set for network discovery and a dynamically configured set for communication. A device that joins the network has a priori knowledge only of the first set of PHYs. If it successfully authenticates, it receives specific set of PHYs to be used by this for communication (either from a neighbor in a distributed network or form the gateway in a centralized network). This set may vary from one device to another. This way, it is harder for unauthenticated nodes to know which PHYs are used for communication. Also, in case of an unauthorized join to the network, only a part of the network is compromised since not all the devices use the same set of PHYs. This mechanism is inspired by the "bridge" access mode for the The Onion Routing network that enables it to survive hostile blocking attempts [83].

Second, multi-PHY integration can improve network protection against sniffing or jamming by "random" hopping over a diverse set of PHYs (e.g. modulation, band, coding rate etc.). Future work can explore different hopping schemes that can mitigate the risk of sniffing of a multi-hop TSCH network, such as the sniffing approach proposed by Kovac et al. [84]. For example, Kovac et al.perform sniffing on 16 channels in the 2.4 GHz band. How can the diversity in band (e.g., sub-GHz band) or modulations mitigate this risk of sniffing?.

8.2.6 Agile Spectrum Access

Future work can explore the potential of multi-band support within the network to improve network QoS in industrial applications. This track is important since network QoS can be degraded as a side-effect of the interference in the unlicensed band.

As discussed in Section 2.3, the use of the unlicensed band introduces throughput limitations due to interference, specially with the use of long-range PHYs. This is because in highly industrialized or urbanized zones, hundreds or thousands of wireless devices are expected to co-exist, yet without any coordination among them on the use of the shared spectrum. This can lead to degraded QoS of the network because of external interference.

This research track can be interesting in three focus points. First, it can help networks develop more resilience against external interference by simply changing any PHY that seems to suffer low PDR (especially if it is combined with high RSSIs). Second, network operators may choose to offload some traffic using licensed bands or using TV white-spaces for an improved reliability. This way, the network operators can create QoS trade-offs for each end device depending on the use case. Existing proposals, such as the proposal of Labib et al. [85], have introduced off-loading Long Term Evolution (LTE) traffic to the unlicensed spectrum. This confirms the intuition behind integration of the licensed and unlicensed bands. Therefore, future work can explore the off-loading *from* the unlicensed band into the licensed band. For example, alarms messages can be off-loaded to the licensed band for improved latency and reliability. Less critical use-cases, such as smart utility meter readings, can be transmitted in the unlicensed band with higher latency. Third, there is an existing interest in dynamic spectrum sharing for efficient utilization of the licensed spectrum [86]. The reason is that licensed bands usually have the fixed costs of their purchase, yet they are not always in use by the end customers, which means a waste of bandwidth resources. Since the spectrum is already a scarce resource, there is interest in its commoditization: operators can "rent out" licensed bands temporarily for efficient utilization. Renters can be operators in the unlicensed bands who may benefit from partial access to licensed bands for improved QoS. This can be subject to pricing dynamics based on supply and demand [87].

Since g6TiSCH in combination with 6DYN enables multi-PHY support, it can increase the spectral agility of the network by allowing the network to dynamically switch bands or PHYs (fully or partially). This way, there is more space for QoS trade-offs in the network. The challenge in this focus track is how should the network scan and discover the available spectral options during its running? Finally, how should a route be selected in this setting when the route is a mixture of free and rented bands? This can be addressed through cost-aware routing which is discussed in the following section.

8.2.7 Routing Metrics for Improving Network Costs

In Chapter 7, we introduced a RPL OF that improves network lifetime. This was motivated by the need to improve network cost by reducing the number of employee hours and trips to replace the batteries of all the devices. However, there can be more cost elements involved, other than the factory trips. For example, as mentioned in

Section 8.2.6, some links can be more costly than others if they use licensed bands (in case of mixing license-free and licensed PHYs). Furthermore, some devices may be in a harder to reach areas than others or may be more critical than others such that removing them can incur excessive labor costs or halting production lines.

Future work can then consider routing metrics to improve the overall network cost, which can follow an LPWAN budget model such as in previous research [78]. The challenge in this work is how to extend RPL DMCs to include cost-related metrics such as cost of licensed bands (when in use), battery replacement cost, and battery capacity. Furthermore, consumption of battery energy can be computed more systematically to include power consumption of the radios as well as non-radio components such as attached sensing modules or local storage such as flash memory as introduced in [88]. This way, the routing topology is more aware of the budget-consuming factors and is more intentional about optimizing for budget saving.

Chapter 9

Publications Resulting from this Work

Journal Articles

1. *No Free Lunch—Characterizing the Performance of 6TiSCH When Using Different Physical Layers.* Mina Rady, Quentin Lampin, Dominique Barthel, Thomas Watteyne. **MDPI Sensors**, vol. 20, no. 17, p. 4989, September **2020**.

2. *g6TiSCH: Generalized 6TiSCH for Agile Multi-PHY Wireless Networking.* Mina Rady, Quentin Lampin, Dominique Barthel, Thomas Watteyne. **IEEE Access**, vol. 9, pp. 84465-84479, **2021**.

3. *6DYN: 6TiSCH with Heterogeneous Slot Durations.* Mina Rady, Quentin Lampin, Dominique Barthel, Thomas Watteyne. **MDPI Sensors**, special issue on Dependable IoT Networking vol. 21, no. 5, p. 1611, February **2021**.

4. *Bringing Life out of Diversity: Boosting Network Lifetime using Multi-PHY Routing in RPL.* Mina Rady, Quentin Lampin, Dominique Barthel, Thomas Watteyne. **Wiley Transactions on Emerging Telecommunications (ETT)**, *under review.*

Conference Paper and Demonstration

1. *Demo: Blink - Room-Level Localization Using SmartMesh IP.* Yasuyuki Tanaka, Hai Le, Victor Kobayashi, Camilo Lopez, Thomas Watteyne, Mina Rady. **IEEE INFOCOM, CNERT workshop**, Paris, France, 29 April **2019**.

Conference Poster

1. *Extending LPWANs with Heterogeneous Mesh Networks.* Mina Rady, Quentin Lampin, Dominique Barthel, Thomas Watteyne. **Journées thématiques GDR RSD ResCom** Low-Power Wide Area Networks (LPWAN),Lyon, France, July **2019**.

Research Report

1. *Initial Design of a Generalization of the 6TiSCH Standard to Support Multiple PHY Layers*. Mina Rady, Quentin Lampin, Dominique Barthel, Thomas Watteyne. **Inria Research Report** RR-9392, **2021**.

Software Contributions

1. to the OpenWSN project (`http://www.openwsn.org`), the reference open-source implementation of the 6TiSCH protocol stack. Specifically, I lead the development of:

   - the `openradio` interface (`https://github.com/minarady1/openwsn-fw/tree/develop_FW-866_v2`),
   - the `g6TiSCH` OpenWSN implementation (`https://github.com/minarady1/openwsn-fw/tree/develop_FW-877`),
   - the `OpenVisualizer` support for the multi-PHY network (`https://github.com/minarady1/openvisualizer/tree/develop_FW-877`),
   - the `6DYN` OpenWSN implementation (`https://github.com/minarady1/openwsn-fw/tree/develop_FW-877`).

   My contributions are published under an open-source BSD license.

2. to the OpenTestbed Project (`http://testbed.openwsn.org/`), an open-source low-power wireless testbed solution based on off-the-shelf hardware. Specifically, I lead the development of the KPI Monitor (`https://github.com/minarady1/kpi_monitor`). My contribution is published under an open-source BSD license.

3. RPLSim a discrete-event high-level RPL Simulator written in Python. RPLSim has allowed us to mimic the evolution of network lifetime as a function of RPL OF configuration. I am the lead developer on this project.

Bibliography

[1] F. Civerchia, S. Bocchino, C. Salvadori, E. Rossi, L. Maggiani, and M. Petracca, "Industrial Internet of Things Monitoring Solution for Advanced Predictive Maintenance Applications," *Elsevier Journal of Industrial Information Integration*, vol. 7, pp. 4–12, Sep. 2017. DOI: 10.1016/j.jii.2017.02.003.

[2] *Waht is Zigbee?* https://zigbeealliance.org/solution/zigbee/, Accessed: 31 August, 2021.

[3] T. Watteyne, L. Doherty, J. Simon, and K. Pister, "Technical Overview of SmartMesh IP," in *Seventh International Conference on Innovative Mobile and Internet Services in Ubiquitous Computing*, Taichung, Taiwan: IEEE, Jul. 2013, pp. 547–551. DOI: 10.1109/IMIS.2013.97.

[4] J. Muñoz, T. Chang, X. Vilajosana, and T. Watteyne, "Evaluation of IEEE802.15.4g for Environmental Observations," *MDPI Sensors*, vol. 18, no. 10, p. 3468, Oct. 2018. DOI: 10.3390/s18103468.

[5] J. Muñoz, E. Riou, X. Vilajosana, P. Muhlethaler, and T. Watteyne, "Overview of IEEE802.15.4g OFDM and Its Applicability to Smart Building Applications," in *Wireless Days (WD)*, IEEE, Dubai, UAE, Apr. 2018, pp. 123–130. DOI: 10.1109/WD.2018.8361707.

[6] A. H. Kazmi, M. J. O'grady, D. T. Delaney, A. G. Ruzzelli, and G. M. P. O'hare, "A Review of Wireless-Sensor-Network-Enabled Building Energy Management Systems," *ACM Transactions on Sensor Networks*, vol. 10, no. 4, pp. 1–43, Jun. 2014. DOI: 10.1145/2532644.

[7] T. Watteyne, A. Laura Diedrichs, K. Brun-Laguna, J. Emilio Chaar, D. Dujovne, J. Carlos Taffernaberry, and G. Mercado, "PEACH: Predicting Frost Events in Peach Orchards Using IoT Technology," *EAI Endorsed Transactions on Internet of Things*, vol. 2, no. 5, Dec. 2016. DOI: 10.4108/eai.1-12-2016.151711.

[8] C.-S. Sum, M.-T. Zhou, F. Kojima, and H. Harada, "Experimental Performance Evaluation of Multihop IEEE 802.15.4/4g/4e Smart Utility Networks in Outdoor Environment," *Wireless Communications and Mobile Computing*, vol. 2017, pp. 1–13, 2017. DOI: 10.1155/2017/7137406.

[9] Y. Tanaka, H. Le, V. Kobayashi, C. Lopez, T. Watteyne, and M. Rady, "Demo: Blink – Room-Level Localization Using SmartMesh IP," in *International Conference on Embedded Wireless Systems and Networks (EWSN)*, ACM, Lyon, France, Feb. 2020, pp. 198–199.

[10] T. Chang, T. Watteyne, B. Wheeler, F. Maksimovic, O. Khan, S. Mesri, L. Lee, I. Suciu, D. Burnett, X. Vilajosana, and K. Pister, "6TiSCH on SCμM: Running a Synchronized Protocol Stack without Crystals," *Sensors*, vol. 20, p. 1912, Mar. 2020. DOI: 10.3390/s20071912.

[11] E. Fadel, V. Gungor, L. Nassef, N. Akkari, M. A. Malik, S. Almasri, and I. F. Akyildiz, "A Survey on Wireless Sensor Networks for Smart Grid," *IEEE Computer Communications*, vol. 71, pp. 22–33, Nov. 2015. DOI: 10.1016/j.comcom.2015.09.006.

[12] F. Adelantado, X. Vilajosana, P. Tuset-Peiró, B. Martinez, J. Melia-Segui, and T. Watteyne, "Understanding the Limits of LoRaWAN," *IEEE Communications Magazine*, vol. 55, no. 9, pp. 34–40, 2017. DOI: 10.1109/mcom.2017.1600613.

[13] *Sigfox Technology*, https://www.sigfox.com/en/what-sigfox/technology, Accessed: 04 August, 2021.

[14] Y.-P. E. Wang, X. Lin, A. Adhikary, A. Grovlen, Y. Sui, Y. Blankenship, J. Bergman, and H. S. Razaghi, "A Primer on 3GPP Narrowband Internet of Things," *IEEE Communications Magazine*, vol. 55, no. 3, pp. 117–123, Mar. 2017. DOI: 10.1109/mcom.2017.1600510cm.

[15] K. Mekki, E. Bajic, F. Chaxel, and F. Meyer, "Overview of Cellular LPWAN Technologies for IoT Deployment: Sigfox, LoRaWAN, and NB-IoT," Mar. 2018. DOI: 10.1109/PERCOMW.2018.8480255.

[16] J. Muñoz, "km-Scale Industrial Networking," Ph.D. dissertation, Sorbonne University, Paris, France, 2019.

[17] T. Watteyne, J. Weiss, L. Doherty, and J. Simon, "Industrial IEEE802.15.4e Networks: Performance and Trade-Offs," in *IEEE International Conference on Communications (ICC)*, London: IEEE, Jun. 2015, pp. 604–609. DOI: 10.1109/ICC.2015.7248388.

[18] IEEE, *802.15.4e-2012 - IEEE Standard for Local and metropolitan area networks–Part 15.4: Low-Rate Wireless Personal Area Networks (LR-WPANs) Amendment 1: MAC sublayer*, IEEE, Apr. 2012.

[19] T. Watteyne, V. Handziski, X. Vilajosana, S. Duquennoy, O. Hahm, E. Baccelli, and A. Wolisz, "Industrial Wireless IP-based Cyber Physical Systems," *Proceeding of the IEEE*, vol. PP, no. 99, pp. 1–14, Mar. 2016.

[20] IEEE, *IEEE Standard for Local and Metropolitan Area Networks–Part 15.4: Low-Rate Wireless Personal Area Networks (LR-WPANs)*, Piscataway, NJ: IEEE, 2016.

[21] Texas Instruments, *Datasheet: CC2538 Powerful Wireless Microcontroller System-On-Chip for 2.4-GHz IEEE 802.15.4, 6LoWPAN, and ZigBee Applications*, Red. D, 2015.

[22] The European Commission, *M/441 Standardisation Mandate to CEN, CENELEC And ETSI in the field of Measuring Instruments for the Development of an Open Architecture for Utility Meters Involving Communication Protocols Enabling Interoperability*, Brussels, Apr. 2009.

[23] The European Council, "Directive 2006/32/EC of the European Parliament and of the Council on Energy End-Use Efficiency and Energy Services and Repealing Council Directive 93/76/EEC," *OJ*, vol. L 114, pp. 64–85, Apr. 2006.

[24] *Couverture LoRa® Orange*, `https://www.orange-business.com/fr/reseau-iot`, Accessed: 20 August, 2021.

[25] Nordic Semiconductor, *nRF52840 Product Specification*, v1.1, 2019.

[26] IEEE, *IEEE Standard for Local and metropolitan area networks–Part 15.4: Low-Rate Wireless Personal Area Networks (LR-WPANs) Amendment 3: Physical Layer (PHY) Specifications for Low-Data-Rate, Wireless, Smart Metering Utility Networks*, IEEE, Apr. 2012.

[27] Atmel, *Atmel AT86RF215 Device Family Datasheet*, 42415E, 2016.

[28] F. Kojima, C.-S. Sum, M.-T. Zhou, L. Lu, and H. Harada, "System Evaluation of a Practical IEEE 802.15.4/4e/4g Multi-Physical and Multi-Hop Smart Utility Network," *IET Communications*, vol. 9, no. 5, pp. 665–673, Mar. 2015. DOI: `10.1049/iet-com.2014.0240`.

[29] X. Vilajosana, K. Pister, and T. Watteyne, *Minimal IPv6 over the TSCH Mode of IEEE 802.15.4e (6TiSCH) Configuration*, RFC8180, Internet Engineering Task Force (IETF), May 2017. [Online]. Available: `https://datatracker.ietf.org/doc/html/rfc8180`.

[30] X. Vilajosana, T. Watteyne, T. Chang, M. Vucinic, S. Duquennoy, and P. Thubert, "IETF 6TiSCH: a Tutorial," *IEEE Communications Surveys & Tutorials*, vol. 22, no. 1, pp. 595–615, 2019. DOI: `10.1109/COMST.2019.2939407`.

[31] D. Dujovne, T. Watteyne, X. Vilajosana, and P. Thubert, "6TiSCH: Deterministic IP-Enabled Industrial Internet (of Things)," *IEEE Communications Magazine*, vol. 52, no. 12, pp. 36–41, Dec. 2014. DOI: `10.1109/MCOM.2014.6979984`.

[32] T. Winter, P. Thubert, A. Brandt, J. Hui, R. Kelsey, P. Levis, K. Pister, R. Struik, J. Vasseur, and R. Alexander, *RPL: IPv6 Routing Protocol for Low-Power and Lossy Networks*, RFC6550, Internet Engineering Task Force (IETF), Mar. 2012. [Online]. Available: `https://datatracker.ietf.org/doc/html/rfc6550`.

[33] J. Vasseur, M. Kim, K. Pister, N. Dejean, and D. Barthel, *Routing Metrics Used for Path Calculation in Low-Power and Lossy Networks*, RFC6551, Internet Engineering Task Force (IETF), Mar. 2012. [Online]. Available: `https://datatracker.ietf.org/doc/html/rfc6551`.

[34] P. Thubert, *Objective Function Zero for the Routing Protocol for Low-Power and Lossy Networks (RPL)*, RFC6552, Internet Engineering Task Force (IETF), Mar. 2012. [Online]. Available: https://datatracker.ietf.org/doc/html/rfc6552.

[35] Q. Wang, X. Vilajosana, and T. Watteyne, *6TiSCH Operation Sublayer (6top) Protocol (6P)*, RFC8480, Internet Engineering Task Force (IETF), Nov. 2018. [Online]. Available: https://datatracker.ietf.org/doc/html/rfc6719.

[36] T. Chang, M. Vucinic, X. Vilajosana, S. Duquennoy, and D. Dujovne, *6TiSCH Minimal Scheduling Function (MSF)*, RFC9033, Internet Engineering Task Force (IETF), May 2021. [Online]. Available: https://datatracker.ietf.org/doc/html/rfc9033.

[37] J. Hui and P. Thubert, *Compression Format for IPv6 Datagrams over IEEE 802.15.4-Based Networks*, RFC6282, Internet Engineering Task Force (IETF), Sep. 2011. [Online]. Available: https://datatracker.ietf.org/doc/html/rfc6282.

[38] A. Yang, A. Sundararajan, C. B. Schindler, and K. Pister, "Analysis of Low Latency TSCH Networks for Physical Event Detection," in *Wireless Communications and Networking Conference Workshops (WCNCW)*, Barcelona, Catalunya, Spain: IEEE, Apr. 2018, pp. 167–172.

[39] F. Theoleyre and G. Z. Papadopoulos, "Experimental Validation of a Distributed Self-Configured 6TiSCH with Traffic Isolation in Low Power Lossy Networks," in *International Conference on Modeling, Analysis and Simulation of Wireless and Mobile Systems (MSWIM)*, Malta, Malta: ACM, 2016, pp. 102–110.

[40] R. Teles Hermeto, A. Gallais, and F. Theoleyre, "On the (over)-Reactions and the Stability of a 6TiSCH Network in an Indoor Environment," in *International Conference on Modeling, Analysis and Simulation of Wireless and Mobile Systems (MSWIM)*, Montreal, QC, Canada: ACM, 2018, pp. 83–90.

[41] S. Ben Yaala, F. Theoleyre, and R. Bouallegue, "Performance Study of Co-Located IEEE 802.15.4-TSCH Networks: Interference and Coexistence," in *Symposium on Computers and Communication (ISCC)*, Messina, Italy: IEEE, Jun. 2016, pp. 513–518.

[42] M. Vucinic, T. Chang, B. Skrbic, E. Kocan, M. Pejanovic-Djurisic, and T. Watteyne, "Key Performance Indicators of the Reference 6TiSCH Implementation in Internet-of-Things Scenarios," *IEEE Access*, vol. 8, pp. 79 147–79 157, 2020. DOI: 10.1109/ACCESS.2020.2990278.

[43] M. R. Palattella, N. Accettura, M. Dohler, L. A. Grieco, and G. Boggia, "Traffic Aware Scheduling Algorithm for Reliable Low-Power Multi-Hop IEEE 802.15.4e Networks," in *IEEE 23rd International Symposium on Personal, Indoor and Mobile Radio Communications - (PIMRC)*, 2012, pp. 327–332. DOI: 10.1109/PIMRC.2012.6362805.

[44] M. R. Palattella, N. Accettura, L. A. Grieco, G. Boggia, M. Dohler, and T. Engel, "On Optimal Scheduling in Duty-Cycled Industrial IoT Applications Using IEEE 802.15.4e TSCH," *IEEE Sensors Journal*, vol. 13, no. 10, pp. 3655–3666, Oct. 2013. DOI: 10.1109/jsen.2013.2266417.

[45] S. Ridha, P. Minet, and E. Livolant, "MODESA: an Optimized Multichannel Slot Assignment for Raw Data Convergecast in Wireless Sensor Networks," in *IEEE 31st International Performance Computing and Communications Conference (IPCCC)*, Dec. 2012, pp. 91–100. DOI: 10.1109/PCCC.2012.6407742.

[46] Y. Kim and M. Lee, "Scheduling Multi-Channel and Multi-Timeslot in Time Constrained Wireless Sensor Networks via Simulated Annealing and Particle Swarm Optimization," *IEEE Communications Magazine*, vol. 52, no. 1, pp. 122–129, Jan. 2014. DOI: 10.1109/mcom.2014.6710073.

[47] R. T. Hermeto, A. Gallais, and F. Theoleyre, "Scheduling for IEEE802.15.4-TSCH and Slow Channel Hopping MAC in Low Power Industrial Wireless Networks: A survey," *Computer Communications*, vol. 114, pp. 84–105, Dec. 2017. DOI: 10.1016/j.comcom.2017.10.004.

[48] R. Musaloiu-E and A. Terzis, "Minimising the Effect of WiFi Interference in 802.15.4 Wireless Sensor Networks," *International Journal of Sensor Networks*, vol. 3, no. 1, p. 43, 2008. DOI: 10.1504/ijsnet.2008.016461.

[49] A. Gonga, O. Landsiedel, P. Soldati, and M. Johansson, "Revisiting Multi-channel Communication to Mitigate Interference and Link Dynamics in Wireless Sensor Networks," in *IEEE 8th International Conference on Distributed Computing in Sensor Systems*, IEEE, May 2012. DOI: 10.1109/dcoss.2012.15.

[50] X. Liu, X. Zhai, W. Lu, and C. Wu, "QoS-guarantee Resource Allocation for Multibeam Satellite Industrial Internet of Things with NOMA," *IEEE Transactions on Industrial Informatics*, pp. 2052–2061, 2019. DOI: 10.1109/tii.2019.2951728.

[51] ETSI, *Electromagnetic Compatibility and Radio Spectrum Matters (ERM); Short Range Devices (SRD); Radio Equipment to be Used in the 25 MHz to 1000 MHz Frequency Range with Power Levels Ranging up to 500 mW; Part 1: Technical Characteristics and Test Methods*, Sophia Antipolis Cedex - FRANCE: ETSI, 2012.

[52] T. Watteyne, A. Mehta, and K. Pister, "Reliability through Frequency Diversity," in *Proceedings of the 6th ACM Symposium on Performance Evaluation of Wireless Ad Hoc, Sensor, and Ubiquitous Networks - PE-WASUN*, ACM Press, 2009. DOI: 10.1145/1641876.1641898.

[53] J. Munoz, P. Muhlethaler, X. Vilajosana, and T. Watteyne, "Why Channel Hopping Makes Sense, even with IEEE 802.15.4 OFDM at 2.4 GHz," in *Global Internet of Things Summit (GIoTS)*, IEEE, Jun. 2018. DOI: 10.1109/giots.2018.8534544.

[54] O. Gnawali and P. Levis, *The Minimum Rank with Hysteresis Objective Function*, RFC6719, Internet Engineering Task Force (IETF), Sep. 2012. [Online]. Available: https://datatracker.ietf.org/doc/html/rfc6719.

[55] L. Ben Saad, C. Chauvenet, and B. Tourancheau, "IPv6 (Internet Protocol Version 6) Heterogeneous Networking Infrastructure for Energy Efficient Building," *Energy*, vol. 44, no. 1, pp. 447–457, Aug. 2012. DOI: 10.1016/j.energy.2012.06.008.

[56] F. Lemercier, N. Montavont, L. Toutain, K. Vijayasankar, R. Vedantham, C. Pissard-Gibollet, and C. Philippe, "Support for hybrid network in RPL," in *IEEE International Conference on Smart Grid Communications (SmartGridComm)*, IEEE, Sydney, Australia, Dec. 2016, pp. 527–532. DOI: 10.1109/SmartGridComm.2016.7778815.

[57] F. Lemercier, N. Montavont, L. Toutain, and P. Chiummiento, "A New Objective Function for Hybrid Network in the Smart Grid," in *IEEE 19th International Symposium on "A World of Wireless, Mobile and Multimedia Networks" (WoWMoM)*, IEEE, Chania, Greece, Jun. 2018, pp. 14–16. DOI: 10.1109/WoWMoM.2018.8449744.

[58] O. Iova, F. Theoleyre, and T. Noel, "Using Multiparent Routing in RPL to Increase the Stability and the Lifetime of the Network," *Ad Hoc Networks*, vol. 29, pp. 45–62, Jun. 2015. DOI: 10.1016/j.adhoc.2015.01.020.

[59] M. Brachmann, S. Duquennoy, N. Tsiftes, and T. Voigt, "IEEE 802.15.4 TSCH in Sub-GHz: Design Considerations and Multi-Band Support," in *Conference on Local Computer Networks (LCN)*, IEEE, Osnabrueck, Germany, Oct. 2019, pp. 2169–3536. DOI: 10.1109/LCN44214.2019.8990806.

[60] Van Leemput, Dries and Bauwens, Jan and Elsas, Robbe and Hoebeke, Jeroen and Joseph, Wout and De Poorter, Eli, "Adaptive Multi-PHY IEEE802.15.4 TSCH in Sub-GHz Industrial Wireless Networks," *Ad Hoc Networks*, vol. 111, p. 102 330, 2021. DOI: https://doi.org/10.1016/j.adhoc.2020.102330.

[61] C. Garrido-Hidalgo, D. Hortelano, L. Roda-Sanchez, T. Olivares, C. Ruiz, and V. Lopez, "IoT Heterogeneous Mesh Network Deployment for Human-in-the-Loop Challenges Towards a Social and Sustainable Industry 4.0," *IEEE Access*, vol. 6, pp. 2169–3536, May 2018. DOI: 10.1109/ACCESS.2018.2836677.

[62] A. Al-Saadi, R. Setchi, Y. Hicks, and S. M. Allen, "Routing Protocol for Heterogeneous Wireless Mesh Networks," *IEEE Transactions on Vehicular Technology*, vol. 65, no. 12, pp. 9773–9786, Feb. 2016. DOI: 10.1109/TVT.2016.2518931.

[63] J. Muñoz, F. Rincon, T. Chang, X. Vilajosana, B. Vermeulen, T. Walcarius, W. van de Meerssche, and T. Watteyne, "OpenTestBed: Poor Man's IoT Testbed," in *IEEE Conference on Computer Communications (INFOCOM), CNERT Workshop*, Paris, France: IEEE, Apr. 2019, pp. 467–471. DOI: 10.1109/INFCOMW.2019.8845269.

[64] P. Tuset, X. Vilajosana, and T. Watteyne, "OpenMote+: a Range-Agile Multi-Radio Mote," in *International Conference on Embedded Wireless Systems and Networks (EWSN)*, ACM, 2016, pp. 333–334.

[65] Esteban, Municio and Glenn, Daneels and Vucinic, Malisa and Latré, Steven and Famaey, Jeroen and Tanaka, Yasuyuki and Brun-Laguna, Keoma and Vilajosana, Xavier and Muraoka, Kazushi and Watteyne, Thomas, "Simulating 6TiSCH Networks," *Transactions on emerging telecommunications technologies*, Aug. 2018. [Online]. Available: https://hal.inria.fr/hal-01838566.

[66] G. Daneels, E. Municio, B. Van de Velde, G. Ergeerts, M. Weyn, S. Latré, and J. Famaey, "Accurate Energy Consumption Modeling of IEEE 802.15.4e TSCH Using Dual-Band OpenMote Hardware," *Sensors*, vol. 18, no. 2, 2018, ISSN: 1424-8220. [Online]. Available: https://www.mdpi.com/1424-8220/18/2/437.

[67] A. Elsts, "TSCH-Sim: Scaling Up Simulations of TSCH and 6TiSCH Networks," *Sensors*, vol. 20, no. 19, 2020, ISSN: 1424-8220. DOI: 10.3390/s20195663. [Online]. Available: https://www.mdpi.com/1424-8220/20/19/5663.

[68] M. Rady, Q. Lampin, D. Barthel, and T. Watteyne, "No Free Lunch—Characterizing the Performance of 6TiSCH When Using Different Physical Layers," *MDPI Sensors*, vol. 20, no. 17, p. 4989, Sep. 2020. DOI: 10.3390/s20174989.

[69] M. Rady, Q. Lampin, D. Barthel, and T. Watteyne, "g6TiSCH: Generalized 6TiSCH for Agile Multi-PHY Wireless Networking," *IEEE Access*, vol. 1, no. 1, 2021. DOI: 10.1109/ACCESS.2021.3085967.

[70] M. Rady, Q. Lampin, D. Barthel, and T. Watteyne, "6DYN : 6TiSCH with Heterogeneous Slot Durations," *Sensors*, vol. 21, no. 5, 2021. DOI: 10.3390/s21051611.

[71] K. Pister, T. Phinney, P. Thubert, and S. Thubert, *Industrial Routing Requirements in Low-Power and Lossy Networks*, RFC 5673, Oct. 2009. DOI: 10.17487/RFC5673. [Online]. Available: https://rfc-editor.org/rfc/rfc5673.txt.

[72] J. Muñoz, X. Vilajosana, and T. Chang, *Problem Statement for Generalizing 6TiSCH to Multiple PHYs*, Internet Engineering Task Force (IETF), Jul. 2018. [Online]. Available: https://datatracker.ietf.org/doc/html/draft-munoz-6tisch-multi-phy-nodes-00.

[73] A. Kim, J. Han, T. Yu, and D. S. Kim, "Hybrid Wireless Sensor Network for Building Energy Management Systems Based on the 2.4GHz and 400MHz Bands," *Information Systems*, vol. 48, pp. 320–326, Mar. 2015. DOI: 10.1016/j.is.2014.06.005.

[74] J. H. Saltzer, D. P. Reed, and D. D. Clark, "End-to-End Arguments in System Design," *ACM Transactions on Computer Systems (TOCS)*, vol. 2, no. 4, pp. 277–288, Nov. 1984.

[75] T. Watteyne, X. Vilajosana, B. Kerkez, F. Chraim, K. Weekly, Q. Wang, S. Glaser, and K. Pister, "OpenWSN: a standards-based low-power wireless development environment," *Transactions on Emerging Telecommunications Technologies*, vol. 23, no. 5, pp. 480–493, 2012. DOI: 10.1002/ett.2558.

[76] M. Vucinic, J. Simon, K. Pister, and M. Richardson, *Constrained Join Protocol (CoJP) for 6TiSCH*, RFC9031, Internet Engineering Task Force (IETF), May 2021. [Online]. Available: https://datatracker.ietf.org/doc/html/rfc9031.

[77] S. Duquennoy, B. Al Nahas, O. Landsiedel, and T. Watteyne, "Orchestra: Robust Mesh Networks Through Autonomously Scheduled TSCH," in *Proceedings of the 13th ACM Conference on Embedded Networked Sensor Systems - SenSys*, New York, NY, USA: ACM Press, 2015, pp. 337–350. DOI: 10.1145/2809695.2809714.

[78] M. Rady, J.-P. Georges, and F. Lepage, "Can Energy Optimization Lead to Economic and Environmental Waste in LPWAN Architectures?" *ETRI Journal*, pp. 1–14, Sep. 2020. DOI: 10.4218/etrij.2019-0524.

[79] *SX1276/77/78/79 - 137 MHz to 1020 MHz Low Power Long Range Transceiver*, Accessed: 07 September, 2021.

[80] X. Foukas, G. Patounas, A. Elmokashfi, and M. K. Marina, "Network Slicing in 5G: Survey and Challenges," *IEEE Communications Magazine*, vol. 55, no. 5, pp. 94–100, May 2017. DOI: 10.1109/mcom.2017.1600951.

[81] C. A. Oroza, J. Giraldo, M. Parvania, and T. Watteyne, "Wireless-Sensor Network Topology Optimization in Complex Terrain: A Bayesian Approach," *IEEE Internet of Things Journal*, pp. 1–1, 2021. DOI: 10.1109/jiot.2021.3082168.

[82] M. Rady, M. Hafeez, and S. A. R. Zaidi, "Computational Methods for Network-Aware and Network-Agnostic IoT Low Power Wide Area Networks (LPWANs)," *IEEE Internet of Things Journal*, vol. 6, no. 3, pp. 5732–5744, Jun. 2019. DOI: 10.1109/jiot.2019.2905134.

[83] M. Rady, "Anonymity Networks: New Platforms for Conflict and Contention," *SSRN Electronic Journal*, 2013. DOI: 10.2139/ssrn.2241536.

[84] J. Kovac, J. Crnogorac, E. Kocan, and M. Vucinic, "Sniffing Multi-hop Multi-channel Wireless Sensor Networks," in *28th Telecommunications Forum (TELFOR)*, IEEE, Nov. 2020. DOI: 10.1109/telfor51502.2020.9306544.

[85] M. Labib, V. Marojevic, J. H. Reed, and A. I. Zaghloul, "Extending LTE into the Unlicensed Spectrum: Technical Analysis of the Proposed Variants," *IEEE Communications Standards Magazine*, vol. 1, no. 4, pp. 31–39, Dec. 2017. DOI: 10.1109/mcomstd.2017.1700040.

[86] Y. Xing, R. Chandramouli, S. Mangold, and S. S. N., "Dynamic Spectrum Access in Open Spectrum Wireless Networks," *IEEE Journal on Selected Areas in Communications*, vol. 24, no. 3, pp. 626–637, Mar. 2006. DOI: 10.1109/jsac.2005.862415.

[87] Y. Xing, R. Chandramouli, and C. Cordeiro, "Price Dynamics in Competitive Agile Spectrum Access Markets," *IEEE Journal on Selected Areas in Communications*, vol. 25, no. 3, pp. 613–621, Apr. 2007. DOI: 10.1109/jsac.2007.070411.

[88] M. Rady, "Budget of IoT Low Power Wide Area Networks," M.S. thesis, Lappeenranta University of Technology, Lappeenranta, Finland, Sep. 2018.